Optical resonances of sphere-on-plane geometries

Dissertation zur Erlangung des Grades

„Doktor der Naturwissenschaften“

am Fachbereich Physik, Mathematik und Informatik

der Johannes Gutenberg-Universität

in Mainz

Adriana Rueda Gomez

geboren in Bucaramanga, Kolumbien

Mainz, Juli 2008

1. Gutachter: [Removed]

2. Gutachter: [Removed]

Tag der mündlichen Prüfung: 27.10.2008

Dieser Arbeit wurde in der Zeit von Juli 2005 bis Juli 2008 unter der Betreuung von [Removed] und [Removed] am Max-Planck-Institut für Polymerforschung in Mainz angefertigt.

Contents

1 Introduction

The first indications of a special kind of interaction in systems consisting of a metal sphere with dimensions in the range of the wavelength of light placed at nanometer distances to a metal plane were found in tunnel junction experiments (Lambe and McCarthy 1976; Hansma and Broida 1978). Tunnel junctions were seen to emit light when a voltage was applied across the junction. This effect was first interpreted to be due to the excitation of surface plasmons by the tunneling electrons. The surface plasmons decayed by sending out light. Surface plasmons on perfectly smooth surfaces do not radiate. Nevertheless, it was thought that in these experiments the surface roughness of the junctions made the mechanism possible. With the invention of scanning near field optical microscopes, investigations started to study the role of the tip in the rate of light emission from the tunnel junction created between the tip and the surface studied (Johansson, Monreal et al. 1990). It was found that the tip itself and not only the surface were important. The tip was recognized to play a similar role as the surface roughness by breaking the translational invariance along the surface. The light emission and frequency were dependent on parameters such as the tip curvature and distance of the tip to the surface. The effect was re-interpreted as to be due to an optical resonance termed "localized interface plasmon" built up between the tip and the surface.

Independently in molecular spectroscopy, large enhancements of the Raman cross section were encountered in experiments combining electrochemistry and Raman spectroscopy of the molecule pyridine. Fleischmann et al. (Fleischmann, Hendra et al. 1974) had the idea to increase the amount of adsorbate on the surface by increasing the surface area. For this, they made the silver electrode very rough. They observed a huge increase in Raman signal, a process which is commonly very inefficient. Soon it was found out (Albrecht and Creighton 1977; Jeanmaire and van Duyne 1977) that the effect could not be explained by the increase of scatterers on the surface. Other mechanisms were proposed in which the Raman cross section of the individual molecules was enhanced in the adsorbate state (Jeanmaire and van Duyne 1977) and in which enhancement mechanisms due to optical resonances played a role (Philpott 1975). It was not clear whether the effect had an electromagnetic or chemical origin. The mechanisms behind this process, called Surface Enhanced Raman Scattering (SERS) became the subject of a lively debate. Though the debate remains until today (Weatherby

2005), it is generally accepted that the effect is due to both electromagnetic and chemical enhancement mechanisms. The electromagnetic part is due to large field enhancements in certain "hot spots" of the rough substrate (Dieringer, McFarland et al. 2006). The origin of these "hot spots" is thought to be due to the interaction between metallic protrusions of the rough surface at the nanometer scale. Raman scattering is enhanced by the field in the excitation and emission transitions and depends on the fourth power of the field amplitude E^4. The Raman scattering cross-section can increase by 10 to 12 orders of magnitude in these hot spots (Xu, Wang et al. 2004). Again, like in the case of tunnel junctions, an effect that was thought to be due to the surface roughness found its origins in the electromagnetic interaction of metallic structures at nanometer scales. Even though thirty years have passed since the discovery of SERS, up to now, its mechanisms are not fully quantitatively understood.

This electromagnetic field enhancement plays a role as well in fluorescence experiments where the fields can be used to modify the fluorescence intensity and decay rates of molecules placed near a surface. First experiments were done on silver island films (Glass, Liao et al. 1980; Ritchie and Burstein 1981; Aussenegg, Leitner et al. 1987). But the effect was found to take place not only near metal surfaces but also near dielectric spheres (Benner, Barber et al. 1980) and metallic nanostructures (Gersten and Nitzan 1981). Soon it was understood that surface enhanced fluorescence, Raman scattering, and in general all enhanced luminescence processes had a common origin (Weitz, Garoff et al. 1983): the huge modification of the electromagnetic field by the surface or nanostructures with resonant optical modes which opened new channels to which the molecules could couple.

Apart from the obvious potentials in applications of the high field enhancements, like optical tweezers (Xu and Käll 2002) and sensors (Lyon, Pena et al. 1999; Hutter, Cha et al. 2001; Tsuboi, Fukuba et al. 2007), these enhancements are interesting from a fundamental point of view. The appearance of such enhancements in small volumes raises the question of the applicability of the macroscopic description of matter at the nanoscales. The near fields, with their high wavevector components interact with surface states of the metal (Kolb 1988) or can make the systems sensitive to non-local effects (Barnes 1998) which are normally not included in the description by a bulk dielectric function of the system.

The reason for the lack of quantitative understanding relies on the lack of a defined geometry in the systems in which these effects were usually observed, like for example colloidal metals

in suspension (Kneipp, Wang et al. 1997), which made it impossible to model the systems quantitatively. Nowadays, the field of what is called nanotechnology has advanced tremendously making possible to fabricate a huge variety of metallic structures on the nanoscale, allowing for a better control of the geometry.

A special kind of system with an overall resonance localized in a small gap is the sphere-on-plane system, consisting of a metal nanoparticle placed at nanometer distances from a metal plane. Enhancements of the electromagnetic field take place in the small gap between the sphere and the plane. The reason for our interest in this system is due to a balance between its performance, laboratory feasibility and theoretical modeling (Aravind and Metiu 1983). In sphere-on-plane systems the largest field enhancements can be achieved due to the small gap in which the resonances of the sphere and the plane can couple. The frequency range of the resonance covers the visible region and most important: the system is very easy to fabricate in a way it resembles the models used for its description. The experimental challenge consists in realizing the very small gaps in a defined way and determining the role of the geometrical deviations of the experimental system from the idealized model. A quantitative understanding of this system is still lacking. The main problem arises from the experimental difficulty to determine the thickness and the dielectric environment in the gap, which are parameters needed to compare the response of the system with the theoretical predictions. The quantitative comparisons lead always to unphysical small gaps (Okamoto and Yamaguchi 2003; Tsuboi, Abe et al. 2006). Mainly, the far field response of the system has been studied where the resonances are detected by their extinction. A direct quantification of the near-field enhancement, the most interesting quantity, remains an experimental challenge.

In this work, a contribution towards a quantitative understanding of the electromagnetic resonances of these systems will be presented. First, quantitative investigations on the effect of the surface roughness of metal layers described by a single dielectric function were done (chapter 3). Second, a highly sensitive method to measure the resonance of an ensemble of sphere-on-plane resonators by utilizing propagating surface plasmons was developed (chapter 4). Then, a systematic characterization was done by varying several parameters which influence its resonant behavior: the nanoparticle size, distance to the plane and surrounding medium. In combination with surface plasmon spectroscopy the gap distance and spacer dielectric function could be determined without adjustable parameters (chapter 5). Of great importance was the successful fabrication of sphere-on-plane systems using a new class of

versatile molecules to separate the spheres from the metal plane. These spacers can be functionalized to introduce chromophores in the gap where the field enhancements are present and thus can be used as a probe for the near fields. Experiments were performed to see in how far the fluorescence of these molecules changed due to the sphere-on-plane interaction and surface roughness. The experiments were done using different surface roughness and different types of metals (chapter 6).

2 Basic concepts

In this chapter some basic concepts used throughout the work will be explained. Many of the concepts can be found in textbooks about optical properties of small particles (Bohren and Huffmann 1983; Kreibig and Vollmer 1995; Novotny and Hecht 2006) and in solid-state physics books (Ashcroft and Mermin 1976; Kittel 1996).

2.1 Metal optics

There is a very big difference between the optical properties of non-conductors and conductors of electricity. Dielectrics tend to be transparent and reflect light very weakly for light with less energy than the band gap. Metals are highly absorbing and reflect light at visible and infrared wavelengths.

The optical response of metals can be described using Drude's model (Ashcroft and Mermin 1976). In Drude's model the conduction electrons in a metal are treated as a gas to which the kinetic theory of gases is applied. The ions are assumed to be immobile and create a background against which the conduction electrons move. The electrons move in straight lines until they suffer an instantaneous scattering process which abruptly changes their velocity. The velocity is assumed to change in a way which maintains local thermal equilibrium. The probability of collision per unit time is given by $1/\tau$. τ is called the relaxation time or mean free time. The corresponding path $l = v_o \tau$ is called the mean free path, with v_o the average electron's velocity. Even though this model represents a huge oversimplification, it can be surprisingly well used to obtain rough estimates of properties whose more precise comprehension would require an incredibly complex analysis.

Under the influence of a field, Newton's laws apply. The fields of other electrons or ions are neglected. In this framework the dielectric function under the influence of a harmonic field with frequency ω can be derived as:

$$\varepsilon(\omega) = 1 - \frac{\omega_p^2}{\omega^2 + i\frac{\omega}{\tau}} \tag{2.1}$$

with ω_p the plasma frequency:

$$\omega_p^2 = \frac{n_e e^2}{\varepsilon_0 m_e} \tag{2.2}$$

Here, n_e is the electron density, e the electron charge, ε_0 the permittivity of free space and m_e the electron's effective mass. In this derivation, the forces due to magnetic fields were ignored in the equation of motion, and the spatial variation of the field was neglected. Whereas the corrections due to forces exerted by the magnetic field are very small, the assumption that the field does not vary in space makes the derivation valid only when the mean free path of the electrons is much smaller compared with the wavelength of light ($l << \lambda$) which is normally fulfilled for metals in the optical region. When this condition is not fulfilled, non-local theories have to be applied. Equation 2.1 implies that the optical properties of the metal are given by ω_p and τ which can be determined from experiments. The name plasma frequency originates from the fact that for $\omega = \omega_p$ the electron gas can sustain charge density oscillations called plasma oscillations or plasmons. For frequencies greater than ω_p the inertia of the conduction electrons prevents from instantaneous screening of the field and charge density waves are created.

Figure 2.1 shows a comparison between the dielectric function of gold calculated using Drude's model and values extracted experimentally (see chapter 2.1.2) (Johnson and Christy 1972). The points represent the experimental data and the solid lines the calculations using $\omega_p = 1.22\text{x } 10^{16}\ \text{s}^{-1}$ and $\tau = 7\text{x } 10^{-15}$ s. For $\lambda > 650$ nm, Drude's model describes very well the experimental data. In Drude's model, the complex dielectric function approaches the value $1 + \text{i}0$ (dielectric) for increasing ω and $-\infty + \text{i}\infty$ for decreasing ω (perfect conductor). The plasma frequency is determined by $\text{Re}(\varepsilon_{\text{Au}}) = 0$. For smaller wavelengths, the model of the metal as a free electron gas cannot be applied anymore. Bound electrons contribute at these wavelengths significantly (interband transitions). The visible light region corresponds to frequencies below the plasma frequency of the metal. The plasma frequency is a cut-off frequency where the material's properties are in a transition from a perfect conductor to an insulator. Due to this drastic change in the optical response, experiments with metallic nanostructures in the visible regime cannot be replaced by experiments with microwaves and

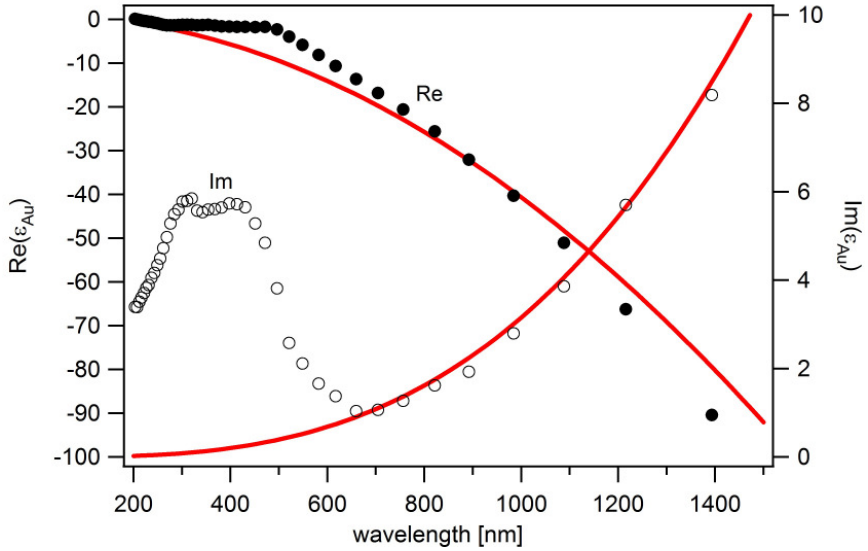

Figure 2.1: Complex dielectric function of gold. The filled and empty circles show the experimental values for the real and imaginary part taken from (Johnson and Christy 1972). The solid lines show the values calculated according to equation 2.1 with ω_p = 1.22x 10 ^{16} s^{-1} and τ= 7x 10 $^{-15}$ s. The corresponding plasma wavelength $\lambda_p = 2\pi c/\omega_p$ =154.5 nm with c the speed of light.

correspondingly larger metal structures using the scale invariance of Maxwell's equations because the material would have a completely different optical response. The study of the optical properties of metallic nanostructures in the visible regime has its own name and is called "plasmonics".

2.1.1 Modifications to the bulk dielectric function

In Drude's model the dielectric function was derived by assuming a time-dependent but spatially uniform field. This assumption is valid if the field does not vary considerably over distances comparable to the mean free path. Additionally, an important factor is not included in the model: the presence of the surface. Obviously, the presence of the surface has a repercussion in the way the electrons can move. At the surface the lattice terminates changing the band structure of the material and the screening forces experienced by the electrons. One can imagine that for example, for small spheres, where the surface to volume ratio is much higher, these effects play an important role. The validity of the concept of an effective dielectric function in which the material is treated as bulk was hoped to yield at least average values of the material properties. In extreme cases, like for very thin films (monolayer films) or very small spheres (radius < 10 nm) this is not the case. The calculation of these effects is still a matter of controversy and has lead experts in the area to loose their optimism (Kolb 1988) in understanding them. In the following, some comments about the repercussions of

these assumptions to the dielectric function will be presented.

2.1.1.1 Surface states

Surface states are states which may be strongly localized at the surface of a solid. They arise due to the lattice termination and are energetically located in the band gap. Although it is thought that metals do not posses a band gap, a band gap is present due to the surface. Surface states extend outside the metal surface for distances in the order of 0.1 nm. It is interesting to note that any changes in the surface structure have an impact on the surface states (Kolb 1988). A way to see the influence of the surface states is by applying an electrostatic potential to the surface. The surface states see a different portion of the potential as the bulk. Experiments in which reflectivity measurements are made when simultaneously changing the potential of the surface (electroreflectance spectroscopy) give indications of these states (Henglein, Kolb et al. 1993). One of the great virtues of electroreflectance at the metal interface is the very high sensitivity with which reflectivity changes can be detected.

In this context it is interesting to note that in spheres, depending on the radius the surface to volume ratio changes drastically with decreasing radius. Hence, surface effects will correspondingly play an increasingly important role in very small metallic nanostructures. For the optical description of small nanoparticles a radius dependent dielectric function $\varepsilon(\omega,R)$ is needed. A summary of all theories developed to approach this problem can be found in (Kreibig and Vollmer 1995).

2.1.1.2 Non-locality

In deriving the macroscopic dielectric function only the time dependence of the field was taken into account which leads to a frequency dependent dielectric function $\varepsilon(\omega)$. It was assumed that the field did not vary considerably in space over distances comparable with the mean free path of the electrons. The field at a certain point depends on what happened to the electrons since their last collisions which took place approximately one mean free path away. In other words, the response of an electron at one time and place depends on the electron's velocity. The velocity depends on the force acting earlier in another place, hence the name *non local* (Barnes 1998). The dielectric function becomes a function of the wavevector k $\varepsilon(\omega, k)$.

An example for a factor which makes the fields spatially inhomogeneous is the

presence of the plasma oscillations in the metal (Ashcroft and Mermin 1976). At frequencies greater than the plasma frequency this longitudinal waves propagate inside the metal in addition to the transverse waves of the electromagnetic field contributing to the reflectivity.

Another situation in which non-local effects can arise is when the material is brought sufficiently near to an electromagnetic field source. In the near field, high k components are present which do not propagate into the far field. If the metal is brought sufficiently near so that it can interact with the near field, these high k components can excite optical (surface plasmons) and non-optical modes (excitation of electron-hole pairs) in the material. The high k components can reach wavelengths $\lambda << l$ introducing the non-locality.

Methods to calculate the dependence of ε on k can be found for example in the book of Kolb (Kolb 1988) for surfaces and in Fuchs and Claro (Fuchs and Claro 1987) for small metal spheres. Non-locality has consequences for example in the reflectivity of metal films (Kolb 1988; Henglein, Kolb et al. 1993) and the extinction cross-sections of small metal spheres (Fuchs and Claro 1987). Recently, an approximate description taking into account non-locality showed how it can affect the fluorescence of molecules adsorbed on metal layers (Vielma and Leung 2007).

2.1.2 Tabulated dielectric function of gold

In this work the optical properties of thin gold films with different surface roughness were investigated. The following section discusses some considerations which should be taken into account when comparing experimental values of the dielectric function.

A huge amount of tabulated data exists for the dielectric function of gold. Figure 2.2 shows some selected sources which are frequently mentioned in the literature. Large variations of up to 10% are observed in the measured dielectric function of gold. The largest variations are seen in the real part from 500 nm to 700 nm which is the region of interest in this work. In the imaginary part, the largest variations are seen for wavelengths below 450 nm. These deviations are not due to systematic errors in the measurements but constitute a limit to the applicability of using surface measurements to determine the bulk properties of a layer. Their origin lies in the microscopic origin of the averaged macroscopic quantity measured (Aspnes 1982). When measuring ε, the macroscopic dielectric response is being measured. This

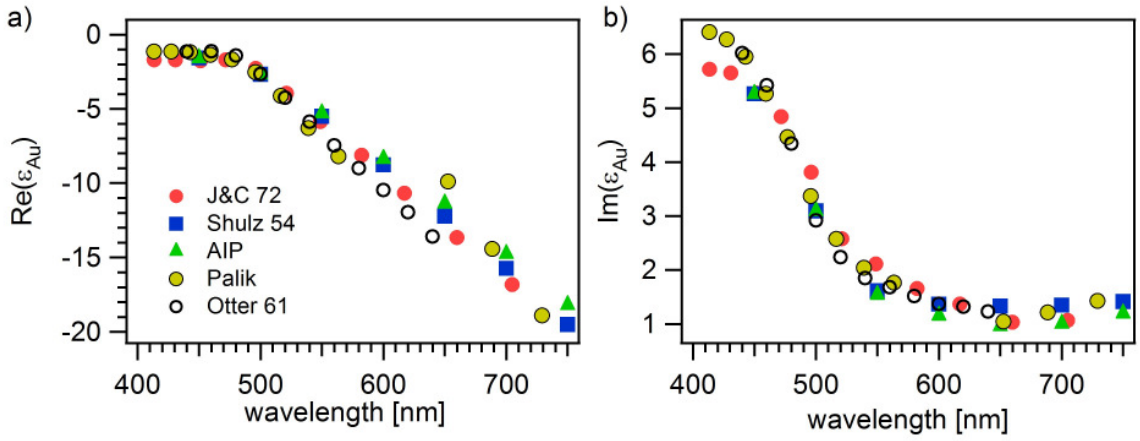

Figure 2.2: Experimental values for the a) real and b) imaginary part of the dielectric function of gold ε_{Au}. Values taken from: Otter 61 (Otter 1961), J&C72 (Johnson and Christy 1972), Schulz 54 (Schulz 1954; Schulz and Tangherlini 1954), AIP Handbook (Gray 1972), Palik (Palik 1984).

constitutes an average over the entire layer and depends on microscopic features like grain size, voids and the presence or absence of long range order. Screening charges develop at the boundaries between grains creating differences between the local field and the macroscopic field applied. Other facts, like the presence of oxides on the surface, which necessarily form when the metal layer is exposed to air also play a major role. Therefore, great care has to be taken when using tabulated data and details about the sample preparation have to be known.

The values for ε_{Au} in Figure 2.2 from Otter (Otter 1961) are for monocrystalline perfectly plane gold. Otter fabricated 5 mm diameter half spheres of gold single crystals. Their crystalline structure was almost perfect, sometimes being composed of few crystallites. He measured the change in intensity and phase of light at reflection angles of 70° in vacuum. The ε_{Au} obtained were found not to depend on the reflection angle chosen. He found out, that despite the good quality of the sample's surface, variations in the response from sample to sample could still be observed.

The values tabulated in the American Institute of Physics (AIP) Handbook (Gray 1972) in the wavelength region under investigation come from measurements done by Weiss in 1948 (Weiss 1948). At that time, it was already conjectured that the problem in the variations could be due to impurities of the samples during the evaporation. Weiss modified the evaporation machine to avoid impurities due to fat that evaporates during the heating procedure. He fabricated 300 µm to 400 µm gold layers on glass and quartz and tested the dependence of their optical response on the evaporation times and on the substrate used. The measurements

were done by measuring the change in phase and intensity of the reflected light.

Schulz (Schulz 1954; Schulz and Tangherlini 1954) measured the absorption coefficient k and the index of refraction n independently in different set of samples using different measuring techniques. To measure k he fabricated interference filters composed of silver/mica/gold layers and compared the transmission with silver/mica/silver layers using 60 nm gold layers. To measure n he measured reflectivity at 45° incidence with gold layers of 150 nm to 200 nm. He tested the effect of aging and annealing and found out that when heated below 130°C the samples were not modified in their optical properties. He tested the effect of aging for more than 2 years and found that aging makes the variations in n disappear.

The values tabulated by Palik in (Palik 1984) come from Thèye (Thèye 1970). Thèye measured reflectivity and transmittance of evaporated gold samples of 10 nm to 25 nm, annealing the samples at 150°C. She characterized the samples using x-ray and electron microscopy and found huge variations in $\mathrm{Im}(\varepsilon_{Au})$ depending on the surface morphology and annealing times.

Johnson and Christy (Johnson and Christy 1972) investigated the effects of the thickness, annealing and rate of evaporation. They measured reflectance and transmission at normal incidence, and transmission at 60° using p polarized light simultaneously to determine the thickness and dielectric function at the same time. They found that the best films were fabricated by fast evaporation rates (0.6 nm/s). They also found 25 nm to be a critical thickness over which the results were independent of the thickness, annealing and aging. Below this thickness they concluded the results obtained were not representative for bulk. These measurements explain why Thèye observed such big variations in her results.

In summary, every value tabulated was measured in a different way in different types of samples. None of these values should be taken as an absolute value for the bulk dielectric response of gold.

2.2 Optical resonances of metallic nanostructures

This work deals with the optical properties of systems made up of gold or silver nanostructures with dimensions in the order of nanometers when interacting with light in the visible region (500 nm - 850 nm). At these wavelengths, metallic nanostructures show very

interesting optical properties. Resonances arise which can be seen for example in their absorption or extinction cross-sections or in their reflectivity. Furthermore, the incoming field is enhanced very near the structure's surface at wavelengths near the resonance.

The systems studied consisted of metallic nanoparticles placed at nanometer distances from metal planes which we call 'sphere-on-plane' systems. In this chapter, some properties about metallic nanospheres, metallic planes and about what happens when they interact in the 'sphere-on-plane' system will be presented.

2.2.1 Metal spheres

The scattering and absorption cross sections of a sphere can be calculated using Mie's Theory (Mie 1908). Exactly 100 years ago, Gustav Mie developed his theory to understand the absorption and scattering phenomena of small gold colloids suspended in water which showed a great variety of colors. They were already observed in 1857 by Faraday (Faraday 1857) who at that time correctly interpreted the differences in color of different suspensions to be due to small metal particles of different shape and degree of aggregation. Although almost only known as Mie theory, Debye (Debye 1909) developed the same theory simultaneously but in another context. He calculated the mechanical pressure onto a small particle when interacting with light. At that time, this pressure could not be measured experimentally whereas scattering and absorption spectra were available.

The calculation is performed by solving Maxwell's equations in polar coordinates using multipole expansions of the incoming electric and magnetic fields. The boundary conditions are defined by an infinitely sharp discontinuity of the electron density at the surface. The material's properties are introduced via the dielectric function $\varepsilon_m(\omega)$ of the material and of the surrounding medium ε_a (a for ambient). $\varepsilon_m(\omega)$ is taken to be an average over the contributions of all electronic and atomic constituents over the volume (Bohren and Huffmann 1983).

In the quasi-static regime $R << \lambda$ (R is the sphere's radius), the phase retardations and high multipole order effects can be neglected and the extinction cross-section due to the dipolar term can be approximated to (Kreibig and Vollmer 1995):

$$\sigma_{ext}(\omega) = 9\frac{\omega}{c}\varepsilon_a^{3/2}\frac{4\pi}{3}R^3\frac{\mathrm{Im}[\varepsilon_m(\omega)]}{(\mathrm{Re}[\varepsilon_m(\omega)]+2\varepsilon_a)^2+\mathrm{Im}[\varepsilon_m(\omega)]^2} \tag{2.9}$$

with ε_a the dielectric function of the embedding material and ε_m the dielectric function of the particle material. The cross section has a resonance when $(\mathrm{Re}[\varepsilon_m(\omega)]+2\varepsilon_a)^2+\mathrm{Im}[\varepsilon_m(\omega)]^2$ has a minimum which can be simplified to $\mathrm{Re}[\varepsilon_m(\omega)]=-2\varepsilon_a$ provided that $\mathrm{Im}[\varepsilon_m(\omega)]$ can be neglected or does not vary much at this frequency. This condition is fulfilled by alkali metals but unfortunately not by noble metals like gold due to the interband transitions. Furthermore in the nanoparticle size range from 10 nm to 100 nm the quasi-static approximation does not exactly hold and retardation does play a role. The phase retardation introduces a shift in the maximum position. Figure 2.3 shows an absorption spectrum of gold nanoparticles in water where a clear resonance in the absorbance can be observed around 525 nm.

Calculations of the near field show that at wavelengths near the resonances seen in the extinction cross-section the incident field is enhanced near the surface of the sphere. These resonances are called in the literature Mie resonances or particle resonances. They have also a great variety of other names which can sometimes result in confusion. They are called sometimes particle plasmon, surface plasmon (although Mie explicitly writes (Mie 1908) in the first page of his publication that these particle resonances have no relation with surface plasmons which at that time were called Wood anomalies (see chapter 2.2.2)) or sometimes just plasmon in connection to the plasma oscillations mentioned in chapter 2.1.

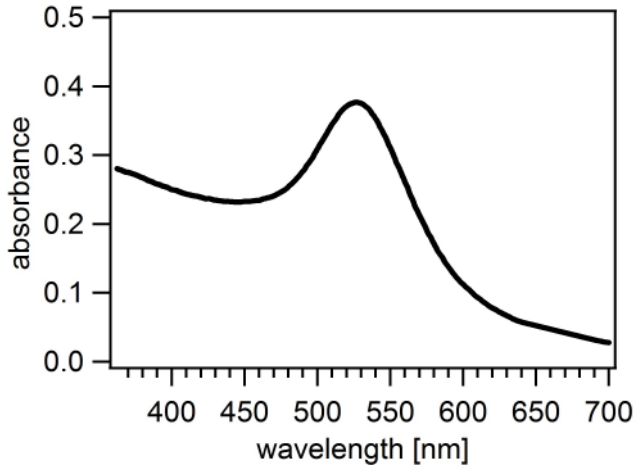

Figure 2.3: Absorbance of a suspension of gold nanoparticles with an approximate diameter of 15 nm (Vasilev 2004).

A nice summary of the optical properties of metallic nanostructures can be found in the book of Bohren and Huffmann (Bohren and Huffmann 1983) from a theoretical and in the book of Kreibig and Vollmer (Kreibig and Vollmer 1995) from an experimental point of view.

2.2.2 Metal planes

A metal plane constitutes another geometry for which optical resonances can be excited and described analytically. Like in the case of metallic spheres, the existence of these resonances has been known for more than 100 years. They were first observed by Wood (Wood 1902) who observed them as black fringes in the spectra of metallic diffraction-gratings when illuminated with white light. He called them anomalies because he could not understand their origins until they were explained later by Fano (Fano 1938). Many years later, they were observed in experiments with inelastic electron scattering (Ritchie 1957) where they were given the name “surface plasmons” (Ritchie and Marusak 1966) due to the connection the energy losses had with the interaction with plasma oscillations of the conduction electrons in the metal. The first time they were observed in optical experiments with non-corrugated metal plane layers was in experiments done on multilayer systems by Turbadar (Turbadar 1959). Turbadar introduces the use of a glass prism to couple the light momentum to the excitation in the metal. This coupling mechanism is known as the Kretschmann configuration due to Kretschmann who developed this coupling mechanism independently 10 years later (Kretschmann 1971) and was apparently not familiar with the work of Turbadar. Kretschamnn and Otto (Otto 1968) (who actually had the idea of the Kretschmann configuration first but did not recognize its potential due to a mistake in his calculations) are recognized as the pioneers of surface plasmon spectroscopy because they not only developed the coupling mechanisms but understood the physical mechanisms underlying the excitation of these surface waves at the metal dielectric interface and recognized their huge sensitivity to surface processes.

Surfaces plasmons and their applications are described in many textbooks, for example in the book from Raether (Raether 1988; Homola, Yee et al. 1999) and from Homola (Homola, Yee et al. 1999). In the following only some concepts needed to understand surface plasmon spectroscopy, which is the technique used throughout this work, will be described.

2.2.2.1 Dispersion relations

The following derivation was adapted from the book of Raether (Raether 1988) and from Knoll (Knoll 1998).

There exists a solution of Maxwell's equations for which a surface wave is generated at the boundary between a semi-infinite metal plane and a dielectric. Being a surface wave, the electromagnetic fields decay exponentially into the space perpendicular to the surface having its maximum at the surface. These waves propagate with a broad spectrum of frequencies. Their dispersion relation (dependence of their frequency ω on their wavevector k) $\omega(k)$ lies right of the light line meaning that they have a longer wavevector than light waves of the same energy and are therefore nonradiative because they cannot be excited by light.

To derive the dispersion relation Maxwell's equations are solved at an interface in the xz-plane between two half-infinite spaces 1 and 2 of materials described by their complex dielectric function ε_1 and ε_2 (see Figure 2.4a). The interface is assumed to be infinitely sharp and magnetic materials are ignored. A solution is sought for which the electromagnetic fields extend into the two materials perpendicular to the surface (in z direction):

$$\begin{aligned}\vec{A}_1 &= \vec{A}_{10}\exp[i(k_{x1}x + k_{z1}z - \omega t)] \\ \vec{A}_2 &= \vec{A}_{20}\exp[i(k_{x2}x + k_{z2}z - \omega t)]\end{aligned} \tag{2.10}$$

A_{i0} is the field's amplitude and k_{xi} and k_{zi} are the wavevectors in the x and z direction. The solution sought is an evanescent wave which has a maximum at the interface and decays into both media. For this, it is required that $\mathrm{Im}(k_{zi}) > 0$ (for the wave to be evanescent) and $k_{z1} < 0$ and $k_{z2} > 0$ (for the wave to decay into both media). For p-polarized light (transverse magnetic TM) with $\vec{E} = (E_x, 0, E_z)$ and $\vec{H} = (0, H_y, 0)$ the following relations are obtained when solving this problem.

From the boundary conditions it follows that:

$$k_{x1} = k_{x2} = k_x \tag{2.11}$$

The only non-trivial solution exists when:

$$\frac{k_{z1}}{k_{z2}} = -\frac{\varepsilon_1}{\varepsilon_2} \tag{2.12}$$

The wavevectors in x and z are related by:

$$k_{z1} = \sqrt{\left(\frac{\omega}{c}\right)^2 \varepsilon_1 - k_x^2} \tag{2.13}$$

and the desired dispersion relation is given by:

$$k_x = \frac{\omega}{c}\sqrt{\frac{\varepsilon_1 \varepsilon_2}{\varepsilon_1 + \varepsilon_2}} \tag{2.14}$$

Normally, ω is taken to be real. Since ε is complex, k_x is a complex quantity. If it is assumed that ε_2 is real and $\varepsilon_2 > 0$ then material 1 must fulfill $\varepsilon_1 < 0$ (equation 2.12) which is fulfilled by metals in the optical regime. This solution describes an evanescent wave having its maximum at $z = 0$ and decaying exponentially into both media. In x it describes an oscillatory wave with a finite propagation length $l = 1/\mathrm{Im}(k_x)$. This electromagnetic mode is called a surface plasmon and therefore k_x is sometimes called k_{sp}.

Figure 2.4b) shows how the surface plasmon's dispersion looks like. For small k_x, the dispersion relation approaches the light line. For big values of k_x, the frequency remains almost constant independent of k_x at a frequency called the surface plasmon frequency ω_{sp} which can be calculated (Raether 1988) to be:

$$\omega_{sp} = \frac{\omega_p}{\sqrt{1+\varepsilon_2}} \tag{2.15}$$

with ω_p denoting the plasma frequency.

A huge variety of names can be found also in the literature for this resonance. Besides surface plasmon, one can find: surface plasma oscillation, Fano mode, Wood anomaly, surface plasmon resonance, surface plasmon polariton and sometimes just plasmon.

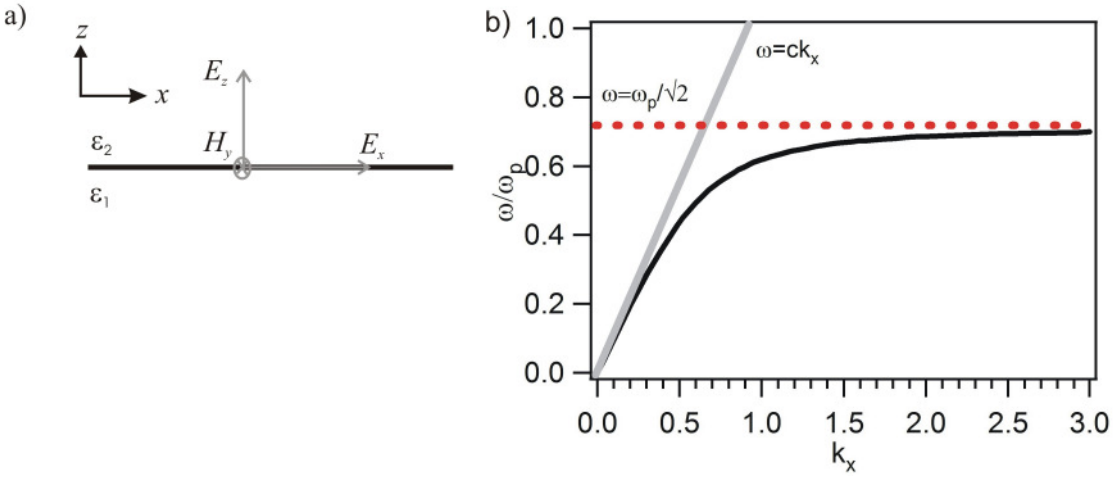

Figure 2.4: a) Coordinate system used to derive the dispersion relation. b) Dispersion relation (black solid line) of surface plasmons in air ($\varepsilon_2 = 1$). The light line is indicated by the gray solid line. The surface plasmon frequency is indicated by the red dotted line.

2.2.2.2 Prism coupling

From equation 2.14 it can be seen that the k_x vector of the surface plasmon k_{sp} is bigger than the wavevector k_0 of free light in medium 2 and can therefore not be excited by just illuminating with light travelling through this medium. A simple method to solve this problem is by letting the light pass first through a material with a dielectric function bigger than 1 as for example glass. The wavevector is increased to:

$$k_x = \sqrt{\varepsilon_{glass}}\frac{\omega}{c}\sin(\theta_i) \tag{2.16}$$

θ_i being the angle of incidence inside the prism. In the coupling mechanism called the Kretschmann-configuration shown in Figure 2.5a), this is achieved by the use of a glass prism. The incoming light's wavevector k_0 is increased when passing through the prism and can be tuned by changing the external angle of incidence θ. Depending on the angle this light can couple to the surface plasmon which propagates at the metal/air interface (see Figure 2.5b).

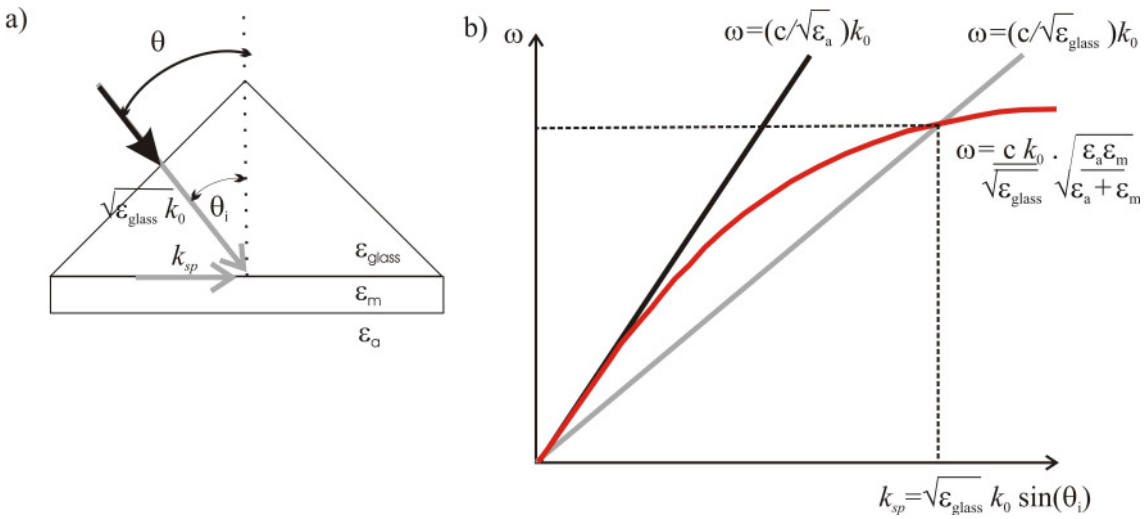

Figure 2.5: a) The Kretschmann configuration. By the use of a prism with dielectric function ε_{glass} the k_x vector is increased. b) Dispersion relation for light in air (black line), light inside the prism (gray line) and for the surface plasmons at the metal/air interface (red line). For a certain combination of the angle of incidence θ and the frequency of the incoming light, excitation of the surface plasmon can be achieved.

Another configuration, called the Otto configuration uses the same principle but another geometry. There, a very thin air gap separates the prism from the metal plane and is therefore more difficult to achieve experimentally. There are other methods to couple light to surface plasmons by the use of gratings for which the increase of momentum is given by the grating. Throughout this work, only the Kretschmann configuration was used.

Figure 2.6a) shows the measured reflectivity for p polarized light in the Kretschmann configuration for a 50 nm gold layer in air. The reflectivity is shown in a gray scale as a function of the external angle of incidence θ and of the wavelength. This representation of $\lambda(\theta)$ is equivalent to the $\omega(k)$ representation. The dispersion relation of the surface plasmons can be nicely seen as a black region. Figure 2.6b) shows corresponding sections from the plot at different wavelengths. For small wavelengths a very broad dip in the reflectivity is seen which becomes narrower with increasing wavelength. This dip in the reflectivity is due to the surface plasmon resonance as it will be explained in section 2.2.2.4.

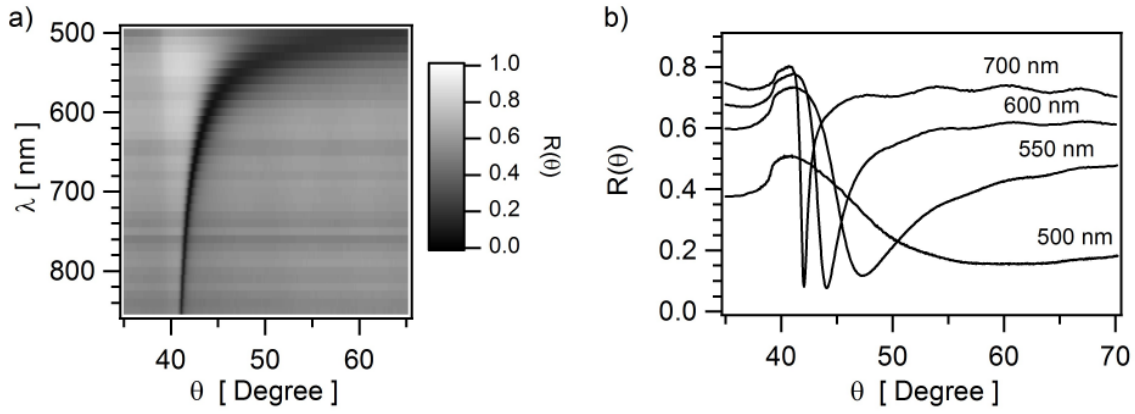

Figure 2.6: a) Measured reflectivity for p polarized light in Kretschmann configuration for a 50 nm gold layer in air. The reflectivity is shown in a gray scale as a function of the external angle of incidence θ and of the wavelength λ of the incident light. b) Cuts through the measurements in a) at different wavelengths.

2.2.2.3 Transfer matrix algorithm

A complete description of the optical response of these multilayers systems (for example the glass/metal/air system) can be achieved by solving the Fresnel equations for the incident, reflected and transmitted fields as they traverse each layer taking into account the change in phase during propagation. The changes at the boundaries and during propagation are written in matrix form making this algorithm very practical when extending to a large number of layers. The algorithm is explained for example in the book of Yeh (Yeh 1998). It allows for the calculation of quantities like the reflectivity of p-polarized light

$$R^p(\theta, \varepsilon_1, d_2, \varepsilon_2, ..., d_{n-1}, \varepsilon_{n-1}, \varepsilon_n) \tag{2.17}$$

with ε_i, d_i the dielectric function and thickness of each layer. Figure 2.7 shows reflectivity curves calculated using the transfer matrix algorithm. A clear resonance dip is seen. It is associated with the surface plasmon resonance. This approach shows that the existence of the surface plasmon arises directly due to the material's properties when Maxwell's equations are solved for a multilayer system. It should be noted that when calculating the reflectivity, all contributions from the reflected fields at the interface of the different layers are taken into account. The dispersion relation derived before assumed a semi-infinite material. Usually, the position of the minimum in the reflectivity is associated with the k_{sp} calculated in section 2.2.2.1 but it should be kept in mind that this is only an approximation. In a first approximation, the change in the minimum position (θ_0 to θ_f) and width (w_0 to w_f) (see Figure 2.7) can be related to the change in the complex surface plasmon wavevector Δk_{sp}

$$\begin{aligned} \mathrm{Re}(\Delta k_{sp}) &= \frac{2\pi}{\lambda}\sqrt{\varepsilon_{glass}}\cdot(\sin\theta_f - \sin\theta_0) \\ \mathrm{Im}(\Delta k_{sp}) &= \frac{2\pi}{\lambda}\sqrt{\varepsilon_{glass}}\cdot(\sin w_f - \sin w_0) \end{aligned} \qquad (2.18)$$

2.2.2.4 Surface plasmon spectroscopy

As seen in Figure 2.6 it is possible to observe the surface plasmon resonance by measuring the reflectivity of thin metal films as a function of the angle of incidence θ. The minimum position and width of the resonance is extremely sensitive to changes of the dielectric response of the medium in contact with the metal layer. By comparing the calculated reflectivity (equation 2.17) with the measurement it is possible to determine the film thickness d_f if its dielectric function ε_f is known or vice versa. Through this displacement, films of thicknesses in the Angstrom scale can be detected. This method is nowadays a standard method to monitor chemical and biological processes taking place at the surfaces of metals (Knoll 1998).

For films which are real dielectrics ($\mathrm{Im}(\varepsilon_f) = 0$), only the minimum position changes. Absorbing films additionally change the width of the resonance (see Figure 2.7b). There exists an approximate analytical expression (Kretschmann 1971; Kolb 1988; Plunkett, Wang et al. 2003) for the change in k_{sp}, Δk_{sp} called here $\Delta k_{linear\ d}$ produced by a layer with dielectric function ε_f and thickness d_f:

$$\Delta k_{linear\ d} \approx \frac{2\pi\omega}{\lambda c}\left(\frac{\varepsilon_m\varepsilon_a}{\varepsilon_m+\varepsilon_a}\right)^2 \cdot \frac{1}{\left(-\varepsilon_m\varepsilon_a\right)^{1/2}\left(\varepsilon_a-\varepsilon_m\right)} \cdot \frac{\left(\varepsilon_f-\varepsilon_a\right)\left(\varepsilon_f-\varepsilon_m\right)}{\varepsilon_f} d_f \qquad (2.19).$$

Here ε_m is the dielectric function of the metal and ε_a of the ambient. This quantity is sometimes called the ellipsometric moment (Plunkett, Wang et al. 2003) and has the advantage to compress the information about the layer in one complex quantity. It has nevertheless the disadvantage to be an approximation for small changes in k_{sp}, i.e. for very thin films and the assumption that a semi-infinite metal layer is used in its derivation.

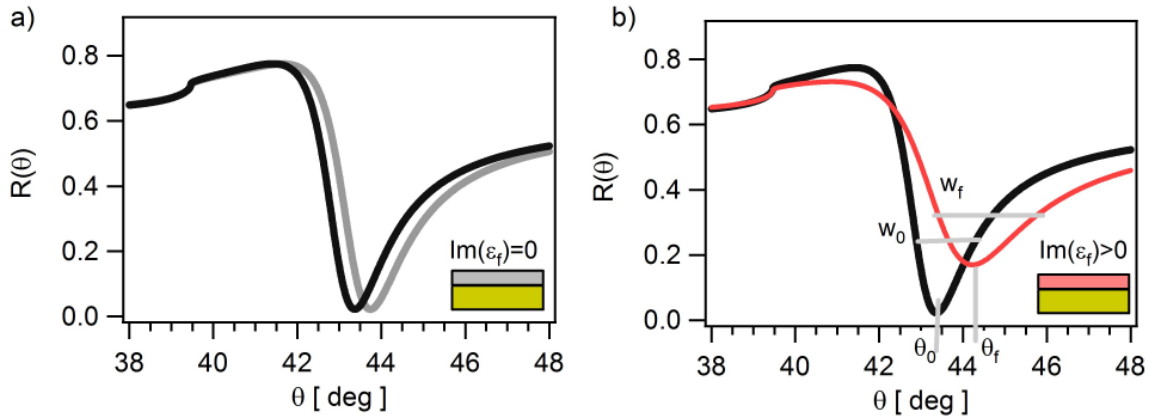

Figure 2.7: Reflectivity *R* as a function of the incident angle *θ* calculated using the transfer-matrix-algorithm for a glass/gold/film/air multilayer system. The plots show the change in the minimum position of the surface plasmon resonance of a 50 nm gold layer (black line) upon deposition of a a) 2 nm film with dielectric function $\varepsilon_f = 2.25+0i$ (gray line) and b) 2 nm film with dielectric function $\varepsilon_f = 0 + 5i$. $\lambda = 630$ nm.

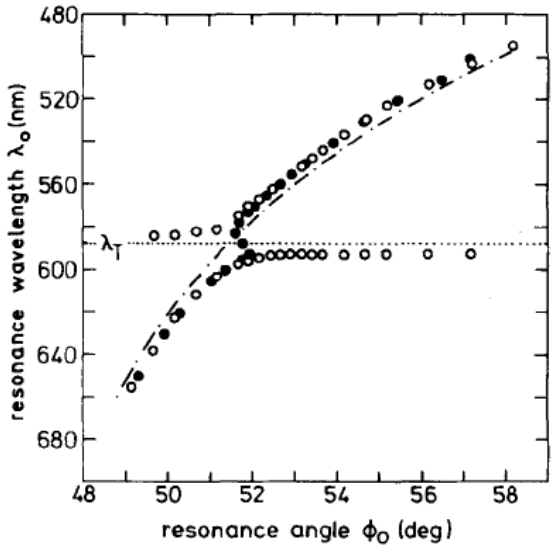

Figure 2.8: Graph taken from (Pockrand, Brillante et al. 1982). The film investigated contained the dye 1-octadecyl-1'-methyl-2, 2'cyanine perchlorate. The points represent the position of the minimum from angular and wavelength scans. The dash-dotted line represents the position of the minimum assuming a constant ε_f.

By measuring at different wavelengths it is possible to extract the signature of $\varepsilon_f(\omega)$ by following the changes in minimum position and width. Figure 2.8 shows an example of the resonance wavelength as a function of its minimum position for Langmuir-Blodgett films containing dye molecules which undergo a resonance at around 590 nm (Pockrand, Brillante et al. 1982).

The change of the dispersion relation when going through a resonance can be used to detect

the resonances due to the sphere-on-plane resonators as it will be shown in chapter 4.

2.2.3 On sphere-on-plane systems

Having discussed the optical properties of metal spheres and metal planes, this subsection describes how these two resonances can couple to create a new resonance called the "gap resonance". This coupling is not linear. Hence, the gap resonance cannot be described in terms of the isolated resonances of the sphere or of the plane.

The optical response of the system can be calculated by solving the Laplace equation in quasi-statical approximation. It was solved by Rendell (Rendell and Scalapino 1981) to explain experiments with tunnel junctions, by Wind et al. (Wind, Vlieger et al. 1987) to explain the behaviour of island films, by Aravind et al. (Aravind and Metiu 1983) as first steps to understand surface enhanced Raman scattering and by Ruppin et al. (Ruppin 1983) to describe systems of small metal spheres deposited on a substrate.

In quasi-statical approximation the response of the system is a function of the dielectric function of the materials, of the sphere radius R and of the gap distance d. For these small scales, the system is scale invariant (Nordlander and Le 2006) i.e. the interaction depends only on the d/R ratio.

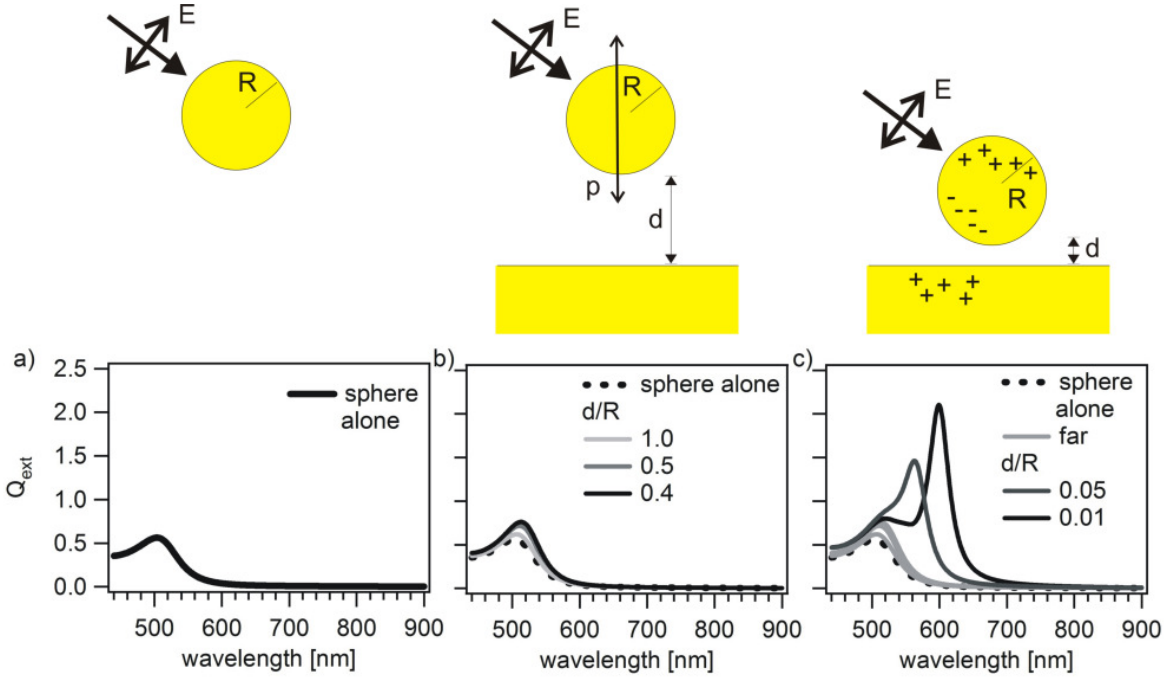

Figure 2.9: Extinction cross section for a) isolated sphere, b) d/R > 0.4 and c) d/R > 0.05.

Figure 2.9a) shows the extinction cross-section of a gold sphere when illuminated under an angle of 60° with polarized light. A resonance in the extinction cross section can be seen at an incident wavelength of about 500 nm. When a sufficiently small sphere is placed on top of a plane at a certain distance d, the sphere can be approximated as a point dipole. The interaction can be regarded as a dipole on mirror interaction. The field emitted by the sphere is reflected by the plane and interacts again with itself producing a shift in the resonance wavelength of the system compared with the resonance of the sphere alone (Figure 2.9b). When d is very small compared with the sphere radius, the sphere can no longer be regarded as a point dipole. The multipole moments due to the charge distributions have to be taken into account. At these distances, huge red-shifts and a significant increase in the extinction cross section (Figure 2.9c).

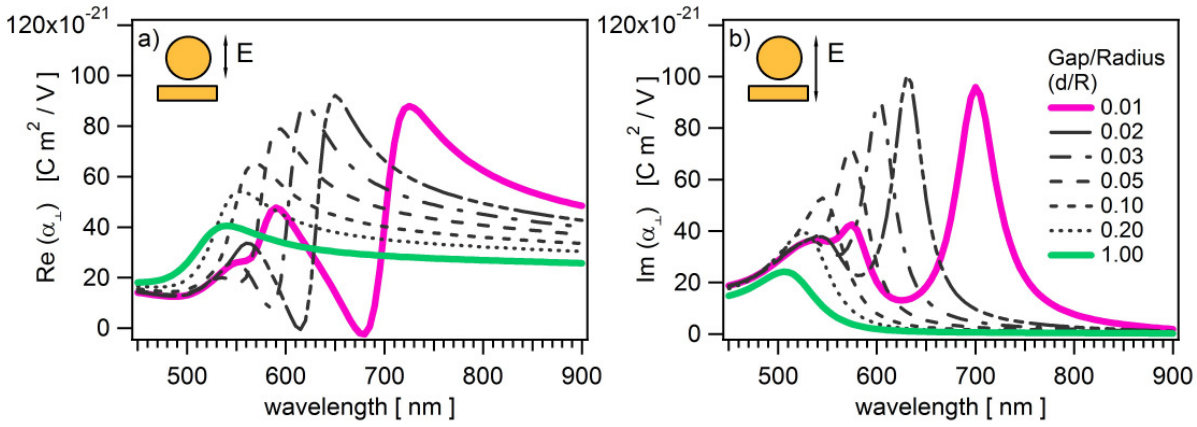

Figure 2.10: a) Real and b) Imaginary part of the complex polarizability of the sphere-on-plane system for a 10 nm radius gold sphere on a gold plane. The different lines show different d/R ratios.

A polarizability α_{SOP} for the system can be calculated by dividing the dipole moment of the system by the incident field E_0. Figure 2.10 shows the complex polarizability for the sphere-on-plane system. Its behavior resembles the behavior of a Lorentz resonator with an imaginary part which increases its value in resonance and a real part which changes signature when going through the resonance.

Calculations of the fields in the gap show strong field enhancements at wavelengths near the resonance. Figure 2.11 shows calculations taken from (Aravind and Metiu 1983) for systems

using gold and silver. The enhancement $(E/E_0)^2$ is defined as the ratio between the field in the gap E^2 and the incident field E_0^2. Field enhancements in the order of 10^4 for gold and of $5x10^4$ for silver can be achieved with sphere-on-plane systems.

Due to the high field enhancements predicted in sphere-on-plane systems there is a great interest in understanding these systems quantitatively. Holland and Hall (Holland and Hall 1984) separated silver and gold island films from a continuous silver film. Kume et al. (Kume, Nakagawa et al. 1995) investigated silver films covered with silver nanoparticles embedded in a SiO2 matrix. They had the idea to use surface plasmon spectroscopy to detect the signature of the gap resonances in the dispersion relation of the surface plasmons and in their scattering pattern (Kume, Hayashi et al. 1996; Kume, Hayashi et al. 1997). Later on, more defined geometries were achieved using alkanethiol spacers (Lyon, Pena et al. 1999; Hutter, Cha et al. 2001; Hutter, Fendler et al. 2001). Okamoto et al. (Okamoto and Yamaguchi 2003) observed the gap resonances in the absorption spectrum. By a systematic variation of the sphere radius he was able to reproduce the trend predicted by the theory. Tsuboi et al. (Tsuboi, Abe et al. 2006) varied additionally the type of spacer used. Nevertheless, a quantitative analysis of these experiments had the drawback to not be able to resolve the ambiguity in the choice of spacer thickness and spacer dielectric function which are needed as parameters to calculate the problem analytically. A problem when comparing with the analytical theories is the absence of the spacer layer in the model.

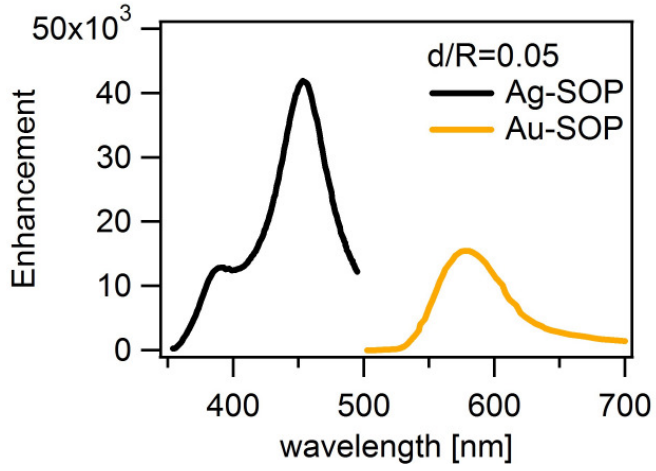

Figure 2.11: Data taken from (Aravind and Metiu 1983). Maximum enhancement of the field in the gap for silver sphere-on-plane systems Ag-SOP and for gold sphere-on-plane systems Au-SOP.

Although the spacer constitutes only a small part of the environment surrounding the sphere, in the gap high enhancements of the incident field arise. The importance of the dielectric environment in the gap was shown (Futamata, Maruyama et al. 2004; Futamata, Maruyama et al. 2005) in Raman scattering experiments. Models in which the spacer layer has been included have been developed with numerical calculations (Leveque and Martin 2006; Leveque and Martin 2006). The group of Nordlander developed a different concept to understand the interaction between the resonances of metallic nanoparticles. The resonances are treated like atomic orbitals which can hybridize giving a more intuitive physical insight to the problem (Prodan, Radloff et al. 2003). A great variety of systems have been calculated using this model including sphere on plane systems (Le, Lwin et al. 2005; Nordlander and Le 2006).

2.3 Surface enhanced luminescence

In chapter 6 experiments in which the fluorescence signal of a chromophore placed in the gap between a metal nanostructure and a metal plane will be presented. At such close distances from the metal sphere and metal plane the fluorescence of the chromophore is greatly affected. Under the influence of the gap resonances and the high fields which accompany them, dramatic changes in all luminescence mechanisms take place.

Luminescence is the emission of photons from an excited electronic state. This process can be altered by the presence of an interface. An interface modifies the boundary conditions of the electromagnetic field interacting with the emitter (atom, molecule or ion in an excited state). Hence a change in luminescence provides a way to access information about the electromagnetic fields present for example near planar or rough surfaces and nanostructures where a strong modification of the electromagnetic field takes place. As mentioned in the introduction the most famous surface enhanced luminescence process is surface enhanced Raman scattering (SERS) discovered more than 30 years ago (Fleischmann, Hendra et al. 1974; Jeanmaire and van Duyne 1977). SERS has developed into a ultra-sensitive spectroscopic technique with single molecule sensitivity (Kneipp, Wang et al. 1997; Nie and Emory 1997). Although the Raman scattering cross section is very small (10^{-30} cm^2 for non-resonant Raman scattering and 10^{-24} cm^2 for resonant Raman scattering) (Xu, Wang et al. 2004) by placing the molecule near a rough surface or for example between two

nanoparticles, the Raman scattering cross section is increased by 10 to 12 orders of magnitude. Fluorescence is another process which is modified by the presence of an interface. It was observed also for the first time 30 years ago near metal surfaces (Glass, Liao et al. 1980) or dielectric spheres (Benner, Barber et al. 1980). Although the mechanisms behind SERS, surface enhanced fluorescence and other luminescence processes is the same, the main difference with fluorescence is that Raman scattering involves coherent absorption and emission events. Hence, the enhancement is experienced in the excitation and by virtue of the reciprocity theorem also in the emission. Consequently the cross section which scales with the electric field E is enhanced by a factor of E^4 for Raman, whereas it scales with E^2 for fluorescence (Xu, Wang et al. 2004).

Although discovered decades ago, a quantitative understanding of surface enhanced processes is still lacking. The reasons for this lie in the undefined geometries in which these processes are observed. Nowadays, experiments using techniques like electron beam lithography (Le Ru, Etchegoin et al. 2007; Muskens, Giannini et al. 2007), atomic force microscopy (Bek, Jansen et al. 2008), single object microscopy (Anger, Bharadwaj et al. 2006; Kuhn, Hakanson et al. 2006) and the advances in nanotechnology which allow for particle geometry designs (Fedutik, Temnov et al. 2007; Tam, Goodrich et al. 2007) renewed interest in a quantitative understanding of these processes.

In the following, surface enhanced fluorescence will be discussed. Though, the mechanisms for the enhancement apply, like already mentioned for other luminescence processes like Raman scattering. The following explanation was adapted from Barnes (Barnes 1998).
Surface Enhanced Fluorescence

Fluorescence is an example of a quantum mechanical process. It is a spontaneous emission process and hence only the probability of decay for an ensemble of emitters can be predicted. The probability of emission is given by Fermi's golden rule:

$$\Gamma_{ij} \propto |M_{ij}|^2 \rho(\upsilon_{ij}) \tag{2.20}$$

with Γ_{ij} the rate for the transition between an excited state *i* and a lower energy state *j*. M_{ij} is a matrix element determined by the wavefunctions of the energy levels *i* and *j*. $\rho(\nu_{ij})$ is the density of the optical field at the transition frequency ν_{ij} and is called the photonic mode density. The photonic mode density can be pictured in a classical way as the ability of

the structure surrounding the emitter to support the emitted photon. A very near interface can modify $|M_{ij}|$ by modifying the energy levels of the emitter. For this, it should be separated from the emitter at distances characteristic for the wavefunctions, i.e. in the Angstrom regime. The modification of the photonic mode density on the other hand, can be achieved at distances characteristic of the wavelength of light and it is its modification in which we are interested. It is important to note that even though fluorescence is a spontaneous process, an interface provides a way to control and modify it.

To understand how the photonic mode density can be modified an idealized planar interface will be considered. If an emitter is placed close to a plane, the field reflected by the interface interferes with the emitter. Depending on the distance to the interface, the emitter experiences a larger field if the reflected field is in phase and a lower field if it is out of phase. In a classical picture, the emitter is viewed as a forced damped dipole oscillator. The driving force is the reflected field and it is damped because the emitter radiates power. Hence an oscillation of the fluorescence is expected. This fact was proven experimentally already in the 1970's by Drexhage (Drexhage 1970). For very small separations (few nanometers) a strong quenching of the emitter is observed. The quenching mechanism can be explained via energy transfer to optical and non-optical modes like bound and free charges. The quenching via optical modes is due to the high wavevector components in the near field which do not propagate into the far field and interact with surface modes like surface plasmons. As explained in chapter 2.2.2 these evanescent fields posses a higher wavevector as free light. Hence, they are able to interact only with the near field. Being radiationless, these modes provide a non-radiative decay mechanism and cannot be observed without the use of for example prism coupling or by roughening the surface. There are three different quenching mechanisms via non-optical modes. They are divided into bulk mechanisms, surface mechanisms and mechanisms due to the spatial variation of the near field. In the bulk mechanisms the energy is absorbed by the creation of an exciton in the bulk of the substrate, the momentum being supplied by the phonons. In surface mechanisms the excitons are created on the surface, the momentum being supplied by the surface potential. The mechanisms due to the spatial variation need to include non-local effects. In this case the momentum is supplied directly by the high k components of the near field. All these processes are accounted for in the classical picture and are included via the dielectric function $\varepsilon(\omega)$. Nevertheless to include the surface and non-local effects, modifications to the homogeneous bulk dielectric function have to be considered. Hence,

surface enhanced processes provide with means to investigate variations in the dielectric function due to non-locality and to the influence of the surface.

The idealized planar interface is impossible to achieve experimentally. The surface roughness is always present. Three different things happen when the interface is not planar. First, the translational symmetry is broken allowing for non-radiative modes to couple to radiation. Second, in many non-planar structures, surface modes become localized leading to dramatic changes in the photonic mode density. And third, the emitter separation d becomes less defined leading to a range of separations of the emitter to the surface.

Many experiments were done on island films (Glass, Liao et al. 1980; Ritchie and Burstein 1981; Aussenegg, Leitner et al. 1987) observing an enhancement of the fluorescence and a change of the decay rate of the emitter. In non-planar structures, experiments were done near dielectric spheres (Benner, Barber et al. 1980) or near metal silver nanoparticles (Chen, Munechika et al. 2007) to mention some examples. Due to the huge localized fields which arise in the gap between the nanostructures, systems like dimers, aggregates or sphere-on-plane systems play an important role in these investigations. Places, where due to nanoparticle aggregations or surface roughness these huge electromagnetic effects take place are called 'hot spots'. Efforts to define the separation between the emitter and the nanostructures or plane play an important role for the quantitative understanding of the process. Another interesting effect is the possibility of a coherent coupling or strong coupling between the emitter and the modes (Trugler and Hohenester 2008).

2.4 Experimental techniques

In this section some basic concepts about the experimental techniques used for the sample fabrication will be presented. All samples in this work were fabricated in collaboration with Dr. Marco Stemmler (except the template stripped gold samples presented in chapter 3 which were prepared in collaboration with Nicolas Vogel).

2.4.1 Self-assembled monolayers

To fabricate the sphere-on-plane systems studied in this work, a spacer layer of the molecules shown in Figure 2.12 was fabricated. The spacer molecules have the property to attach spontaneously to a metal plane by just dipping the metal substrate for a few minutes in a

solution containing the molecule. In this section, some comments about the mechanisms behind this process called self-assembly will be presented. A review about self-assembled monolayers can be found in (Ulman 1996).

Self-assembled monolayers (SAMs) are monolayers of molecules on a substrate which are able to spontaneously attach to the surface and build an ordered structure due to the interactions between them. To be able to self-assemble the molecule must fulfill some special preconditions. The molecule is divided into three parts: a head group, a body and a tail. A common example is an alkane thiol on gold. The head group consists in this case of the thiol group. Sulfur has a very high affinity for gold. The thiol head will stick to the gold surface, the alkyl chains, which constitute the body of the molecule pack together due to Van der Waals interactions. There has been a great deal of work to determine the way in which the molecules self-assemble. It is thought that the thiol head first binds to the surface but the whole molecule is lying down on top of the surface. As the surface coverage increases, the bodies start interacting. The interaction makes the body and tail to point outward. The whole process is thought to be similar to a two dimensional crystallization process. Alkane thiols are known to bind to many metal surfaces. Besides gold, they attach also to silver, copper and platinum. Another example for types of molecules able to self-assemble is that of silanes, which can bind on silicon oxides.

Figure 2.12a) shows the alkane thiol 2-Aminoethanethiol used in this work. The thiol group constitutes the head (marked in yellow), the alkyl chain the body and the tail is in this case an amino group. The amino group is able to bind the molecule to the gold nanoparticles. Due to the short alkyl chain and the big amino group on the tail 2-Aminoethanethiol does not self assemble into monolayers (Naud, Calas et al. 2001). A mixture of conformers in which the molecule is lying down (gauche) and pointing out (trans) are present (Michota, Kudelski et al. 2002). Figure 2.12b) and c) shows the polyphenylene dendrimers also used as spacers. In the case of the polyphenylene dendrimers the dithiolane units marked as R constitute simultaneously the head and tail. The body of the molecule is not a linear chain. The molecules can be thought of more like a tetrahedron with the 16 dithiolane groups which can attach either to the surface or to the nanoparticle. Not much is known about the way these molecules cover the surface. One of the tasks of this work was to test whether these molecules could be used as spacers or not.

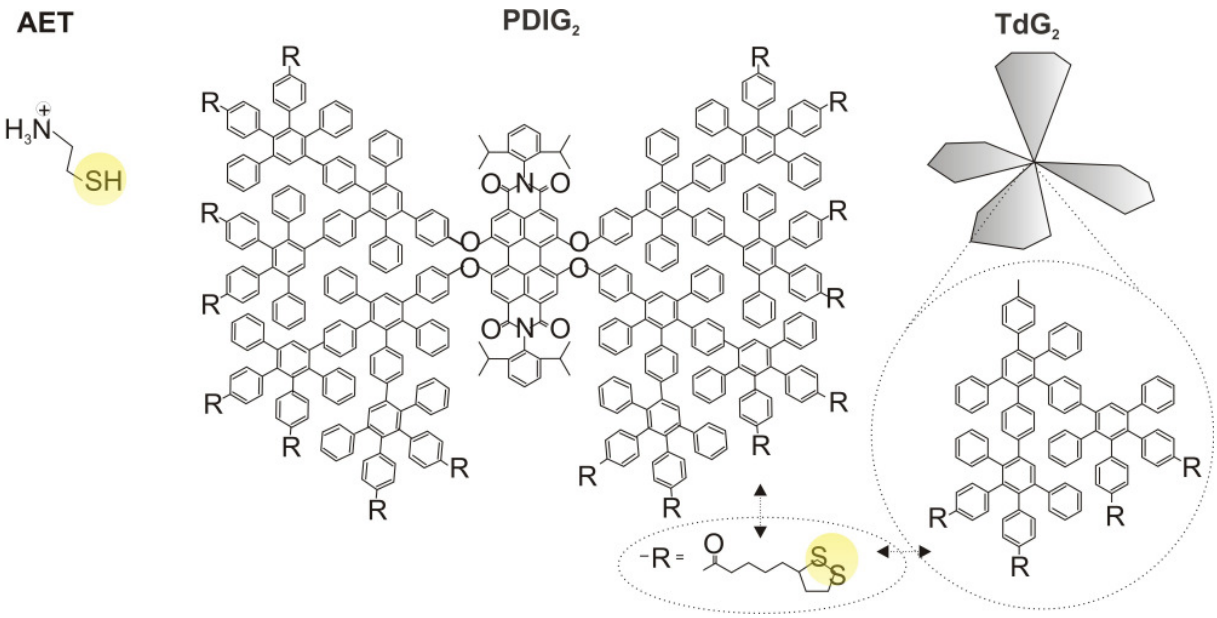

Figure 2.12: The three molecules used as spacers for the sphere-on-plane systems. a) 2-Aminoethanethiol (AET). b) The polyphenylene dendrimer $PDIG_2$ and c) TdG_2.

2.4.2 Fabrication of gold and silver colloids

Colloidal gold or colloidal silver is a suspension of nanometer sized gold or silver particles in a liquid which in this work was always water. There exist many methods to fabricate them (Kreibig and Vollmer 1995; Schmid 2003). The method used here is called the citrate reduction method, pioneered by Turkevich et al. (Turkevich, Stevenson et al. 1951) and later refined by Frens (Frens 1973). For gold, $HAuCl_4$ is dissolved in water and heated until boiling. While constantly stirring a sodium citrate solution is added which acts as a reducing agent. The Au^{3+} ions are reduced to neutral gold. The neutral gold atoms precipitate forming nanoparticles. The stirring is important to produce particles uniform in size. The negatively charged citrate acts as a stabilizing agent attaching to the nanoparticles preventing different nanoparticles from aggregating. The nanoparticle size can be increased by reducing the amount of sodium citrate. With less stabilizing agent present, the nanoparticles aggregate to form bigger nanoparticles. The lower limit for the amount of sodium citrate which can be used is reached when there is not enough reducing agent to reduce the gold. In this work nanoparticles varying from 20 nm to 200 nm in diameter were fabricated. Up to 50 nm the nanoparticles fabricated have a very narrow size distribution (of about 10% FWHM) and are almost spherical. The larger nanoparticles are not so narrow distributed and contain nanoparticles of different forms: spheres, rods, triangles. The gold nanoparticles suspensions

vary in color (from light red to yellow-brown) depending on their size.

To produce silver nanoparticles the $HAuCl_4$ is replaced by $AgNO_3$. The nanoparticle size distribution in this case is very broad with a particle size distribution ranging from 20 – 160 nm in diameter. The suspension has a yellow-brown color and various nanoparticle forms are present as in the case of the large gold nanoparticles.

2.4.3 Template stripping of gold

The method of template stripping is a method to fabricate much smoother surfaces than those achieved by evaporation. It makes use of the poor adhesion of the material evaporated to an atomically flat template surface like mica or silicon single crystals which allows the material to be stripped after evaporation thus leaving the surface in contact with the template uncovered.

The method was first developed by Butt et al. (Butt, Wang et al. 1991) for carbon surfaces to be able to image bio-molecules immobilized at the surface. They applied the same technique with Pt/C and gold successfully (Butt, Müller et al. 1993). Hegner et al. successfully fabricated gold layers with the method simultaneously (Hegner, Wagner et al. 1993) and introduces the term template stripped gold for the fabricated gold surfaces.

The steps for the sample fabrication are first evaporation of the gold layer onto mica, gluing the gold layer onto glass and finally stripping the surface by chemical or mechanical methods. Stamou et al. (Stamou, Gourdon et al. 1997) were the first to use silicon as a template. Hegner et al. (Hegner, Wagner et al. 1993) investigated the stability of different glues in solution showing that they were stable enough to be dipped in solutions of self assembled monolayers of alkanethiols opening a wide area of applications for these smooth surfaces. The same method can also be used for silver instead of gold.

3 Characterization of gold films by surface plasmon spectroscopy: Large errors and small consequences

In this chapter a quantitative investigation of the effect of the surface roughness of thin metal layers described by a single dielectric function when characterized with surface plasmon spectroscopy will be presented. As explained in section 2.2.2, surface plasmon spectroscopy has become a widespread ultrasensitive tool for the characterization of thin layers and interfaces (Knoll 1998; Homola, Yee et al. 1999). It relies on the optical response of a thin (around 50 nm) noble metal film which separates two media with different refractive indices, e.g. glass and air. The thin metal film is illuminated by a plane light wave from the half space with high refractive index and the reflected light intensity is recorded as a function of the angle of incidence. A sharp dip is observed in the reflected intensity which, upon variations of the optical response near the interface between the metal and the low refractive index medium, shows pronounced changes. This dip is attributed to surface plasmon excitation (Raether 1988). Mostly, thin dielectric films are investigated which lead to a shift in the minimum angle.

The quantitative analysis is based on the comparison between the measured angle dependent reflectivity and a calculation for the multilayer architecture glass/gold/thin film/air (Yeh 1998). The best fit for the glass/gold/air system yields the thickness and complex dielectric function of the gold. A second fit after deposition of a thin dielectric film allows for the determination of its thickness if its refractive index is known.

Due to the great success of this method for thin film analysis, the model of the gold as a homogenous layer with constant refractive index may be taken as physical reality. Though, the evaporated gold films generally have a flat interface with their substrate opposed to a much rougher side facing the ambient. In this chapter an experiment is presented where surface plasmons are excited both on the top side and on the smooth side which was facing the substrate and was processed by the method of template stripping (Stamou, Gourdon et al. 1997). The limitations in the characterization of thin metallic layers by surface plasmon spectroscopy are discussed and the implications of these shortcomings for the analysis of thin dielectric coatings are analyzed.

3.1 Experimental

A gold layer of 40 nm nominal thickness was thermally evaporated (Balzers PLS500) on clean BK7 glass and on a silicon single crystal wafer simultaneously. The silicon slide was obtained as a 26 x 45 mm^2 pre-cut wafer (Crystec Kristalltechnologie). It was pre-cleaned for one hour in a solution of 50 ml H_2O, 10 ml NH_3 and 10 ml of H_2O_2 at 75°C, rinsed extensively in ultra clean water (Milli-Q Gradient A10) and dried under nitrogen flow. It was then directly placed into the vacuum chamber for evaporation. The evaporated gold layer on the BK7 glass was taken directly as one of the two samples and will be called the evaporated gold sample (see Figure 3.1b). The gold layer evaporated on the silicon wafer was used to prepare a smoother gold surface by the method of template stripping of gold from silicon (Butt, Wang et al. 1991; Butt, Müller et al. 1993; Hegner, Wagner et al. 1993; Stamou, Gourdon et al. 1997) which is shown schematically in Figure 3.1b). This sample will be called the TSG (template stripped gold) sample (see Figure 3.1b). To fabricate this sample, the evaporated gold on the silicon wafer was immediately glued onto a clean BK7 glass substrate using the epoxy glue EPO-TEK 353ND-4 (Epoxy Technology) following the manufacturer's instructions. For curing, the sample was heated to 150°C for 60 min and allowed to cool down. Prior to the optical measurements the gold surface was mechanically separated from the silicon wafer using a scalpel as a lever.

The specular reflectivity was measured in a home-built surface plasmon spectrometer in Kretschmann configuration (Turbadar 1959; Kretschmann 1971) (see Figure 3.1c*)*. The reflected light of a He-Ne Laser (λ = 632.8 nm) was recorded with a silicon photodiode as a function of the external angle of incidence θ. The incident light was amplitude modulated with a chopper (1369 Hz) and transverse magnetically polarized. The signal from the photodiode was analyzed with a Lock-in-Amplifier (EG&G Instruments 7260) using the chopper frequency as reference. The reflectivity R is defined as the recorded reflected light intensity I_r normalized with the incident light intensity I_0 measured without sample.

The sample's surface was characterized with an atomic force microscope (AFM). The images were taken in air at room temperature with a commercial AFM (Nanocope IIIa, Veeco) in tapping mode.

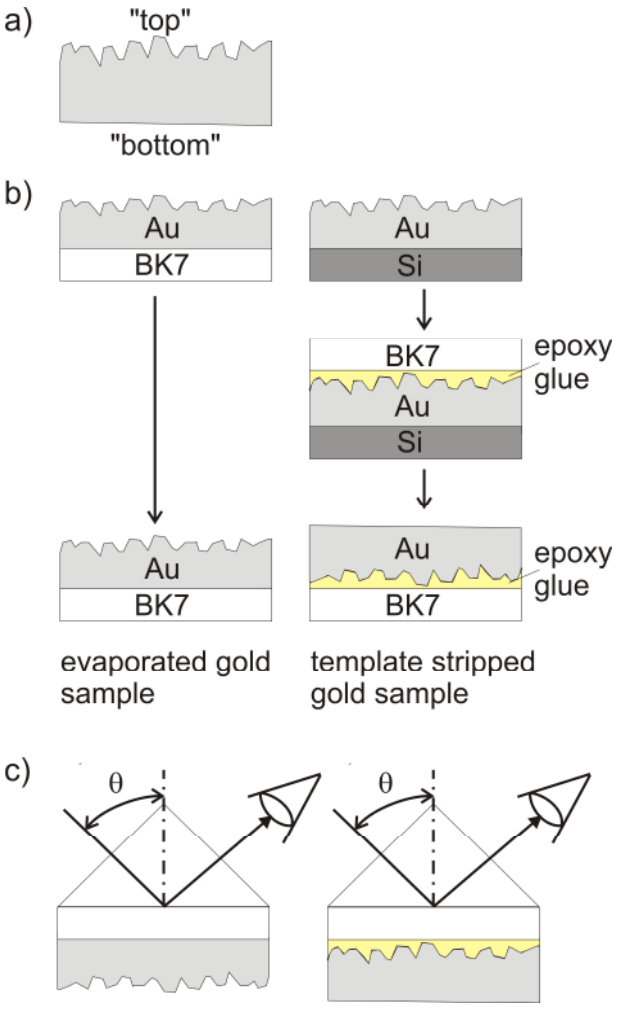

Figure 3.1: Definition for "top" and "bottom" of the gold thin film. b) Schematic representation of the sample fabrication. c) Schematic representation of the reflectivity measurements.

3.2 Results

The objective of this study is to investigate in how far standard gold films with a rough "top" side and a smooth "bottom" side (see Figure 3.1a) are optically inhomogeneous. The experimental basis for the further analysis relies on the fabrication of a gold film with a smooth and rough side and its investigation with surface plasmon spectroscopy both when the smooth and the rough side are exposed to air. To produce samples which approximate this ideal situation as well as possible, two different samples were simultaneously evaporated (see Figure 3.1). The one sample was left as it was and will be called the evaporated gold sample. The other was used to prepare a template stripped sample. The procedure takes advantage of the poor adhesion between gold and silicon. By application of mechanical pressure, the interface of the two materials is "stripped" free. Thus, the natural smoothness of the polished silicon wafer surface is transferred to produce a very smooth gold surface. In this way

measuring the optical properties of the evaporated gold sample gives information about the "top" rough side of the film and measuring the optical properties of the template stripped gold sample (TSG) sample gives information about the "bottom" smooth side of the film.

3.2.1 Indications why the gold seems to be inhomogeneous

Figure 3.2 shows the topography from the two samples as measured by atomic force microscopy. The evaporated gold sample has a surface roughness (rms) of 1.45 nm and a peak to valley distance of 7.9 nm compared to the much smoother TSG sample which has a surface roughness of 0.20 nm and a peak to valley distance of 1.1 nm. In both cases the surface is polycrystalline. The gold grows as crystallites of ~30 nm diameter. However, in the TSG the crystallites adjust to the surface of the silicon used as support creating a much smoother overall surface.

Figure 3.3 shows the reflectivity R as a function of the external angle of incidence θ for the evaporated gold (1) and the TSG sample (2). Differences in the minimum position and width of the surface plasmon resonance are seen indicating differences in the dielectric response. Hence, the reflectivity measurements indicate that the optical properties of the top of the film differ from those at the bottom, indicating that the gold film is heterogeneous.

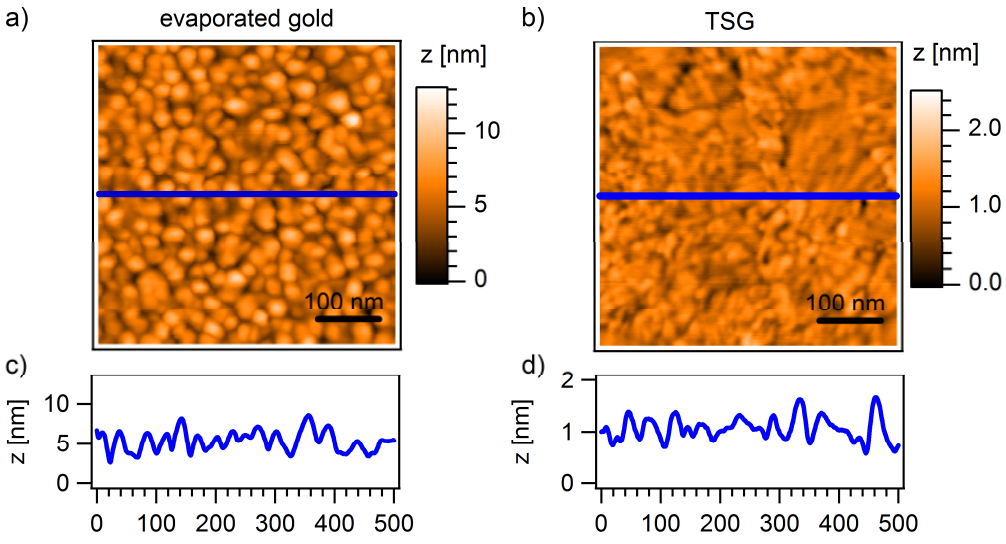

Figure 3.2: AFM images of the a) evaporated gold and b) template stripped gold sample. c) and d) Cross section of a) and b).

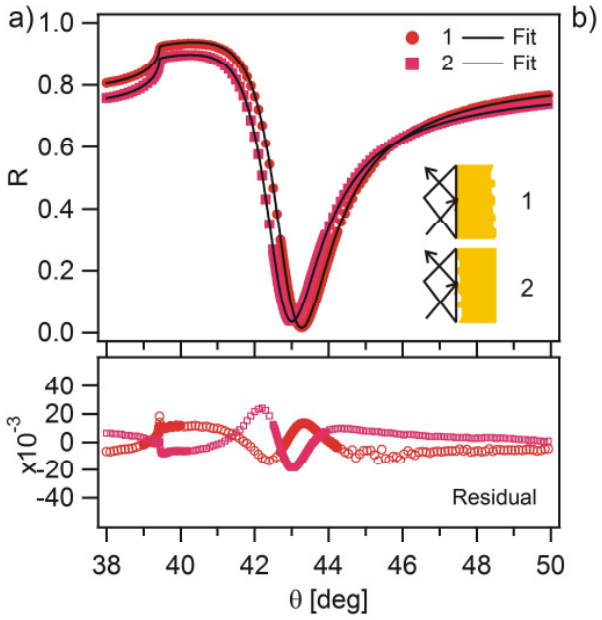

(1) c=0.992±0.001		
layer	d [nm]	ε
glass	∞	2.2935
gold	44.63 ± 0.04	(-11.846 ± 0.003) +i (1.205 ± 0.002)
air	∞	1.00

(2) c=0.943±0.001		
layer	d [nm]	ε
glass	∞	2.2935
gold	41.26 ± 0.02	(-12.863 ± 0.002) +i (1.243 ± 0.001)
air	∞	1.00

Figure 3.3: a) Reflectivity *R* as a function of the angle of incidence *θ* for the evaporated gold sample (1) and the TSG sample (2). The fit results are indicated by the solid curves. The bottom plot shows the residual. b) Parameters for the multilayered system used to fit the experimental data.

For the fit, a multilayer system glass/gold/air is assumed. The reflectivity *R*' of the multilayer system is calculated using the transfer matrix algorithm (Yeh 1998). For this, the external angle of incidence θ is transformed into the internal angle of incidence inside the prism. Additionally, a global constant scaling factor c is included for the fit function $R_{fit}=cR'$. The scaling factor is introduced to account for absorption inside the prism, fluctuations in the laser intensity and differences in the detector response across the detector area. For the fit, the global scaling factor c, the gold thickness d_{gold} and the gold dielectric function $\varepsilon_{\text{gold}}$ are set as free parameters. The dielectric function of glass $\varepsilon_{\text{glass}}$ is determined by matching the total internal reflection edge. A fit of the reflectivity assuming one single homogenous gold layer describes the experimental data very well as shown in Figure 3.3a). Figure 3.3b) shows the parameters obtained for both samples. The errors indicated are the errors from the fit. A plot of the residual, the difference between R_{fit} and the experimentally measured reflectivity, shows discrepancies in the order of 1%. The scaling factor c shows discrepancies of 1% for the evaporated sample and in the order of 5% for the TSG sample, probably due to absorption in the epoxy glue layer and inside the prism. Significantly different values for the gold thickness and gold dielectric function were obtained for both samples, the difference in $\text{Re}(\varepsilon_{\text{gold}})$ being about 10%. Such large variations in the experimental $\varepsilon_{\text{gold}}$ have been

discussed by all authors who tried to measure this quantity (Schulz 1954; Schulz and Tangherlini 1954; Otter 1961; Thèye 1970; Johnson and Christy 1972; Aspnes 1982). In particular, Aspnes (Aspnes 1982) points out that the dielectric function highly depends on the microstructure of the sample. The macroscopic observable ε_{gold} is an average of its microscopic counterpart. Any changes in the local structure contribute to deviations from the value of ε_{gold} from its true bulk value set a principal limit to access the true bulk response of gold. Among other things, grain size and grain length, voids and the long range order of the sample are important. Therefore, details about the sample preparation have to be known to compare tabulated data. Figure 3.4 shows values for ε_{gold} from different classical sources together with the two results found here. Palik (Palik 1984) states the smallest negative value for Re(ε_{gold}). These values actually go back to Thèye (Thèye 1970) where gold films with thicknesses of about 150 Å were used. Johnson and Christy (Johnson and Christy 1972) found 250 Å to be a critical thickness below which the optical properties of the film are not representative for bulk. Their data is based on measurements on thicker samples, resulting in a larger negative value for Re(ε_{gold}) pointing to a higher quality.

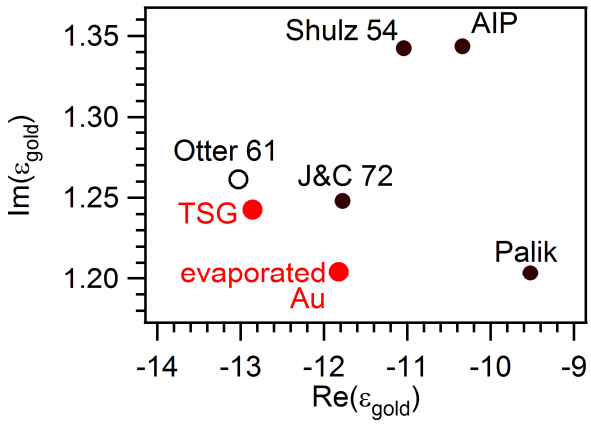

Figure 3.4: ε_{gold} at 633 nm for monocrystalline gold (empty circle), for polycrystalline gold from different classical sources (black circles) and for the two results found in this work (red circles). Otter 61 (Otter 1961), J&C72 (Johnson and Christy 1972), Schulz 54 (Schulz 1954; Schulz and Tangherlini 1954), AIP Handbook (Gray 1972), Palik (Palik 1984).

Earlier work by Schulz and Tangherlini (Schulz 1954; Schulz and Tangherlini 1954) and Weiss (Weiss 1948) (tabulated in the AIP Handbook (Gray 1972)) yield intermediate values. In the experiment it is expected that the surface plasmon located at the air side dominates the optical response. On the rough side, it "sees" a response similar to the tabulated values in

Johnson and Christy. On the smooth side a significantly larger negative value for $\mathrm{Re}(\varepsilon_{gold})$ is found very close to the value reported for monocrystalline gold (Otter 1961), suggesting a high quality of the TSG sample.

3.2.2 Description as a two-layer model

The difference in optical behavior between the top and bottom side of the same film suggest a description of the film by a depth dependent dielectric function $\varepsilon(d)$. The simplest possibility to account for a depth dependency is two layers. This model is clearly a simplification and does not reflect the physical reality. Nevertheless, to model $\varepsilon(d)$ would require infinitely many layers which corresponds to infinite free parameters to be determined experimentally. In the following it will be shown that already the parameters of this two layer model cannot be determined in a unique way. This approach to account for the heterogeneous character of evaporated thin gold films using multilayer models has also been recently discussed (Zhang, Berguiga et al. 2007).

3.2.3 Model – gold only

Next, it is investigated if this simple two-layer model is capable to reproduce both experimental results simultaneously.

To set the thickness and dielectric function of the two layers which will be called gold_1 and gold_2, with thickness and dielectric function d_1, d_2, ε_1 and ε_2 respectively, the measured reflectivity for the evaporated gold sample and TSG were fitted simultaneously considering glass/gold1/gold2/air for the evaporated gold sample and glass/gold2/gold1/air for the template stripped gold sample. The free parameters for the fit were c_1, c_2, d_1, d_2 and the complex ε_1 and ε_2; with c_1 and c_2 the scaling factors for the evaporated gold and the TSG fit respectively.

By testing different sets of start parameters for d_1 and d_2, it was found that there is not a unique solution. A continuous set of possible d_1 and d_2 combinations can be chosen to describe the measured data with similar goodness of the fit. A histogram of the values found by the fit is shown in Figure 3.5a). d_1 and d_2 are highly correlated. The sum of both thicknesses is a constant which amounts to approximately 42.9 nm as shown in Figure 3.5b).

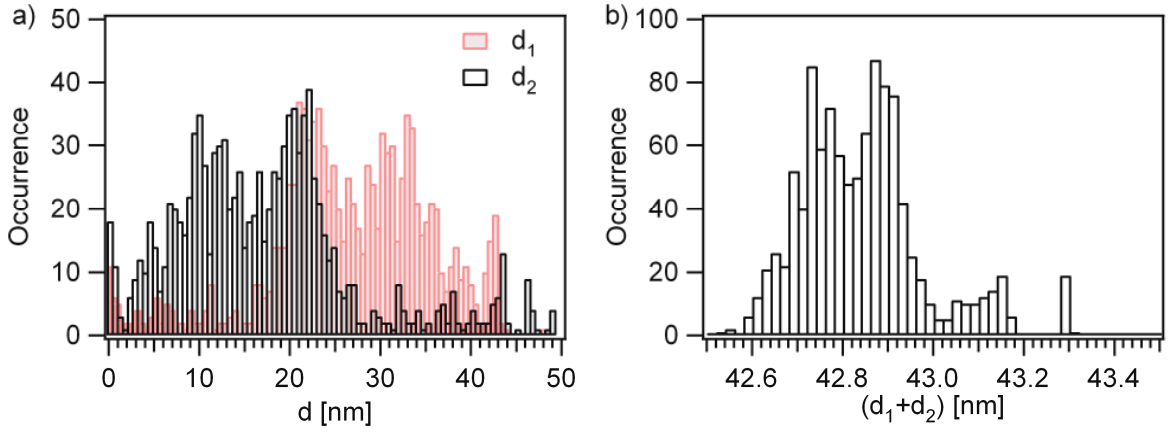

Figure 3.5: a) Histogram of the values found for d_1 and d_2 in the fit. b) Sum of d_1 and d_2 for each fit.

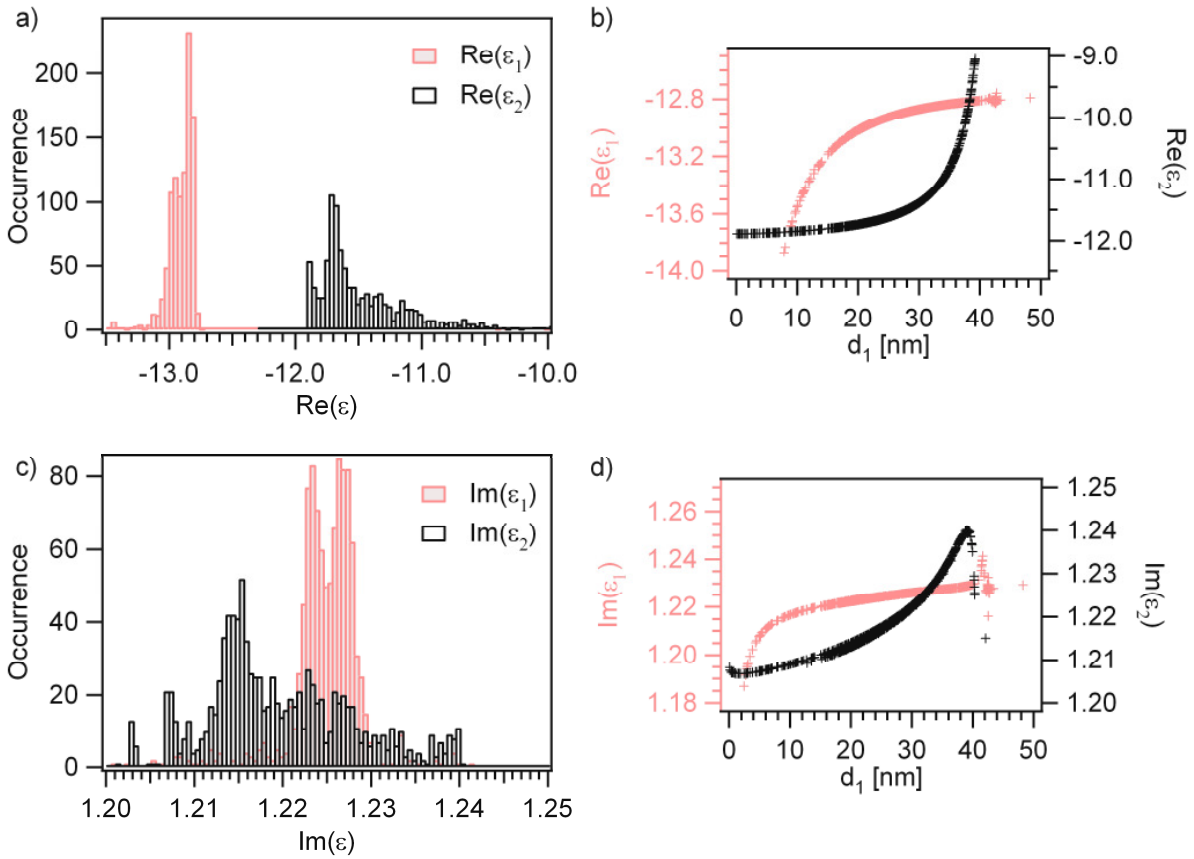

Figure 3.6: a) Histogram of the values found for $Re(\varepsilon_1)$ and $Re(\varepsilon_2)$ in the fit. b) $Re(\varepsilon_1)$ and $Re(\varepsilon_2)$ as a function of the value found for d_1. c) and d) same as a) and b) for $Im(\varepsilon_1)$ and $Im(\varepsilon_2)$.

Figure 3.6a) shows the values found for Re(ε). In all cases, a gold$_1$ layer with a more negative real part of the dielectric function and a gold$_2$ with a less negative real part are found, reflecting the higher quality of this surface. These values are plotted against d_1 in Figure 3.6b). For a fixed d_1 unique values of Re(ε_1) and Re(ε_2) exist. As the thickness of d_1 decreases, progressively larger negative values for Re(ε_1) are found, corresponding to a better conductivity. This is reasonable since a thin film with high conductivity is equivalent to a thicker film with low conductivity for a surface plasmon on the smooth side. A similar argument explains the trend of decreasing conductivity of the gold$_2$ film with decreasing thickness. The same behavior is seen for the Im(ε) as shown in Figures 3.6c) and Figure 3.6d).

Thus, least-squares fitting does not provide a unique set of parameters describing the composite film but once the thickness of one layer is chosen, all other quantities are determined in a unique way.

Figure 3.7 shows measured reflectivities and the fit found using arbitrary chosen starting values: d_1 =30 nm, d_2 =10 nm, ε_1 = -12+i 1.2, ε_2 = -12+i 1.2, c_1 = 1 and c_2 = 1. The high degree of correlation between d_1 and d_2 is reflected in the large uncertainty found by the fit.

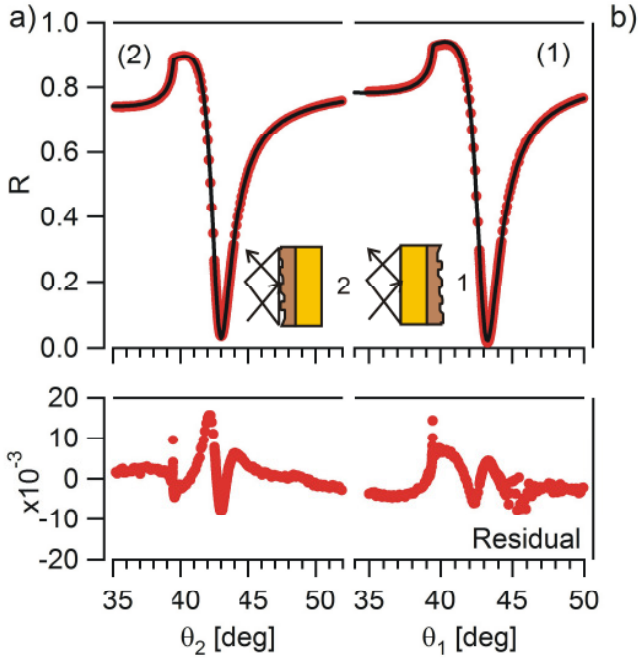

	c_1= 0.9894 ±0.0003	c_2=0.9452 ± 0.0003
layer	d [nm]	ε
glass	∞	2.2935
gold$_1$	34±4	(-12.8 ± 0.1) + i (1.227 ± 0.002)
gold$_2$	9±4	(-11.0 ± 0.6) + i (1.229 ± 0.006)
air	∞	1.00

Figure 3.7: a) Simultaneous fit of $R(\theta)$ for the evaporated gold sample (1) and the TSG sample (2). The fit results are indicated by the solid curves. The residual is shown in the bottom plot. b) Fit parameters.

3.2.4 What can be learned about the gold

Next, it is demonstrated that the two-layer model reproduces the experimental findings. Figure 3.8 shows the multilayered model used for the data generation (left) and for the fit (right). The incident wavelength used was 633 nm. The table in Figure 3.8b) summarizes the parameters used. The start fit parameters were $d_{\text{gold}} = 40$ nm for the gold thickness and $\varepsilon_{\text{gold}} = -12+i\,1.20$ for the gold dielectric function. The best fit results were achieved by a gold thickness of 44.17 nm and $\varepsilon_{\text{gold}} = -11.89 + i\,1.202$, thus very good agreement is obtained with the experiment (see Figure 3.3b). The fit itself is remarkably good as can be seen from the plot of the residual. Thus, also in the modeled situation it has to be concluded that surface plasmon spectroscopy without extra information is unable to resolve even substantial inhomogeneities in the metal films optical response. Even significant less deviations can be seen. This may lead to the speculation that the real films are significantly more inhomogeneous as estimated from our two-layer model. At the same time, it is concluded that the two-layer model is the best description of a realistic film that can be obtained based on the experimental data that available.

3.2.5 Implications for optical investigations of thin dielectric adlayers

Surface plasmon spectroscopy is used mostly to determine the thickness of a thin dielectric film at the interface between gold and the low-refractive index medium. This film is often referred to as the adlayer. A natural question that arises at this point is the possible error in the analysis of this film due to the highly simplified description of the metal. In order to investigate this, synthetic datasets were generated, emulating standard surface plasmon spectroscopy on an inhomogeneous gold film. The reflectivity of a double gold layer (Figure 3.8) and of a double gold layer coated by a dielectric film ($\varepsilon_{\text{film}} = 2.25$, $d_{film} = 1$ nm) were calculated. These two datasets were then analyzed to determine d_{film} with the common assumption of a single homogeneous gold film. In this way the errors made in the determination of the adlayer by modeling the gold as a single homogeneous layer can be estimated. The reflectivity curves were generated again using the glass/gold$_1$/gold$_2$/film/air system. The complex gold dielectric function and gold thickness obtained in the first step were set as fixed. The fitting parameters were the film thickness and scaling factor c. Figure 3.9 shows the parameters used for the modeling and obtained from the fit.

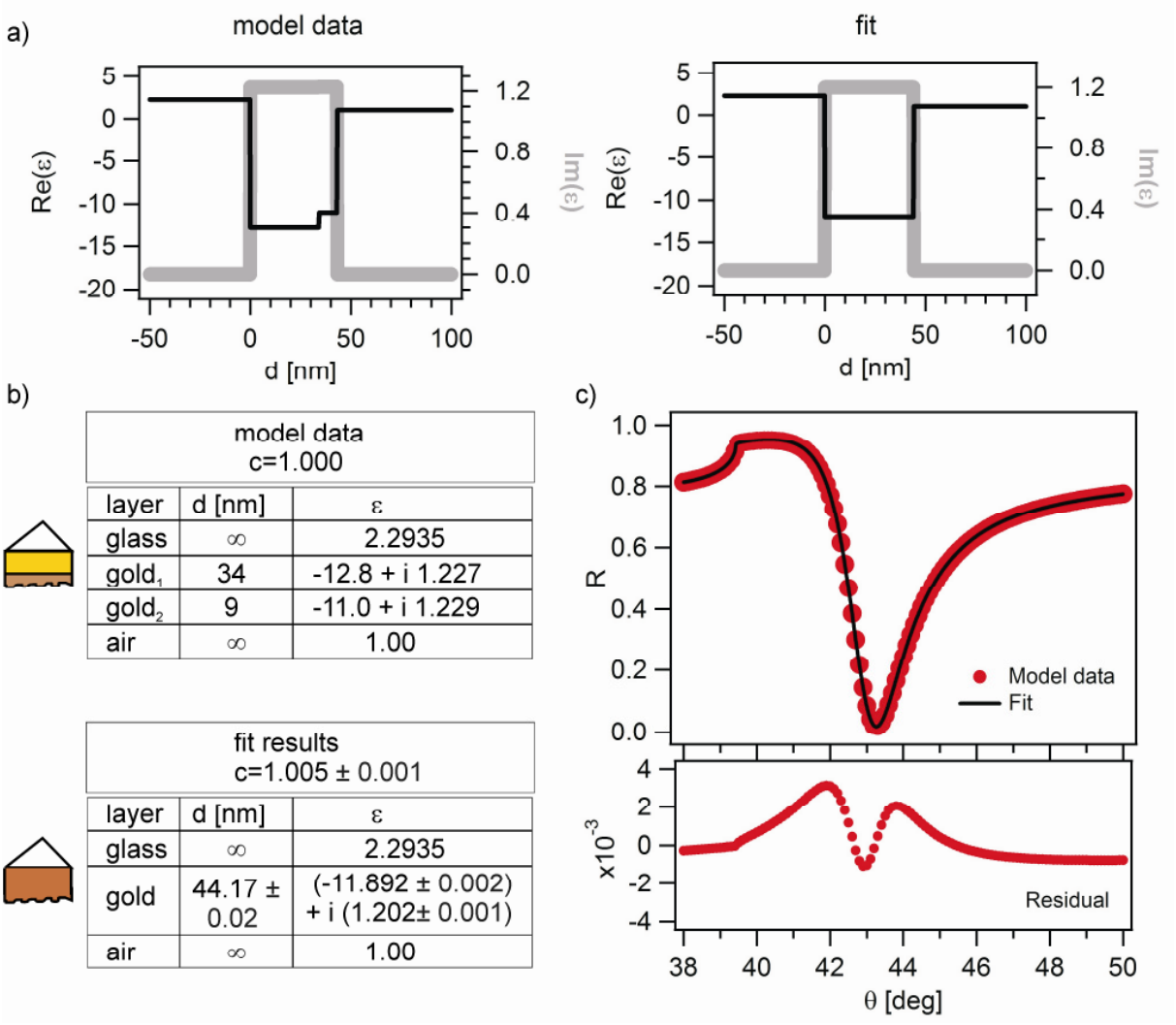

Figure 3.8: a) Dielectric function for the multilayered model used for the data generation and results obtained from the fit. b) Parameters used for the data generation and fit results. c) Fit results and fit residual.

The fit finds a 1.002 nm film, a value that is remarkably well reproducing the initially modeled film given the variations in ε_{gold} which are of the order of 10%. Thus, the highly oversimplified description of the metal film as one homogenous layer does not seem to compromise the precision of surface plasmon spectroscopy for the investigation of thin dielectric films.

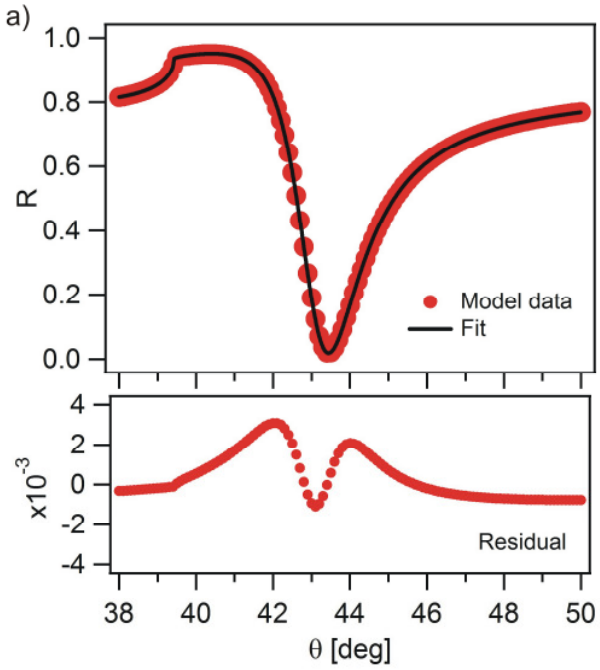

b)

model data c=1.000		
layer	d [nm]	ε
glass	∞	2.2935
$gold_1$	34	-12.8 + i 1.227
$gold_2$	9	-11.0 + i 1.229
film	1	2.25
air	∞	1.00

fit results c=1.005 ± 0.001		
layer	d [nm]	ε
glass	∞	2.2935
gold	44.17	-11.89 + i 1.202
film	1.002 ± 0.002	2.25
air	∞	1.00

Figure 3.9: a) Fit results and fit residual. b) Parameters used for the data generation and fit results.

3.3 Conclusions

Two gold films were prepared with a smooth and a rough side which were as similar as possible. Both gold films were used for surface plasmon spectroscopy in Kretschmann-configuration with surface plasmon excitation on the rough and smooth side respectively.

Their reflectivity is well modeled by a single gold film for each individual measurement. The simultaneous description of both datasets is not possible assuming a homogeneous gold film. A two-layer model though, leads to a very good description of the experimental data in the sense of a small mean squares difference. This leads to a more accurate description of the optical response of the gold film itself, revealing significant differences between the two sides. It is shown however, that only negligible errors occur in the thickness determination of a thin dielectric adlayer if the inhomogeneous gold layer is assumed to be homogeneous.

From this it can be concluded that on the one hand surface plasmon spectroscopy is unable to resolve even substantial inhomogeneities in a metal film. On the other hand, it is not necessary to know the depth dependence of the dielectric function in the gold if the experimental goal is the optical investigation of thin dielectric adlayers. A good fit of the

reference curve is sufficient to obtain the thickness of the added dielectric film with a high accuracy.

3.4 Acknowledgements

[Removed]

4 Localized plasmons seen by propagating surface plasmons: Unique determination of their dielectric response

4.1 Introduction

In chapter 3 the limitations in the characterization of thin metallic layers with thin non-absorbing dielectric coatings by surface plasmon spectroscopy were discussed. If the film under investigation is absorbing it must be described by a complex-valued dielectric response. In this case, both the resonance position and width are changed. The absorption leads mainly to a broadening of the minimum. In particular, when the film under investigation has an absorption maximum peaking at a defined wavelength, in addition to the broadening, the minimum position as a function of frequency displays a characteristic "s" –shape reflecting the dispersion of the polarisability while going through resonance (Pockrand, Brillante et al. 1982). Based on this approach, mostly the complex dielectric response of organic dye molecules (Bellessa, Bonnand et al. 2004; Dintinger, Klein et al. 2005; Wiederrecht, Hall et al. 2007) on a metal surface have been investigated by surface plasmon spectroscopy (see section 2.2.2.4).

In this chapter, surface plasmon resonance spectroscopy will be applied to investigate sphere-on-plane resonances. Optical extinction spectroscopy is the standard way to study the optical answer of the sphere-on-plane systems (Okamoto and Yamaguchi 2003; Tsuboi, Abe et al. 2006). The resonances can be clearly identified and the influence of the shape on the absorption maximum can be investigated in detail. Nevertheless there are potential advantages of using surface plasmon spectroscopy instead. Firstly, one should note the high sensitivity of this method, in particular taking into account the fact that in extinction experiments transmission through a highly absorbing gold film is measured as it will be detailed in section 4.3.7. Secondly, both the real and the imaginary part of the dielectric response are accessible in this scheme. Thirdly, no light has to propagate through the low refractive index medium, therefore stable experiments in liquids are possible even when the liquid's optical response changes as is often the case in biological and chemical applications. First experimental efforts towards using propagating surface plasmons for the study of sphere-on-plane resonances were reported by Kume et al. (Kume, Nakagawa et al. 1995; Kume, Hayashi et al. 1996; Kume,

Hayashi et al. 1997). They investigated silver particles embedded in a SiO_2 matrix on an aluminum substrate and could follow the change in plasmon minimum position and width due to sphere-on-plane resonators. These experiments were interpreted as evidence for a sphere-on-plane resonance in analogy to the earlier investigations on dye molecules (Pockrand, Brillante et al. 1982).

The limited use of surface plasmon spectroscopy for the study of sphere-on-plane resonators today is probably due to difficulties in the quantitative interpretation of the experimental response. In this chapter a strategy will be pointed out to overcome this problem and take advantage of the superior sensitivity and information content of surface plasmon spectroscopy. This approach was motivated by studies on sphere on plane resonators and will be illustrated by experimental data on this type of system. Though, these concepts apply to surface plasmon spectroscopy on absorbing systems in general. First, the problem of fitting the optical response of absorbing films will be addressed. The dependency of the fit result on start parameters is discussed and explained, allowing for a proper choice of start parameters. Second, the problem that in surface plasmon spectroscopy the thickness of an effective layer and its dielectric response cannot be determined simultaneously in a unique way will be addressed. It is proposed to deduce a polarisability per unit area and point out the prerequisites that must be fulfilled so that this quantity can be extracted from the experiment.

4.2 Experimental

A schematic representation of the sample architecture is shown in Figurea): Gold colloids are attached to a gold surface using a thiorane-functionalised hyperbranched dendrimer (**TdG_2**) as spacer. These molecules possess 16 functional groups which can bind covalently to gold and are therefore well-suited to form a well-defined molecular spacer layer between a plane gold surface and colloidal gold particles.

In order to determine changes in the optical response due to colloid deposition, different sample architectures are compared which are depicted schematically in Figure 4.1b) and were prepared as follows.

First, a thin (~ 2 nm) chromium layer was deposited onto a BK7 glass substrate by thermal evaporation (Edwards FL 400). The chromium layer serves as adhesion promoter.

Subsequently it was covered by a gold layer (approximately 50 nm thickness). One of these samples was kept as "Au" reference. The synthesis of **TdG_2** has been described previously (Morgenroth, Kübel et al. 1997; Morgenroth, Reuther et al. 1997; Wiesler, Berresheim et al. 2001; Vossmeyer, Guse et al. 2002). The disulfide groups at the structure's surface attach to gold surfaces and serve as binding sites to interlink the particle with the gold substrate (Nuzzo and Allara 1983). The slides were submerged for 10 min in a 2 µM solution of **TdG_2** in tetrahydrofuran, rinsed in tetrahydrofuran and dried with nitrogen. One of these samples is kept as "Au+spacer". Gold nanoparticle sols (60 nm nominal diameter) were prepared using the citrate reduction method (Turkevich, Stevenson et al. 1951; Frens 1973) (see section 2.4.2). In a 250 ml two-neck round-bottom flask, 100 ml of a 0.25 mM solution of $HAuCl_4 \cdot 3H_2O$ was heated to reflux, and 2 ml of a 0.015 M solution of trisodium citrate in water was injected quickly. After approximately 5 minutes the color changes from pale yellow into a dark red, indicating the formation of spherical particles. The colloidal suspension prepared this way had a mean particle diameter of 60 nm as determined by scanning electron microscopy (Figure 4.1d). The sample was submerged in the gold nanoparticle suspension. A potential was applied between the gold surface and the suspension to promote the attachment of the negatively charged gold nanoparticles. By varying the potential different nanoparticle concentrations at the surface could be achieved. The sample was rinsed with water and dried with an air gun. Two samples with different particle concentrations are discussed in this work (see Figure 4.1b), SOP7 and SOP22 with approximately 7 and 22 particles per μm^2, respectively.

The specular reflectivity $R(\theta)$ of the samples was measured in a home-made surface plasmon spectrometer in Kretschmann configuration (Turbadar 1959; Kretschmann 1971) shown schematically in Figure 4.1c). A halogen lamp and a monochromator (Chromex 250SM scanning monochromator) serve as a tunable light source. The beam divergence is controlled by the use of two aperture holes. At the sample position the beam has a divergence of 0.24° and a diameter of 6 mm. The incident light is transverse-magnetically polarized as required for surface plasmon excitation. The reflected light is detected with a photomultiplier (Hamamatsu H6240-01) in photon counting mode. For each wavelength an angular scan is taken. The sample reflectivity $R(\theta)$ is determined by normalizing the reflected light intensity with the incident light intensity which is measured without sample.

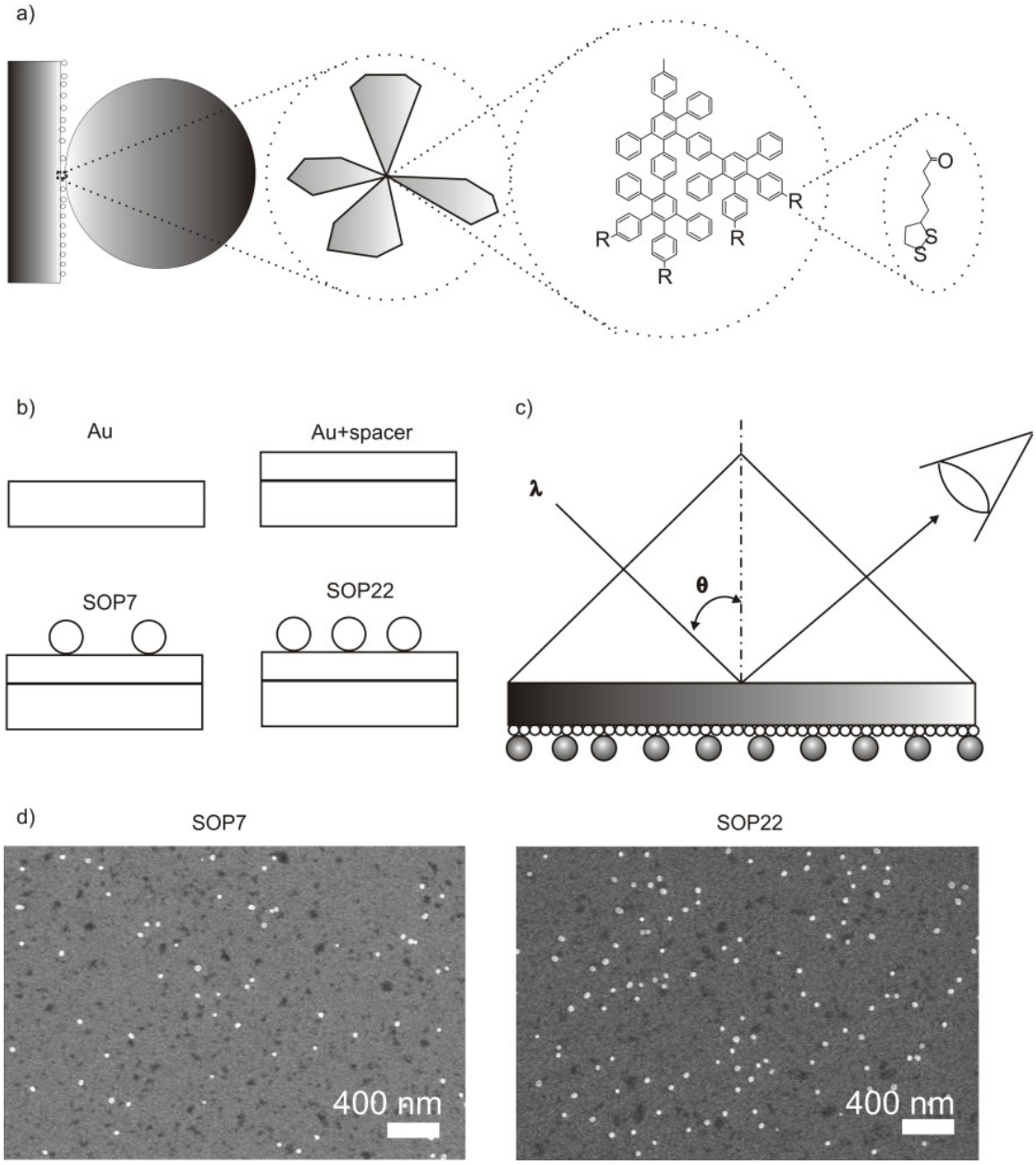

Figure 4.1: a) Sketch of the sample architecture b) Sketch of the 4 different sample architectures used for the experiment: "Au", "Au+spacer", SOP7 and SOP22. c) Schematic representation of the experimental setup. d) Scanning electron micrographs of the samples SOP7 (left) and SOP22 (right).

Additionally the extinction spectrum of samples prepared in the same way was measured using a Perkins Elmers UV-VIS-NIR Lambda 9 Spectrometer. The light was incident at an angle of 60° relative to the samples surface normal and had transverse-magnetic polarisation, resulting in a component of the electric field perpendicular to the surface. The extinction spectrum of the reference sample 'Au+spacer' A_{ref} and of the sample with nanoparticles A_p was measured using the transmitted intensity through clean glass as reference intensity. The extinction of the sphere on plane system is calculated by $A_{SOP} = A_p - n\, A_{ref}$. A normalizing

factor *n* has to be included due to the gold thickness variations of about 0.3 nm from sample to sample. The thickness variations produce greater changes in the extinction spectrum than the effect due to the nanoparticles and have to be corrected for. The correction factor *n* is calculated by assuming that both extinction spectra A_{ref} and A_p should coincide at λ=840 nm where no effect due to the nanoparticles is expected.

4.3 Experimental results and discussion

4.3.1 Qualitative description

Figure 4.2a-d) show the measured reflectivity $R(\theta)$ as a function of the excitation angle θ and wavelength λ in a gray level representation for the four samples under investigation. The minimum corresponding to surface plasmon excitation is clearly seen, its wavelength dependence of position and width is in agreement with the known dispersion relation (Raether 1988). A better comparison between different data sets is possible by plotting the reflected intensities for one fixed wavelength. Such a plot is shown in Figure 4.2e) for $\lambda = 600$ nm.

It is seen that upon deposition of the spacer a change in the minimum position and width of the reflectivity arises. Upon deposition of the colloids a small change in the reflectivity is observed for the sample SOP7 with low concentration of nanoparticles. For the higher concentration (SOP22) a more pronounced change, both in the minimum position and width occurs.

The effect of the colloid deposition for every measured wavelength is analyzed qualitatively by extracting changes in the minimum position and width from the $R(\theta)$ for all wavelengths. For this, the reflectivity near the minimum position is fitted with a parabola

$$R(\theta) = R_0 + (1/w)^2(\theta - \theta_{\min})^2 \qquad (4.1)$$

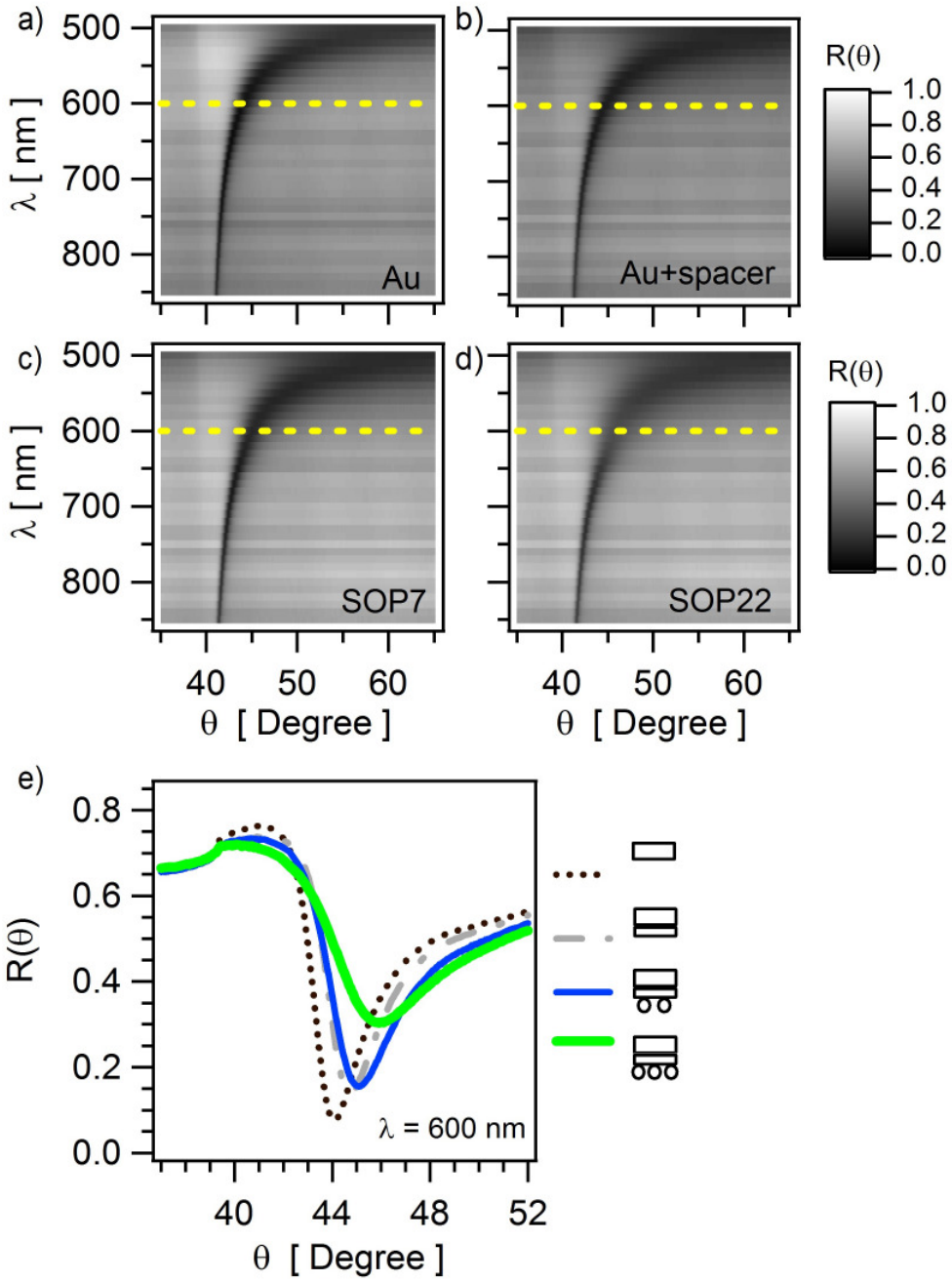

Figure 4.2: a-d) Reflectivity as a function of the external angle of incidence θ and wavelength λ. e) Reflectivity at λ = 600 nm for the samples sketched in the inset.

with R_0 being the reflectivity at the minimum position θ_{min}. w is the width of the parabola.

Figure 4.3a) shows θ_{min} as a function of the wavelength. The "Au+spacer" – sample exhibits a shift relative to the "Au" – sample which does not vary much with wavelength, indicative for the deposition of a dielectric layer. Upon colloid deposition, a further shift is seen which is most pronounced at around $\lambda = 620$ nm. A higher amount of colloids leads to a

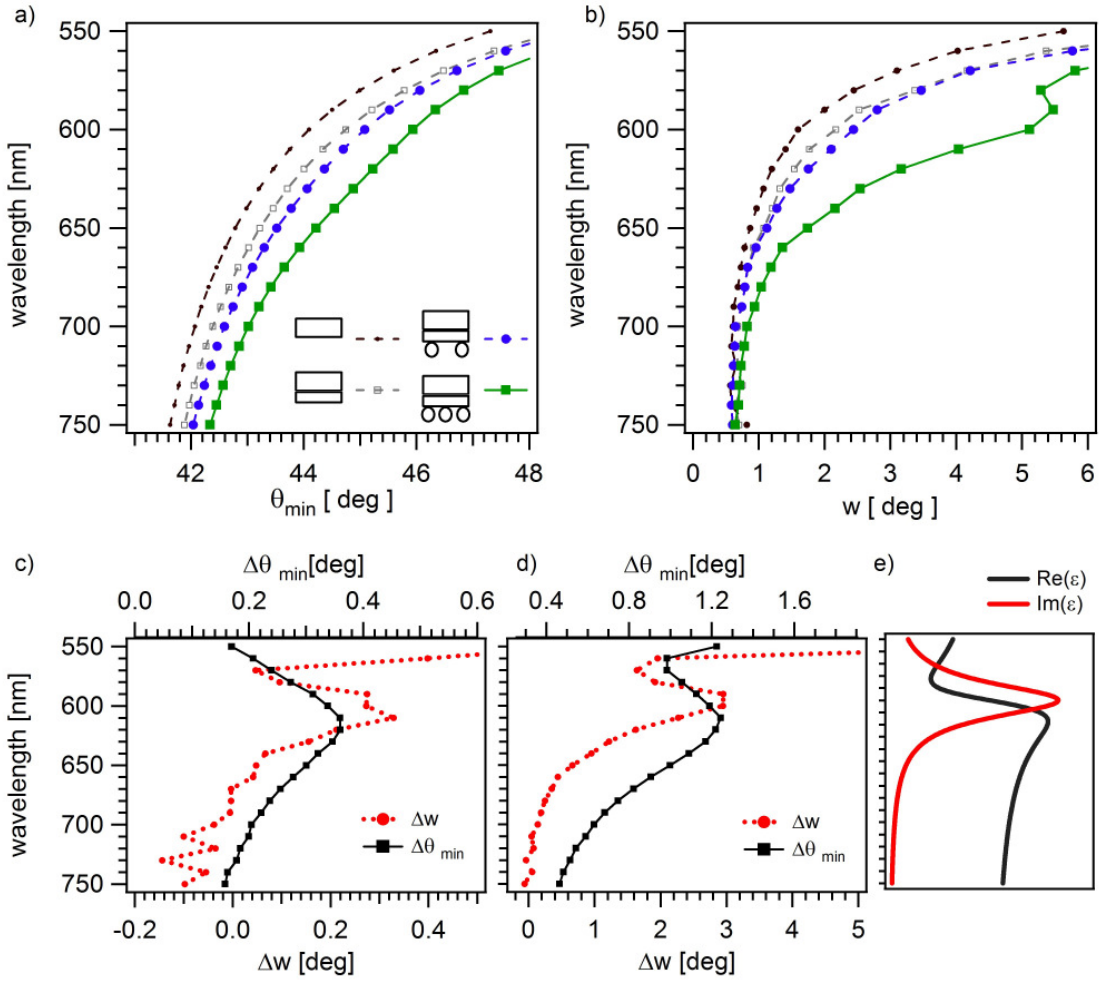

Figure 4.3: Position of the minimum (a) and width (b) of *R(θ)*c) Difference in minimum position and width between samples "Au+spacer" and SOP7d) Same as c) for the difference between 'Au+spacer' and SOP22 e) Wavelength dependency of the real and imaginary part of the dielectric function ε for a Lorentz type resonance.

larger shift. A comparably small displacement is seen for short and long wavelengths. Simultaneously, an increase in width around $\lambda = 600$ nm upon particle deposition is seen (Figure 4.3b).

The effect can be better seen in Figure 4.3c,d) where the change in minimum position and width w upon colloid deposition are plotted. The wavelength dependency of $\Delta\theta$ and Δw resemble the real and imaginary part of the dielectric function of a Lorentz oscillator (Bohren and Huffmann 1983) which is plotted in (Figure 4.3e) for comparison. Based on this type of analysis, the dispersion of the dielectric function ε has been assigned qualitatively to the dispersion of the polarisability of the sphere-on-plane resonators (Kume, Nakagawa et al.

1995) in analogy to the investigations of organic dye molecules on silver (Pockrand, Brillante et al. 1982).

4.3.2 Quantitative fitting based on a layer model

Surface plasmon spectroscopy is most commonly used to investigate thin films which are assumed to be homogenous. In this case, a mathematically manageable evaluation is possible which is adapted to the ensemble of sphere-on-plane resonators presented here. Obviously, the representation of scattered polarisable units on a surface as a homogenous layer represents a gross simplification whose validity remains to be checked. Some evidence that the polarizability per unit area of the sphere-on-plane resonators can be extracted will be given during the further discussion.

For the following it will be discussed how the dielectric function $\varepsilon_f(\lambda)$ and thickness d_f of an effective film can be deduced from the experimental data. This analysis is based on fitting the reflectivity curves to the ones that are modeled by a transfer-matrix algorithm (Yeh 1998).

The multilayer system is completely determined for the case where the dielectric function ε and thickness d are known for all layers (glass, chromium (Cr), gold (Au), spacer (sp), effective film formed by the sphere-on-plane resonators (f), air (a)). In brackets, abbreviations are given to be used as subscript for the specification of the corresponding layer.

First, it should be noted that the spacer, being a transparent dielectric, should only introduce a shift of the plasmon angle but not in depth and width. This is not the case (compare Figure 4.2e), probably due to rearrangements on the gold surface induced by the spacer molecules. The spacer thickness is approximately determined d_{sp}=3.0 nm from the minimum shift, assuming a refractive index ε_{sp} = 2.25. These parameters were kept fixed in the following analysis. It is important to note that the precise values for the spacer parameters do not have a measurable influence on the following discussion and that the parameters describing this true film are independent from the effective film to be obtained below.

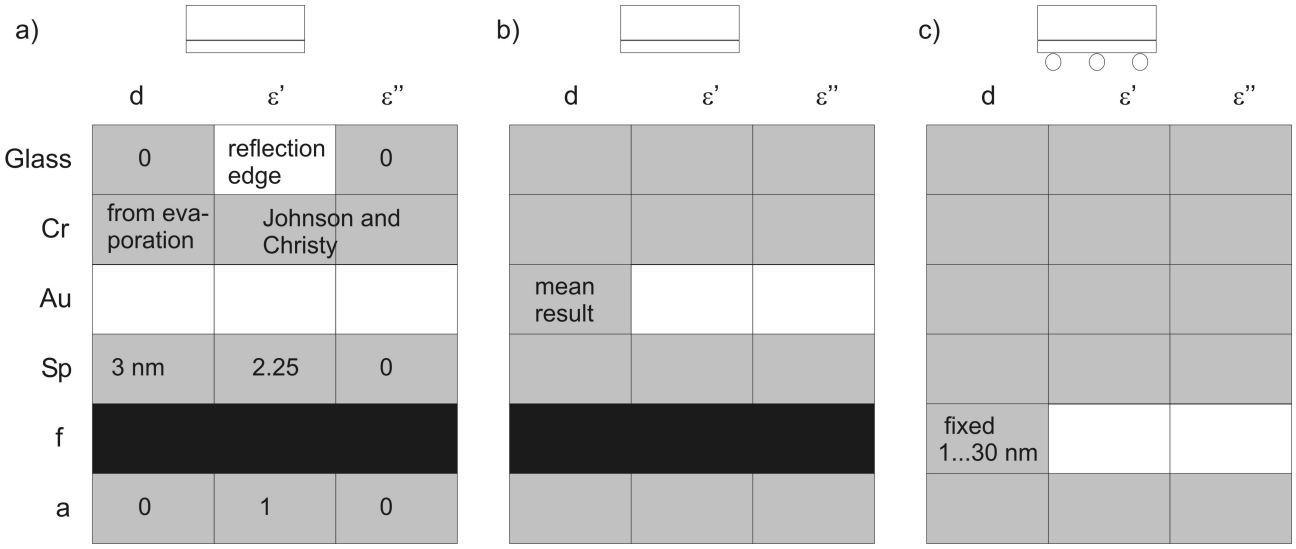

Figure 4.4: Schematic representation of the three fitting steps used to determine the complex $\varepsilon_f(\lambda)$. Each box represents a parameter of the multilayer system. Gray boxes represent parameters set as fixed during the fit. White boxes represent parameters determined by the fit. Black boxes represent parameters not relevant for the specific sample.

The strategy to determine the layer parameters is straightforward and requires three subsequent fitting steps shown schematically in Figure 4.4.

First, a fit of $R(\theta)$ of the reference sample 'Au+spacer' (glass/chromium/gold/spacer/air) is used to determine the (complex) $\varepsilon_{Au}(\lambda)$, d_{Au} , representing an averaged description of the gold layer after deposition of the spacer as well as the (real) $\varepsilon_{glass}(\lambda)$. The chromium dielectric response $\varepsilon_{Cr}(\lambda)$ is taken from literature (Johnson and Christy 1974) and its thickness d_{Cr} is assumed to equal the nominal value given by the evaporation machine. $\varepsilon_{glass}(\lambda)$ is determined by adjusting the reflection edge using $\varepsilon_a(\lambda)$=1. The thickness of the spacer layer d_{sp} is set as 3nm and is set as fixed. The spacer dielectric function is assumed to be $\varepsilon_{sp} = 2.25$. A global scaling factor c with $R(\theta)=c\, R_{calc}(\theta)$ is left as a free parameter to correct for small intensity drifts, were $R_{calc}(\theta)$ is the calculated reflectivity using the transfer matrix algortithm.

It turns out that slight variations in the fitted d_{Au} occur for different wavelengths. The mean value from all fits is calculated and set fixed, a second fit is then performed to finally obtain ε_{Au} for each wavelength. Third, the optical response of the effective film describing the sphere-on-plane resonators is determined from a fit of the samples SOP7 and SOP22. The thickness d_f and the dielectric function ε_f cannot be determined independently. Therefore, the

fit is done for several fixed d_f in the range between 1 and 30 nm.

4.3.3 Occurrence of multiple solutions

It turns out that the last fitting step may yield two different values for ε_f, depending on the choice of ε_f used as start parameter. This problem is illustrated in Figure 4.5 by plotting:

$$s^2 = \frac{\sum_{i=1}^{n} e^2}{n} \tag{4.2}$$

in the complex plane spanned by the initial values (Re(ε_f), Im(ε_f)) for one example. Here, $e = R(\theta_i) - R(\theta_i)_{fit}$ where $R(\theta_i)$ is the measured reflectivity value for a given angle θ_i, $R(\theta_i)_{fit} = cR_{calc}(\theta_i)$ is the fitted value at this same angle and n is the total number of points measured. Apparently, two local minima in s^2 exist and, depending on the starting value the fitting routine retrieves one of them. One solution yields a value for ε_f similar to the gold dielectric function, the other one yields a solution similar to the air dielectric function, the latter giving a better agreement with the data indicated by the smaller s^2.

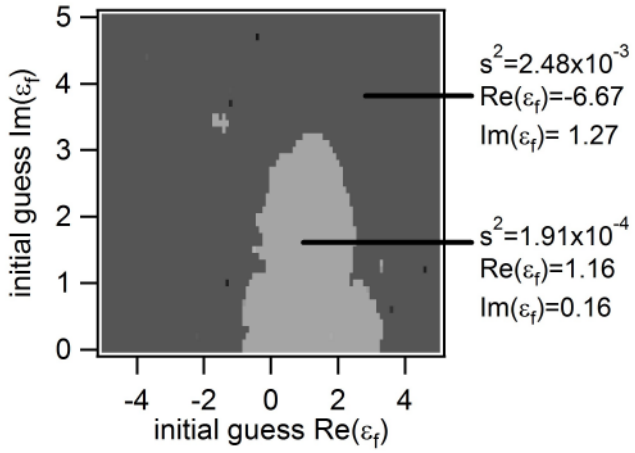

Figure 4.5: s^2 as a function of the initial guess for ε_f. (Sample SOP7, λ = 600 nm, d_f = 5 nm).

A way to understand the existence of these two solutions is by considering the changes made by introducing a film at the metal-dielectric boundary to the surface plasmon in-plane wavevector k_{sp}. In the following, the real and imaginary part of k_{sp} will be identified with the

position and width of the reflectivity dip, respectively. One should note, though, that this is to be regarded as an approximation as is briefly explained in the following. In lossless planar structures well-defined guided modes may exist which are purely harmonic in time and in space and are uniquely defined. In these cases, the fields A as a function of time t and position x in propagation direction are written as $A=A_0\ exp(i(k_x\ x-\omega\ t))$ with real wavevector k_x and frequency ω. As soon as there is loss, one may either consider solutions which have a complex k_{sp} and therefore decay in space, or ones with a complex ω which decay in time.

A common definition of k_{sp} (Raether 1988) assumes a harmonic time-dependence, leading to a complex-valued k_{sp}: the field obtained is stationary and damped in the propagation direction. Experimentally, on the other hand, one enforces a field which indeed is harmonic in time and space.

While the description of the system in terms of k_{sp} has the apparent advantage that the experimental data from one $R(\theta)$ is compressed in one complex number, it lacks the full quantitative validity of the multilayer fitting approach. Assuming small changes in k_{sp}, an approximate analytical expression for the change in surface plasmon wavevector with linear dependency on layer thickness, $\Delta k_{linear\ d}$ (Kretschmann 1971; Kolb 1988; Plunkett, Wang et al. 2003) for an infinitely thick gold layer is known:

$$\Delta k_{linear\ d} \approx \frac{2\pi\omega}{\lambda c}\left(\frac{\varepsilon_{Au}\varepsilon_a}{\varepsilon_{Au}+\varepsilon_a}\right)^2 \cdot \frac{1}{\left(-\varepsilon_{Au}\varepsilon_a\right)^{1/2}\left(\varepsilon_a-\varepsilon_{Au}\right)} \cdot \frac{\left(\varepsilon_f-\varepsilon_a\right)\left(\varepsilon_f-\varepsilon_{Au}\right)}{\varepsilon_f} d_f \qquad (4.3)$$

Note that in this simplified treatment neither the spacer nor the supporting prism plays a role.

To illustrate the appearance of two solutions the dataset shown in Figure 4.6a) was chosen which represents an arbitrarily chosen typical experimental case. The experimentally measured wavevector $k_{R(\theta)}$ is determined using:

$$\begin{aligned} \mathrm{Re}(\Delta k_{R(\theta)}) &= \frac{2\pi}{\lambda}\sqrt{\varepsilon_{glass}} \cdot (\sin\theta_{\min} - \sin\theta_0) \\ \mathrm{Im}(\Delta k_{R(\theta)}) &= \frac{2\pi}{\lambda}\sqrt{\varepsilon_{glass}} \cdot (\sin w_{\min} - \sin w_0) \end{aligned} \qquad (4.4)$$

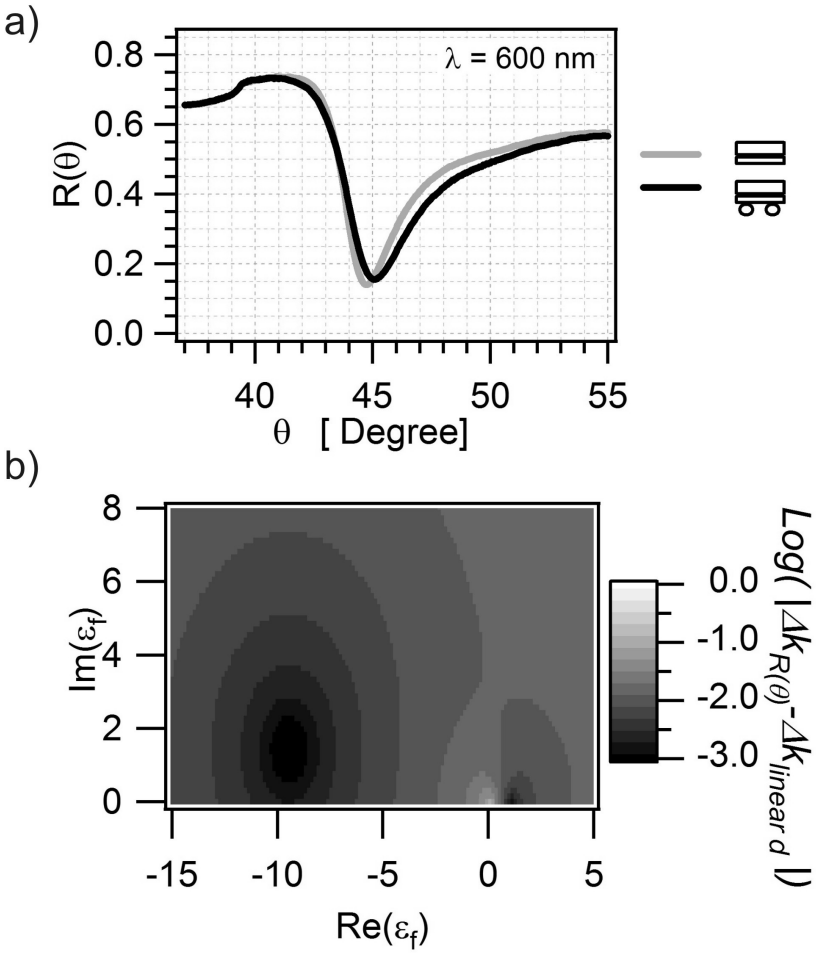

Figure 4.6: a) $R(\theta)$ for samples "Au+spacer" and "SOP7". b) $|\Delta k_{R(\theta)} - \Delta k_{linear\ d}|$, assuming $\lambda = 600$ nm, $\varepsilon_{Au} = -9.53783 + i\ 1.45877$, $\varepsilon_a = 1+i0$ and $d_f = 10$ nm in equation (4.3).

where the subscript $R(\theta)$ stands for reflectivity scan, meaning that the information is extracted from the minimum position and width of the resonance measured. θ_0 and w_0 are the minimum angle position and width for the 'Au+spacer' sample and θ_{min} and w_{min} are the minimum angle position and width for the SOP7 sample. Using equation 4.4, a $\Delta k_{R(\theta)} = 8.41044 \cdot 10^{-5}\ nm^{-1} + i\ 8.39383 \cdot 10^{-5}\ nm^{-1}$ is obtained. Figure 4.6b shows the difference $|\Delta k_{R(\theta)} - \Delta k_{linear\ d}|$ as a function of (Re(ε_f), Im(ε_f)) when $\Delta k_{linear\ d}$ is calculated with equation 4.3 using the appropriate parameters for this example. Two different local minima, one close to ε_a and one close to ε_{Au} are seen. They indicate that two completely different values of ε_f lead to the same $\Delta k_{R(\theta)}$ and, in turn, to similar changes of the reflectivity curves $R(\theta)$. It has to be concluded that an analysis of $\Delta k_{linear\ d}$ alone does not allow for a decision which minimum

corresponds to the physical reality. Though the fit to $R(\theta)$ yields two different values for s^2. The lower one corresponds to $\varepsilon_f = 1.16 + i0.16$ and was chosen for the further analysis. Thus, least squares fitting has to be done with some care and wrong local minima have to be avoided. Clearly, this problem applies to all surface plasmon spectroscopy experiments. Usually, it is a priori known that a lossless dielectric film is deposited therefore the solution near the gold values is not even considered. Here, we are dealing with an effective medium which consists mainly of air. Therefore, the minimum near the ambient ε_a applies for us as well. Technically, this is achieved by fixing the starting value to $\varepsilon_f = 1+i0$.

4.3.4 Ambiguities in the choice of layer thickness and optical response

Figure 4.7 illustrates another problem in surface plasmon spectroscopy that appears to be 'well known' among scientists but has not been discussed in depth to our knowledge: Often exactly identical $R(\theta)$ are obtained by the fit with different choices of d_f, thus only a set of possible combinations of pairs (d_f, ε_f) can be determined. Here, for different wavelengths ten theoretical curves assuming d_f between 1 and 10 nm are plotted. They overlap perfectly, thus a determination of the thickness of the effective layer requires an a priori guess of its dielectric function and vice versa.

Figure 4.8 and Figure 4.9 show the ε_f that is obtained for different choices of d_f for the two samples under investigation. Apparently, thin films with a ε_f that differs strongly from ε_a are equivalent to thick ones that differ only slightly from ε_a. One may again infer a Lorentz-type resonance, though there is a slight dependency of the position of the resonance on the choice of the d_f. For sample SOP7 with low particle concentration (Figure 4.8b and d) from $d_f = 3$ nm onwards the resonance position found becomes independent of d_f . For d_f =1 nm and d_f =2 nm the position of the resonance is shifting to the red. For sample SOP22 with high particle concentration a similar systematic shift is seen for $d_f < 7$ nm. Here a Re(ε_f) below its vacuum value 1 and even below 0 is seen, pointing to a strong effective resonance. The negative values of Im(ε_f) found for SOP7 points to another slight change in the supporting gold layer. Here, for the dilute system the absolute precision of the experiment is apparently reached. Though, the important feature, a peak around 600 nm is clearly seen. One may apply baseline corrections to avoid unphysical negative values of Im(ε_f). For $\lambda < 550$ nm the surface plasmon resonance is too broad and the fit results cannot be taken into account.

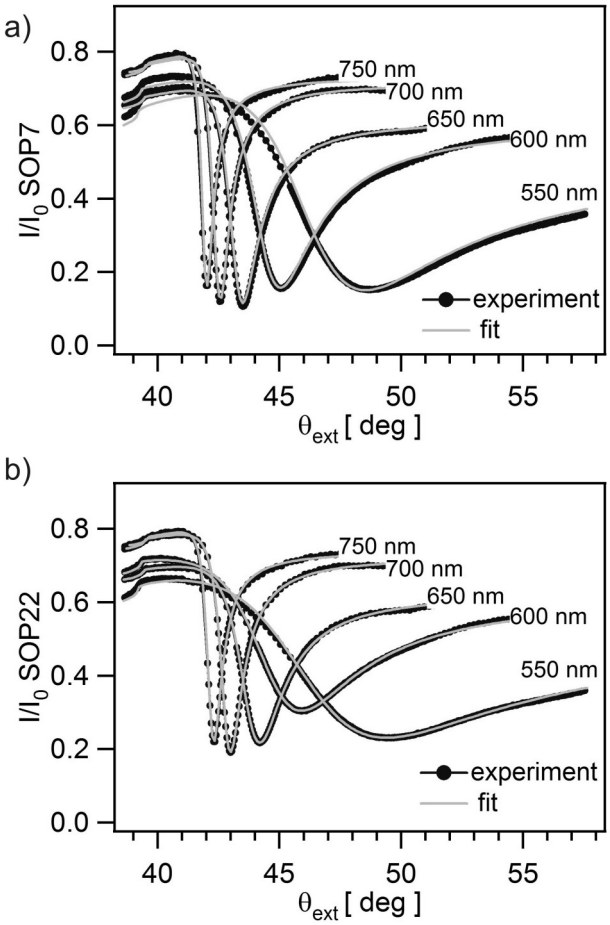

Figure 4.7: Fit results (gray lines) for d_f between 1 and 10 nm at selected wavelengths measured with a) low (SOP7) and b) high (SOP22) colloid concentration. Ten different gray curves for each fit are plotted.

4.3.5 Calculation of the polarizability per surface area

Apparently, due to this ambiguity in determining ε_f and d_f, it would be desirable to derive another quantity from the experiments which can be determined in a unique way. The following approach is proposed: If the effective layer consists of induced dipoles with a polarizability α occupying an area A, then, one may apply the Clausius-Mossotti equation (Schnatterly and Tarrio 1992) to calculate a polarizability per area

$$\frac{\alpha}{A} = 3\varepsilon_0 \frac{\varepsilon_f - 1}{\varepsilon_f + 2} d_f \qquad (4.5)$$

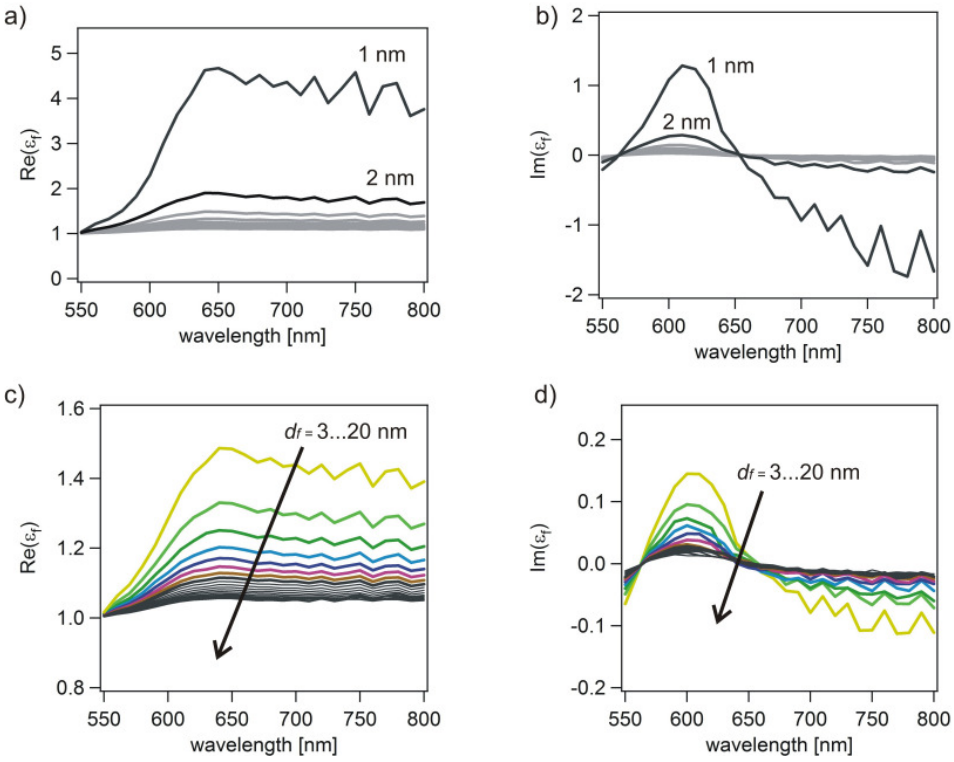

Figure 4.8: Fitted real and imaginary part of ε_f for SOP7 for d_f =1 nm to d_f =20 nm. The gray curves in a) and b) show the results for d_f = 3 nm to d_f = 20 nm which are displayed in a smaller scale again in c) and d).

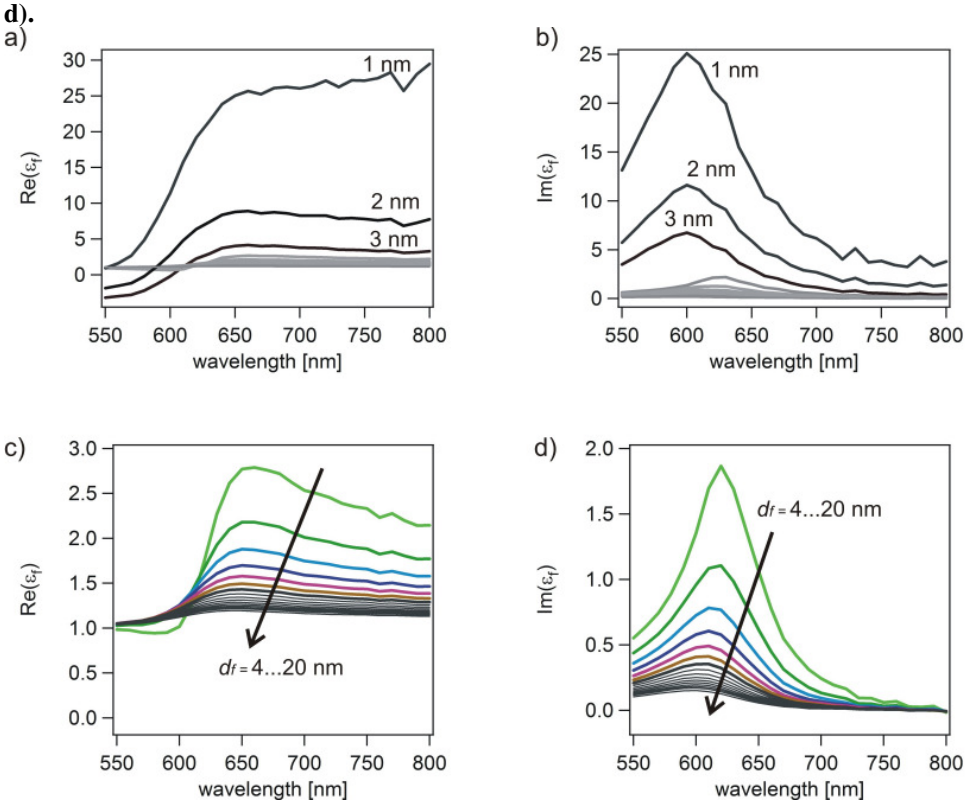

Figure 4.9: Fitted real and imaginary part of ε_f for SOP22 for d_f = 1 nm to d_f =20 nm. The gray curves in a) and b) show the results for for d_f = 4 nm to d_f = 30 nm which are displayed in a smaller scale again in c) and d).

ε_0 being the permittivity of free space. Figure 4.10 shows the resulting α/A obtained for the different values of d_f used. It is seen that this quantity becomes independent from the choice of d_f if d_f is in the range from 3 to 20 nm for SOP7 and in the range from 7 to 30 nm for SOP22. For smaller d_f deviations are observed which appear together with fitted values for Re(ε_f) and Im(ε_f) which differ from the vacuum value by more than approximately 0.5. One may tentatively state that deviation from the vacuum value in the sense of the modulus of the difference between two complex numbers must be small compared to the value itself. It should be noted that for d_f reaching the order of λ_{vac} the wavelength of light, a transition to another regime occurs: For very large d_f the surface plasmon resonance depends exclusively on ε_f and is independent from d_f. For the following discussion, we stay well outside this regime by focusing on $d_f << \lambda_{vac}$. Apparently, in some range of parameters, α/A is a unique, physically well-defined quantity that describes the optical response of the reflectivity curve to an adsorbed layer. Importantly, this quantity has an immediate physical meaning as is well described in textbooks of solid-state physics, for example in (Kittel 1996). It can be directly determined if the area density of polarisable units as well as their polarisability is known, irrespective of the thickness of the layer they form. For the example discussed here, α is identified with the polarisability of one sphere-on-plane resonator, multiplied by their area density which is readily obtained from the electron micrographs. Since for the sphere-on-plane resonators it is conceptually difficult to define an effective layer thickness at all, evaluation of the reflectivity in terms of arbitrary combinations of ε_f and d_f, as is the standard procedure in surface plasmon spectroscopy, does not lead to physically well-defined quantities. The alternative determination of α/A is much better suited to describe their effect on surface plasmon resonance curves.

4.3.6 Comparison to an approximate theory

Furthermore, it is now possible to directly compare the experimental result obtained from surface plasmon spectroscopy to a quantity that can be calculated in a straightforward fashion, the polarisability per resonator, α_{SOP}. An analytical expression for α_{SOP} can be calculated using equation (2.22) from (Wind, Vlieger et al. 1987):

$$\alpha_{SOP} = 4\pi\varepsilon_a R^3 A_{\perp 1} \tag{4.6}$$

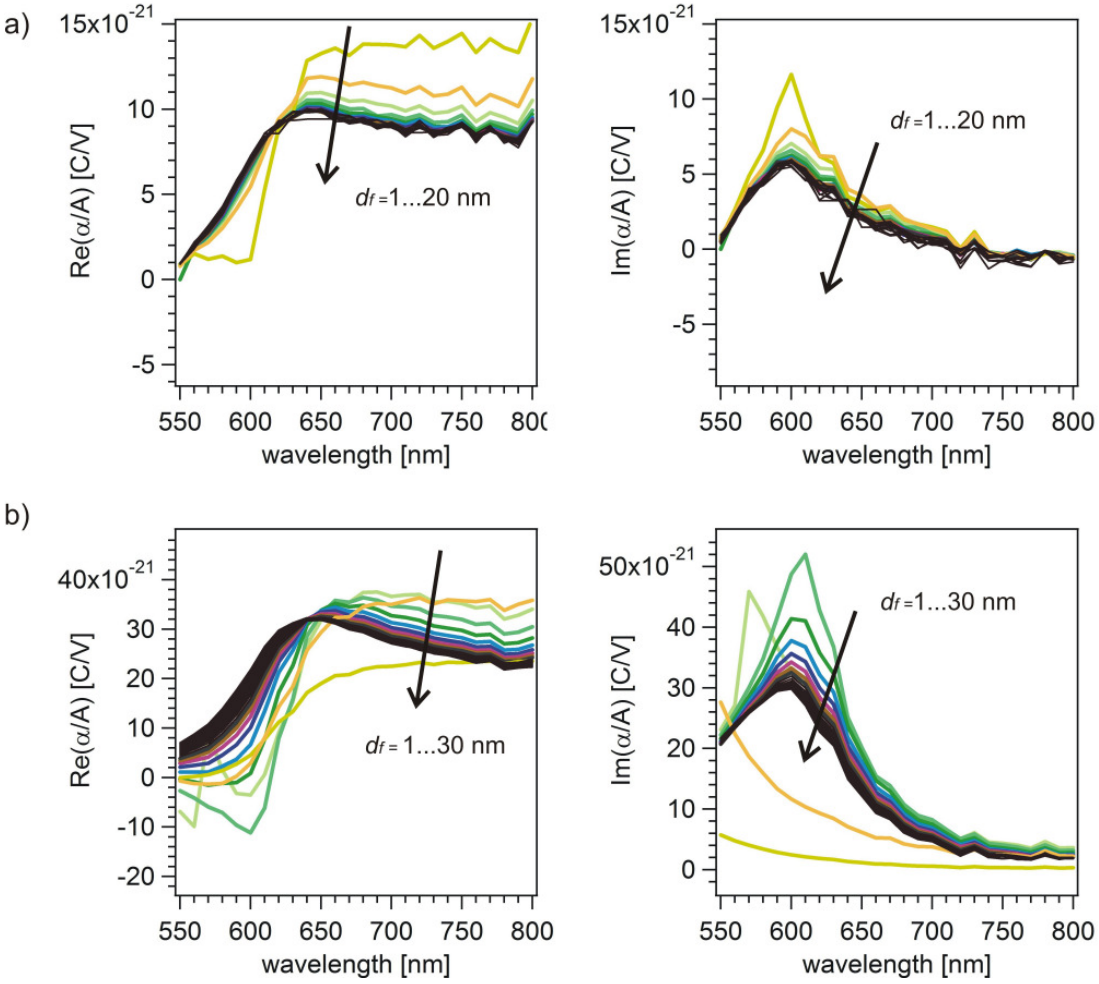

Figure 4.10: Polarizability per resonator area α/A for different d_f for a) low particle (SOP7) and b) high particle concentration (SOP22).

where $A_{\perp 1}$ is obtained by solving the following set of linear equations (eqn 3.6) from (Wind, Vlieger et al. 1987):

$$\sum_{j=1}^{\infty}\left\{\delta_{kj}+\left(\frac{k(\varepsilon_{Au}-\varepsilon_a)(\varepsilon_a-\varepsilon_{Au})}{(k\varepsilon_{Au}+(k+1)\varepsilon_a)(\varepsilon_a+\varepsilon_{Au})}\frac{(k+j)!}{k!\,j!\left(\frac{2(d_{gap}+R)}{R}\right)^{k+j+1}}\right)\right\}A_{\perp j}=\delta_{k1}\frac{(\varepsilon_{Au}-\varepsilon_a)}{(\varepsilon_{Au}+2\varepsilon_a)} \qquad (4.7)$$

d_{gap} indicates the distance between the sphere and the plane. The assumptions used to calculate this expression are that firstly the entire sphere-on-plane resonator is significantly smaller than the wavelength of light and secondly that the sphere is surrounded by a homogenous dielectric medium i.e. ε_{sp} and ε_a are identical. In particular due to the latter

assumption, these analytical expressions can only be regarded as first-order approximations for the experiments presented here. To compare the extracted values with the polarizability calculated analytically, the area per resonator $A = 0.14$ μm^2 for SOP7 and $A = 0.045$ μm^2 for SOP22 and the sphere radius $R = (30 \pm 4)$ nm were estimated from the scanning electron micrographs. The gold dielectric function used to describe the sphere and the plane was taken from the fit results of the reference sample "Au". It turns out that by choosing a dielectric constant ($\varepsilon = 1$) around the sphere and a value of $d_{gap} = 0.9$ nm for the distance between the sphere and the plane, the experimentally measured resonance position can be reproduced and an approximate description of the systems response is obtained. It should be noted that similarly, much smaller d_{gap} values had to be introduced to properly model experimentally observed extinction maxima due to resonances in α_{SOP} (Okamoto and Yamaguchi 2003; Tsuboi, Abe et al. 2006) There, a deeper discussion of the applicability of this approach is given. While a more realistic description of the system would be beneficial, the system with spacer can only be calculated numerically where significant problems with discretizations close to the gap occur. Here, we mainly want to demonstrate that without any adjustable parameter reasonable agreement between the polarisability density α/A in theory and experiment is achieved as shown in Figure 4.11. As another important error source it will be stressed again that the finite polarisability of the spacer was neglected leading to a significant uncertainty in the calculation. It should be noted that for both samples the experimental Re[α/A] is larger than the theoretical prediction by approximately the same factor. The maximum in Im[α/A] is broader in the experiment, probably due to distributions in size and shape of the particles and gap geometry. While the agreement within a factor of two shows in principle the applicability of the data evaluation routine presented here, a detailed analysis of sample-to-sample variations is currently on the way.

4.3.7 Comparison to UV-Vis spectroscopy

The standard way to measure the optical response of thin films in general and SOP-resonances in particular is UV-Vis transmission spectroscopy, thus representing the benchmark for our method. Firstly, the optical response of the nanoparticle film in terms of its imaginary part of the refractive index ($n = \sqrt{\varepsilon_f}$) is compared in Figure 4.12a). A layer

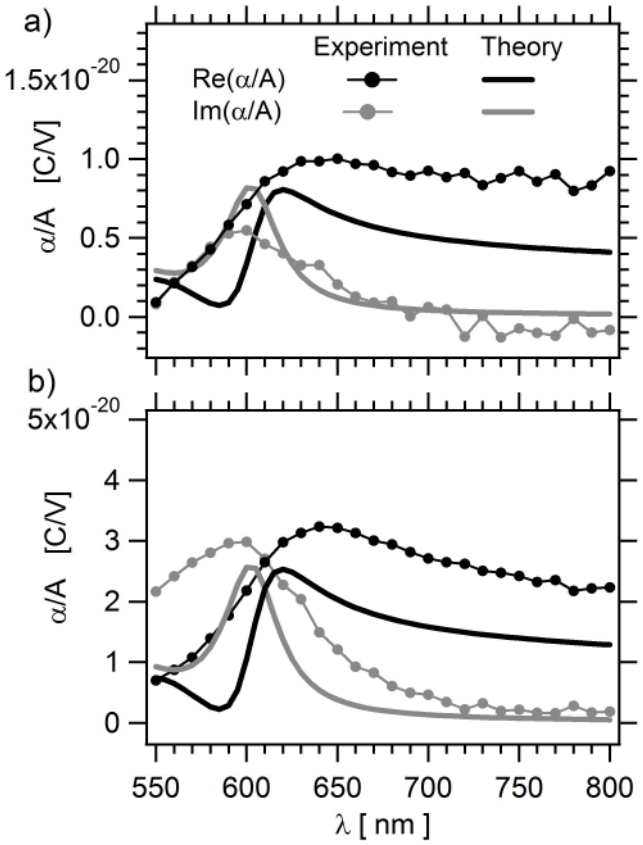

Figure 4.11: Comparison between the calculated and the measured α/A for a) SOP7 (d_f = 20 nm in Figure 4.10) and b) SOP22 (d_f = 30 nm in Figure 4.10).

thickness of 50 nm is assumed, a quantity that is readily calculated both from UV-Vis data and from surface plasmon spectroscopy.

The results show approximate agreement with no adjustable parameters, it should be noted, though, that an extra normalization step (see section 4.2) was necessary to extract these results from the UV-Vis data which may be responsible for the slight discrepancies.

A clear advantage of plasmon spectroscopy is illustrated in Figure 4.12b) where the change in light intensity due to the particle layer, normalized by the incident intensity is shown for the two experimental schemes for one representative wavelength. The reflectivities were normalized with the global scaling factor c extracted from the fit. This quantity, being closely connected to the signal to noise ratio one may obtain, is 40 times higher for the surface plasmon geometry, showing that this approach is the method to be chosen when one seeks to retrieve small signals. One should note that the comparison of the experimental noise appears by far less favorable, this effect being to the comparison of a homebuilt plasmon

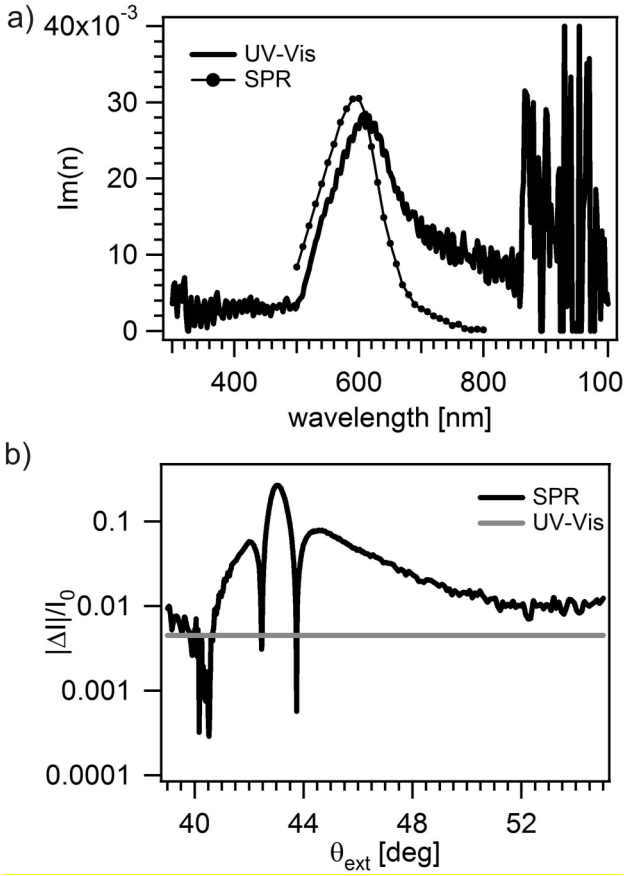

Figure 4.12: a) Imaginary part of the refractive index n calculated from the UV-Vis extinction measurements (solid line) and from the reflectivity measurements (circle-line). b) Change in intensity normalized to incident intensity as a function of the external angle of incidence calculated from reflectivity measurements (black line) at λ=600 nm. The horizontal gray line shows the corresponding normalized change in intensity in the extinction spectrum at 600 nm.

spectrometer with a state-of-the-art UV-Vis spectrometer which is corrected for several drift mechanisms. Similar drift corrections could be implemented in a plasmon setup as well.

4.4 Applicability of the analysis in terms of α/A

While the determination of α/A for our particular sample works, in the following the general applicability of this approach will be discussed. First (4.4.1) the approximations made when describing the resonators as a homogeneous layer are stressed. The following analysis will rely on this assumption and apply to thin films. The criteria that, if met, guarantee that α/A is a well-defined parameter to describe the response of the system are identified. Firstly (4.4.2) a

set of equivalent (ε_f, d_f) must exist. Then (4.4.3), the range of validity of an analytical expression for Δk is discussed. Based on this, a range in the (ε_f, d_f) plane where α/A is well-defined is identified.

4.4.1 Description as a homogenous layer

Clearly, one should bear in mind the approximations made when describing the resonators as a homogenous layer. The modeling of an ensemble of spheres with a diameter of 60 nm and an average distance of more than 100 nm as a homogenous layer represents the first gross simplification that was made. Though, the quality of the fit before and after the deposition of the spheres is comparable ($s^2 = 6.4\text{x}10^{-5}$ and $1.91\text{x}10^{-4}$ respectively). This implies that for the experimental arrangement under study the ensemble of spheres does behave similar to a homogenous layer. Secondly, the Clausius-Mossotti equation holds only in a three-dimensional dielectric. It is nevertheless a good approximation for a two dimensional arrangement of dipoles (Simovski, Popov et al. 2000). Thirdly, it is assumed that the resonators give rise to an isotropic medium disregarding the fact that the optical response of the system is highly dependent on the polarization. However the electric field magnitude in the direction perpendicular to the plane is much higher than in the direction parallel to the plane justifying the use of an isotropic approximation. Finally it is assumed that the optical response of the gold substrate remains unchanged after deposition of the gold nanoparticles. Being well aware of all these limitations that apply when sphere-on-plane resonators are described as a homogenous layer at all, for the following a thin homogeneous films will be considered. In the reminder of this chapter the prerequisites which have to be met so that a unique α/A can be determined for such a thin film by surface plasmon spectroscopy will be discussed.

4.4.2 Reduction of the information on one parameter

A first prerequisite that has to be met if the information from an $R(\theta)$-dataset is to be represented by a single parameter (α/A) is that an identical $R(\theta)$ response is obtained for different d_f if the appropriate ε_f is chosen. In order to identify the range of film parameters where this is the case, $R(\theta)$ was calculated for a range of $\varepsilon_{f,0}$ and $d_{f,0}$ (other layer parameters see Figure 4.13). For each point in the ($\varepsilon_{f,0}$,$d_{f,0}$) - plane, a fit was performed

assuming different, fixed values for $d_{f,1}$, while leaving $\varepsilon_{f,1}$ as free fitting parameter. The analysis was performed assuming either a real ε_f =Re(ε_f)+ i0 (Figure 4.13a) and b)) or an imaginary ε_f =1+i Im(ε_f) (Figure 4.13c) and d)). The s^2-value of this fit represents a measure in how far d_f is really arbitrary – if s^2 reaches the order of magnitude of a realistic fit to experimental data, ε_f and d_f can both be determined independently and α/A alone is not sufficient any more to describe the experimental observations. The results of this analysis are summarized in Figure 4.14. For a large range of ($\varepsilon_{f,0}$,$d_{f,0}$), a $s^2 < 1\text{x}10^{-4}$ is obtained, indicating that here, for typical data in our experiments, the fits would be indistinguishable. This represents at the same time the range of ($\varepsilon_{f,0}$,$d_{f,0}$) where the film response can be described by a single parameter, an obvious choice being the change in the complex surface plasmon wavevector Δk_{sp} which can be correlated to the change in minimum position and width of the resonance in the reflectivity $R(\theta)$. It should be noted that often one is rather seeking for an independent determination of ε_f and d_f. Although this is just the parameter range that has to be excluded for the analysis presented here, the consideration given above allows for a direct answer to this question. Here, we have to point out that this analysis only applies assuming a constant ε_a =1. In standard thin film analysis, independent determination of ε_f and d_f can be achieved by immersion in liquids with different dielectric constants (Debruijn, Altenburg et al. 1991). The prerequisite for this approach, though, is that the film remains unaffected by the liquid which is not the case for the effective layer formed by sphere-on-plane resonators.

4.4.3 Analytical expression for Δk: Range of validity

The further discussion is significantly simplified if the analytical expression for the change in surface plasmon wavevector, equation 4.3, holds. The range of (ε_f, d_f) where this is the case was determined by calculating for each point in the (ε_f, d_f) – plane both $\Delta k_{linear\ d}$ the change in wavevector according to equation 4.3 and $\Delta k_{R(\theta)}$, $R(\theta)$ stands like before for reflectivity scan and is obtained by calculating the reflectivity of a multilayer system and identifying the change in minimum position and width with the real and imaginary part of $\Delta k_{R(\theta)}$ according to equation 4.4.

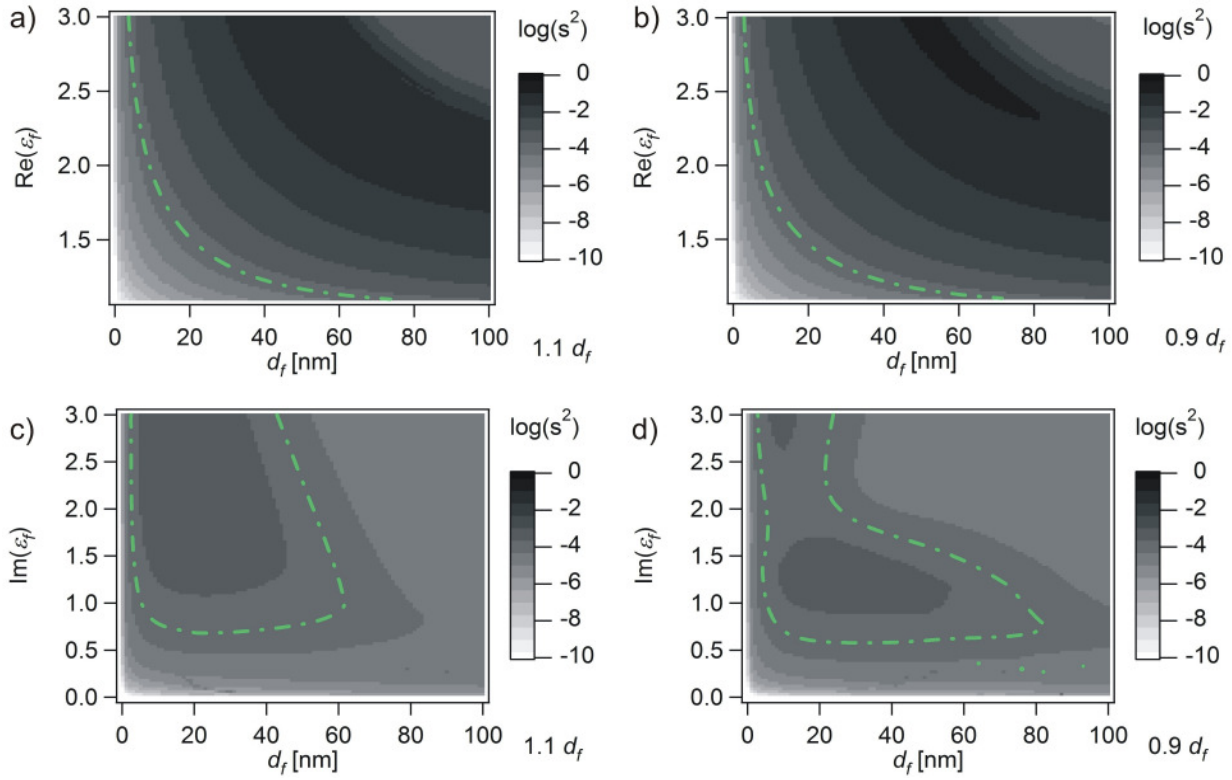

Figure 4.13: s^2 obtained by fitting a) $R(\theta, \mathrm{Re}(\varepsilon_f), 1.1\ d_f)$ and b) $R(\theta, \mathrm{Re}(\varepsilon_f), 0.9\ d_f)$ to match $R(\theta, \varepsilon_f, d_f)$, by letting ε_f vary. $\mathrm{Im}(\varepsilon_f)=0$ remains constant throughout the fit. c) $R(\theta, \mathrm{Im}(\varepsilon_f), 1.1\ d_f)$ and b) $R(\theta, \mathrm{Im}(\varepsilon_f), 0.9\ d_f)$ to match $R(\theta, \varepsilon_f, d_f)$, by letting ε_f vary. $\mathrm{Re}(\varepsilon_f)=1$ remains constant throughout the fit.The contour line delimitates the region where $s^2 < 1\mathrm{x}10^{-4}$. The other layer parameters used for the fit are: $d_{Au} = 50$ nm, $\varepsilon_{glass} = 2.29134$, $\varepsilon_{Au} = -1.5672+i11.27145$ and $\lambda = 630$ nm.

In Figure 4.14 $|\Delta k_{R(\theta)}-\Delta k_{linear\ d}|/\ \Delta k_{R(\theta)}$ the relative error that is made when approximating $\Delta k_{R(\theta)}$ by $\Delta k_{linear\ d}$, is shown. It is seen that the approximation fails already for relatively thin films with low refractive index but, allowing for a 10% error, there is still an appreciable parameter range where $\Delta k_{linear\ d}$ is well suited to describe the entire response of the system.

4.4.4 Analytical expression for Δk: Linear range

If the approximate expression for the change in plasmon wavevector $\Delta k_{linear\ d}$ can be applied, it can be shown analytically that for small deviations δ of the film dielectric function

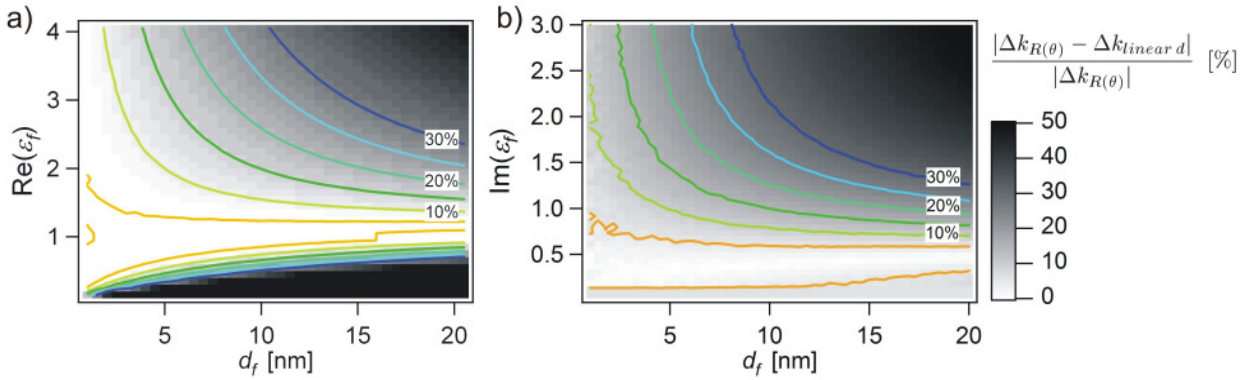

Figure 4.14: Relative difference between a) Re($\Delta k_{R(\theta)}$) determined from simulated reflectivity curves and Re($\Delta k_{linear\ d}$) calculated using equation 4.3. Im(ε_f) = 0. b) Relative difference between Im[$\Delta k_{R(\theta)}$] and Im($\Delta k_{linear\ d}$). Re(ε_f) = 1.The contour lines delimitate the regions of constant relative difference. (ε_{glass} = 2.29134, d_{Au} = 50 nm, ε_{Au} = -1.5672+i11.27145, λ = 630 nm).

$\varepsilon_f = \varepsilon_a + \delta$ from the ambient value $\varepsilon_a = 1$, $\Delta k_{linear\ d}$ is proportional to α/A. In this case the last term in equation 4.3 can be approximated as

$$\Delta k_{linear\ d} \propto \frac{(\varepsilon_f - 1)(\varepsilon_f - \varepsilon_m)}{\varepsilon_{coll}} d_f \cong \frac{(1+\delta-1)(1+\delta-\varepsilon_m)}{1+\delta} d_f = \frac{\delta(1+\delta-\varepsilon_m)}{1+\delta} d_f \cong \delta(1-\varepsilon_m) d_f \tag{4.8}$$

while on the other hand the Clausius-Mossotti relation yields

$$\frac{\alpha}{A} \propto \frac{(\varepsilon_f - 1)}{(\varepsilon_f + 2)} d_f \cong \frac{(1+\delta-1)}{(1+\delta+2)} d_f \cong \frac{\delta}{3} d_f \tag{4.9}$$

leading to an expression for the quantity $\Delta k_{linear\ \alpha}$, the change in plasmon wavevector assuming the linear approximation (4.8) to be valid.

$$\Delta k_{linear\ \alpha} \approx \frac{2\pi\omega}{\lambda c}\left(\frac{\varepsilon_m \varepsilon_a}{\varepsilon_m + \varepsilon_a}\right)^2 \cdot \frac{1}{(-\varepsilon_m \varepsilon_a)^{1/2}(\varepsilon_a - \varepsilon_m)} \cdot 3 \cdot (1-\varepsilon_m) \cdot \frac{\alpha}{A} \tag{4.10}$$

In this case, the system response is uniquely described by α/A irrespective of the thickness d_f of the layer that hosts the polarisable units. In order to assess where this approximation is valid, the relative error that is made by approximating $\Delta k_{R(\theta)}$ by the $\Delta k_{linear\ \alpha}$ according to equation 4.10 is calculated and displayed in Figure 4.15.

The black line indicates the border of the region where the relative error is below 10%. By comparison to the values obtained for (d_f, ε_f) in the experiment, it is seen that for SOP7

and SOP22 significant errors are to be expected when stating a value for α/A if $d_f < 3$ nm and $d_f < 10$ nm, respectively. This agrees perfectly with the observation made in Figure 4.10 that only for sufficiently large d_f consistent values for α/A are obtained. Both approximations discussed before introduce negligible errors for the parameter range under investigation. All data points lie well within the area where the change in $R(\theta)$ is described by a single parameter (dashed or dot-dashed line). The only points where the analytical approximation $\Delta k_{linear\ d}$ introduces a significant error (dotted line) correspond to very small d_f and fall in a region where $\Delta k_{linear\ d}$ is not proportional to α/A.

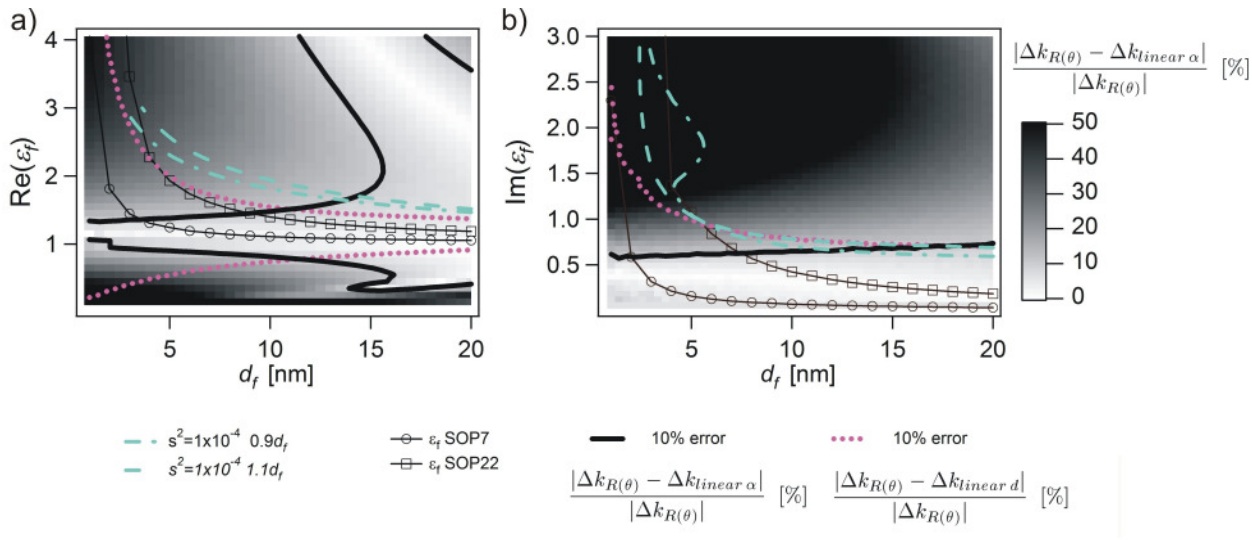

Figure 4.15: a) Comparison between the changes in the real part of $\Delta k_{R(\theta)}$ and $\Delta k_{linear\ \alpha}$ determined using equation 4.10. $\mathrm{Im}(\varepsilon_f) = 0$. The black contour line delimitates the 10% error region. The other contour lines show the regions obtained from the previous analysis (compare Figure 4.13a), Figure 4.13b) and Figure 4.14a)). Same analysis for the imaginary part of $\Delta k_{R(\theta)}$ and $\Delta k_{linear\ \alpha}$ with $\mathrm{Re}(\varepsilon_f) = 1$. The other contour lines show again the regions obtained from the previous analysis (compare Figure 4.13c), Figure 4.13d) and Figure 4.14b)).

The circles and the squares show the values obtained from the fit for $\mathrm{Re}(\varepsilon_f)$ or $\mathrm{Im}(\varepsilon_f)$ at $\lambda = 630$ nm for the low and high concentration samples, respectively.

Most importantly, in Figure 4.15 a region can be identified where a polarisability density α/A can be extracted from surface plasmon spectroscopy irrespective of the thickness of the layer where the polarisable units are distributed.

4.5 Conclusions

In conclusion, multi-wavelength surface plasmon spectroscopy in Kretschmann-

configuration was established as a tool to study the optical response of the plasmonic resonances that occur when metal spheres interact with a metal surface over a thin gap. The resonances lead to characteristic changes in surface plasmon dispersion. It was pointed out that fitting may lead to two fundamentally different results depending on the starting value and care must be taken in automatic data treatment. Then, the impossibility to determine the 'natural' parameters describing a thin film, thickness and dielectric response simultaneously, was discussed. It is proposed that under certain conditions instead a polarisability per surface area α/A should be stated. In this case, equal area densities of polarisable units yield identical responses in surface plasmon spectroscopy irrespective of the thickness of the layer they are distributed in. It was shown that this analysis yields reasonable quantitative agreement for the order of magnitude of the polarizability with a simple theoretical model of the sphere-on-plane resonators. The parameter range where the evaluation of surface plasmon data in terms of α/A is applicable was determined for a typical experimental situation.

We propose that analysis of surface plasmon reflectivity data for very thin films should be performed in terms of α/A. This would in general increase the use of these experiments since α/A is directly connected to area densities of polarisable units as (bio-) molecules in standard sensing applications. We found that surface plasmon spectroscopy is a highly sensitive tool to study sphere-on-plane resonators which are highly dilute and therefore represent a 'clean' system. Systematic studies on sphere-on-plane resonances utilizing this approach are currently pursued in our lab.

4.6 Acknowledgements

[Removed]

5 Optical resonances of gold nanoparticles on a gold surface: Quantitative determination of the geometry

5.1 Introduction

The key feature ascribed to sphere-on-plane systems is a very large electromagnetic field localized in volumes in the nanometer range. Therefore, they play an important role in many physical effects involving emission and collection of light, for example Scanning Tunnel ling Microscopy (STM) induced light (Johansson, Monreal et al. 1990), Scanning Near Field Optical Microscopy (SNOM) (Fischer and Pohl 1989) and Surface Enhanced Raman Scattering (SERS) (Abe, Manzel et al. 1981). Furthermore they can be used in bio-sensing and chemical sensing (Lyon, Pena et al. 1999; Hutter, Cha et al. 2001; Tsuboi, Fukuba et al. 2007) or as an optical tweezer (Xu and Käll 2002).

Estimates of the field enhancement are based on quasi-static calculations of the fields in an ideal geometry. The nanoparticle is modeled as a sphere surrounded by a homogeneous medium on a perfectly flat plane (Ambient-Colloid model, AC, see Figure 5.1a). Experimentally, a spacer layer is needed to suspend the nanoparticle on top of the plane ideally leading to the geometry shown in Figure 5.1b (Ambient-Spacer-Colloid model, ASpC). Realistic experimental systems though, may vary significantly from the ideal geometry. Figure 5.1c) shows a sketch to scale of how a realistic system could look like. The gold surface is not flat but shows considerable roughness. Here, the gold surface topography was taken from an atomic force micrograph from a typical evaporated gold surface (see Figure 3.2). The spacer layer is sketched as an assembly of particles with a diameter of 3 nm. Gold nanoparticles are generally facetted and many different crystal shapes are possible. Here, an icosahedron is sketched according to Buffat et al. (Buffat, Flueli et al. 1991) with an approximate diameter of 60 nm. It should be noted that these rough estimates lead to significant deviations of the contact area from the ideal case. These deviations should affect the optical response. Calculations on rectangular particles on planes show that larger contact areas allow for larger gap distances leading to similar resonance wavelengths (Leveque and Martin 2006) achieved with a sphere-on-plane system. A further assumption in the ideal model is the description of the metal in terms of a bulk dielectric function, although nonlocal effects and surface states are expected to play a role on the length scales under consideration

which are typically in the range from 5 Å to 30 Å. A quantitative understanding of the influence of these factors on the field enhancement calculations is therefore important if their magnitude is to be taken as realistic. A direct measurement of the field enhancement is not possible but the signature of the sphere-on-plane resonance in the far field response of the system can be studied and promises some insight on the electromagnetic effects taking place on these very small length scales.

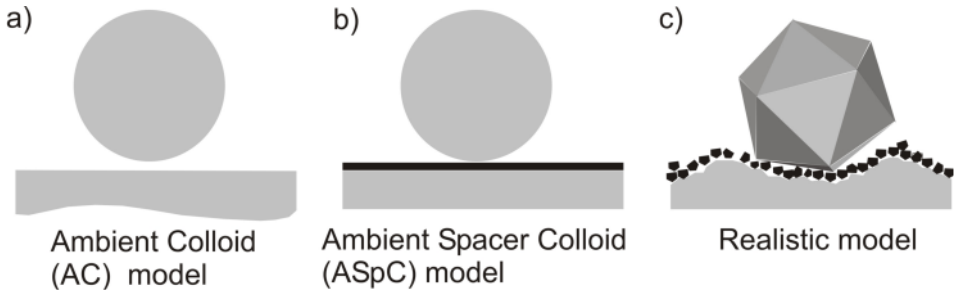

Figure 5.1: a) Model used for analytical calculations. b) Idealized sample architecture. c) Schematic of a realistic sample architecture.

Experiments to systematically investigate the dependence of the gap resonances on the resonator geometry were done using different types of systems (see chapter 4). Okamoto et al. managed to show clearly the gap resonances in the extinction spectrum and investigated the effect of the sphere diameter on the resonance wavelength. Tsuboi et al. (Tsuboi, Abe et al. 2006) investigated also sphere-on-plane systems using different kinds of organic spacers. Le et al. (Le, Lwin et al. 2005) investigated the influence of the finite thickness of the supporting gold layer.

The experiments were described (Okamoto and Yamaguchi 2003; Tsuboi, Abe et al. 2006) by the simple analytical AC (Ambient-Colloid) model although the experiments used a high-refractive index spacer which ideally would correspond to the ASpC (Ambient-Spacer-Colloid) model. The key problem in the analysis is the ambiguity in the choice of the gap distance and the surrounding dielectric function for the calculations. It was found that the gap distances required to model the experiments were much smaller than expected gap. It remains unclear whether this discrepancy was due to the mathematical simplification by using the AC model instead of the ASpC model, or due to the imperfect geometry (compare Figure 5.1c). It

should be noted that, for example, larger contact areas due to the facetted nanoparticles and the rough plane are expected in a realistic geometry which would give a similar far field response but considerably less field enhancements in the gap. Therefore, true quantitative experiments are important to resolve the ambiguity in the choice of the gap distance and gap dielectric function and obtain a realistic picture of the system

In this chapter, a solid experimental basis for a quantitative analysis of sphere-on-plane systems by variation of three central parameters is laid. Firstly, to investigate the influence of the spacer on the gap resonances, sphere-on-plane systems were fabricated using three different kinds of spacers. In addition to the commonly used alkanethiols, polyphenylene dendrimers were used. This new class of spacer molecules can be made much larger (Clark, Wenzel et al. 2007; Clark, Wenzel et al. 2007), are semi-rigid and shape-persistent thus providing defined spacer distances and can be in addition chemically modified to locate chromophores exactly in the gap. Secondly, for each spacer, different systems with gold nanoparticle radii in the range between 11 nm and 80 nm were fabricated. Thirdly, the optical properties of the systems were investigated in surrounding media with different refractive indices, namely air, water and heptane.

Based on these experiments, a way to interpret systems with spacer layers (ASpC-systems) using the analytical AC model which treats homogeneous environments (Figure 5.1a) was developed, avoiding sophisticated numerical calculations. Together with surface plasmon spectroscopy, the ambiguity in the determination of the system geometry is resolved and, surprisingly, no strong evidence of geometrical and material imperfections as suggested in Figure 5.1c) were found.

5.2 Experimental

A schematic representation of the sample architecture is shown in Figure 2a). The sample preparation is in principle identical as in chapter 4 using as spacer **TdG_2**. The only difference being the use of different molecules as spacer and the gold nanoparticle radius variation instead of a variation of gold nanoparticle concentration. The description of the preparation will be repeated for completion. First, a thin (~ 2 nm) chromium layer was deposited onto a BK7 (Menzel-Gläser, for the measurements in air) or a LaSFN9 (Hellma Optik, for the

measurements in liquid) objective slide by thermal evaporation (Edwards FL 400). Subsequently a gold layer (approximately 50 nm thickness) was evaporated. One of these samples was kept as "Au" reference. To create the small gaps needed to separate the gold colloids from the gold plane three different molecules were used: 2-Aminoethanethiol (**AET**, Cysteamin Hydrochlorid HPCL Grade, Fischer Scientific) and two types of functional polyphenylene dendrimers (PPDs) **PDIG$_2$** and **TdG$_2$** shown in Figure 5.3a). **TdG$_2$** was used in chapter 4 and is shown again for completion. To create the spacer layer, the slides were submerged in a solution containing the spacer molecule. One of these samples was kept as "Au+spacer" for later reference measurements. For 2-Aminoethanethiol the submersion time was 16 hours in a 1 mM solution in ethanol (HPCL Grade, Fischer Scientific). The slides were then rinsed in ultra clean water (Milli-Q Gradient A10) and dried with an air gun. For **TdG$_2$** and **PDIG$_2$** the submersion time was generally 10 to 15 minutes in a 2 µM solution of the dendrimer molecule in tetrahydrofurane (HPCL Grade, Sigma Aldrich). The slides were then rinsed in tetrahydrofurane and dried with an air gun.

Gold nanoparticle sols were prepared as described in chapter 4. For 20 nm, 40 nm, 60 nm and 150 nm diameter nanoparticles a concentration of 0.090 M, 0.026 M, 0.015 M and 0.010 M trisodium citrate solution was used respectively. Two different methods were used to attach the nanoparticles to the spacer. In the first method the slide was submerged in the suspension. The submersion time depends on the spacer used. For **AET** 3-6 hours were used. For **TdG$_2$** and **PDIG$_2$** the submersion time needed was 5 to 7 days. This is due to the hydrophobic nature of the surface after addition of the dendrimer molecule. The slides were then rinsed in water and dried with an air gun. Because of the long submersion times needed, an alternative method was used to attach the gold nanoparticles to the dendrimer spacer.

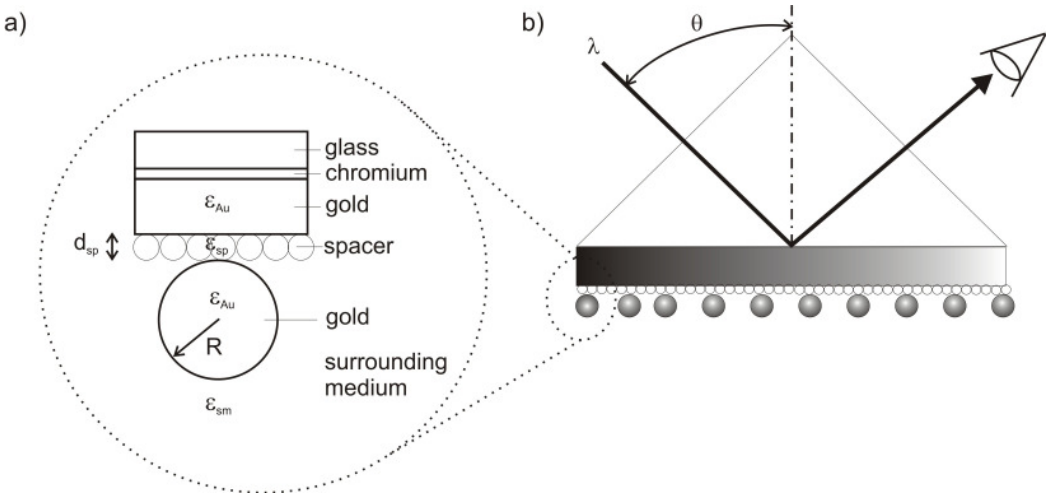

Figure 5.2. a) Schematic representation of the sample architecture. b) Schematic representation of the experimental setup.

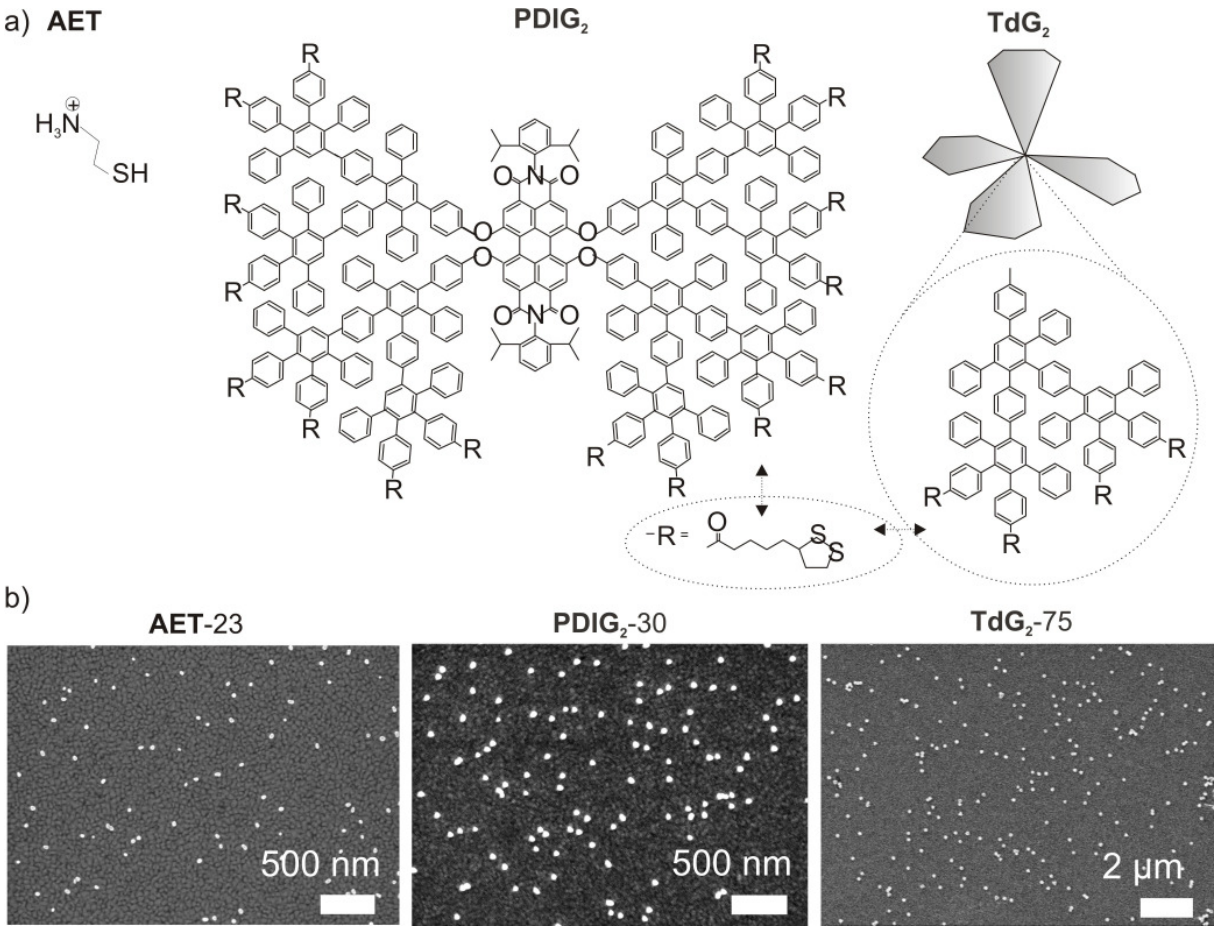

Figure 5.3. a) The three different molecules used as spacers: 2-Aminoethanethiol (AET), $PDIG_2$ and TdG_2. b) Scanning electron micrographs of selected samples.

The slide was submerged in the gold nanoparticle suspension. A potential was applied for 15 minutes between the gold surface and the gold nanoparticle suspension to promote the attachment of the negatively charged gold nanoparticles. By varying the potential in the range between 0.1 V and 0.7 V different nanoparticle concentrations on the surface could be achieved. Scanning electron microscope (SEM) images of the samples were taken with a commercial low voltage, high resolution scanning electron microscope (1530 Gemini Leo).

The specular reflectivity of the samples was measured as described in chapter 4 shown schematically again in Figure 5.2b).

To change the surrounding medium a teflon fluid cell was integrated in the sample holder. Through the cell's aperture holes liquids can be injected and extracted without changing the spot measured. The reflectivity of the samples and its corresponding references ('Au', 'Au+spacer') was measured first in air, then in ultra clean water (Milli-Q Gradient A10) and then in heptane (n-heptane 99% p.a. WTL Laborbedarf GmBH).

5.3 Experiment: Variation of the sphere-on-plane resonator parameters

5.3.1 Variation of the spacer

5.3.1.1 Spacer molecules.

To create the small gaps needed to separate the gold colloids from the gold plane three small organic molecules were used. Theoretically, the gaps need to be of the order of 1 nm to 3 nm for the gap resonances to arise (see section 2.2.3). The alkanethiol 2-Aminoethanethiol (**AET**) (Cysteamin Hydrochlorid HPCL Grade, Fischer Scientific, compare Figure 5.3a) was chosen because of its small size (less than 1 nm) and simple chemistry. Hereby the thiol group binds to the gold surface and the positively charged amino group to the gold nanoparticles. 2-Aminoethanethiol has been used previously in investigations on sphere-on-plane systems (Hutter, Fendler et al. 2001; Okamoto and Yamaguchi 2003; Tsuboi, Abe et al. 2006) and as such the experimental procedures are well established.

A more versatile type of molecules in the above context are dendrimers decorated with

peripheral functional groups with high gold affinity. This class of molecules has a hyperbranched, more or less spherical structure allowing to induce multiple binding sites into the system. A special case among these hyperbranched molecules are polyphenylene dendrimers (Morgenroth, Kübel et al. 1997; Morgenroth, Reuther et al. 1997; Wiesler, Berresheim et al. 2001; Vossmeyer, Guse et al. 2002; Bauer, Liu et al. 2007; Krasteva, Fogel et al. 2007; Zhang, Mullen et al. 2007; Yin, Kuhlmann et al. 2008; Yin, Shen et al. 2008). The molecular structure of these materials, consisting exclusively of phenyl-phenyl linkages furnishes these molecules with an outstanding rigidity and as such shape persistency (Wind, Saalwächter et al. 2002). Moreover their straight forward, modular synthesis permits the easy design and production of nanoparticles with complex functionality (Bauer, Grimsdale et al. 2005).

Two types of functional polyphenylene dendrimers were employed in the present study. The first one, which will be called dendrimer **$PDIG_2$** (shown in Figure 5.3a) was designed to fulfil two different experimental demands: On one side the peripheral lipoic acid rests establish the necessary affinity towards gold (Nuzzo and Allara 1983). On the other hand, a fluorophore unit was embedded into the core of the dendrimer in form of a perylenediimede dye (PDI). As such when using **$PDIG_2$** the fluorophore is located exactly in the gap between the gold nanoparticles and the gold plane and can be used as a probe for near field enhancements in future applications. Here, as a first step in this direction, we focus on the possibility to employ it as spacer for sphere-on-plane systems. The other dendrimer used is a second generation dendrimer and will be called **TdG_2** (which was used in chapter 4 and is shown again in Figure 5.3a). In the case of **$PDIG_2$** a new synthetic protocol had to be followed (see Appendix A).

5.3.1.2 Estimations of the gap thickness from the molecular structure

One can estimate an approximate value for the spacer thickness d_{sp} by calculating the length of the molecule. Nevertheless, the spacer layer thickness is not necessarily given by this length. The actual arrangement of the spacer molecule when adsorbing to form a layer is generally not known and the configuration can change when the gold nanoparticle is bound.

For **AET** Barkowski and Hedberg (Barkowski and Hedberg 1987) determined the length of the conformers in gaseous 2-Aminoethanethiol by means of electron diffraction. Michota et

al. (Michota, Kudelski et al. 2002) found that when adsorbed to a gold surface two conformations are possible. In one conformation called the trans conformer only the thiol group binds to the surface, in the other conformation, called the gauche conformer, the thiol and the amino group bind to the surface. If the amino group binds to the surface, it is not free to bind to the gold nanoparticle which means that locally, for a sphere-on-plane resonator, only the length of the trans conformer is playing a role. The length lies in the range of 0.6 nm to 0.7 nm. In the case of **TdG_2**, a distance of 3.2 nm between the end-groups of any two straight all-para branches was determined by molecular modelling (Brocorens, Lazzaroni et al. 2007) resulting in a vertical distance of 2.6 nm. A diameter of approximately 3.8 nm was determined by light scattering experiments and Atomic Force Microscopy methods (Wiesler, Berresheim et al. 2001). In the case of **$PDIG_2$** there are to our knowledge no molecular modeling calculations. A rough estimation can be made by assuming a planar structure of the molecule giving an upper limit for the diameter. The perilenediimide group with the polyphenyl groups builds the rigid core of the molecule with a diameter of approximately 5.3 nm. This is without taking into account the dithiolane groups which are flexible and can fold.

5.3.1.3 Estimations of the gap thickness from surface plasmon spectroscopy

Surface plasmon spectroscopy is a way to determine the spacer layer thickness d_{sp} experimentally (Raether 1988). The thickness and dielectric function of a thin dielectric layer cannot be determined simultaneously (Debruijn, Altenburg et al. 1991). Figure 5.4 shows the values for d_{sp} obtained assuming different values for ε_{sp}. The values shown are averages over several wavelengths measured (see Appendix A). The error bars take into account the variations from sample to sample.

For **AET** these variations are small. For **$PDIG_2$** and **TdG_2** they constitute the major contribution to the error showing that in this case a thickness cannot be accurately determined. If the values obtained from the surface plasmon analysis for **AET** are compared with the estimated values based on the molecular structure $d_{sp} \approx 0.6$ nm, a value for $\varepsilon_{sp} = 2.0 \pm 0.3$ can be estimated. In the following we will assume this value for all spacers. This assumption will be justified later.

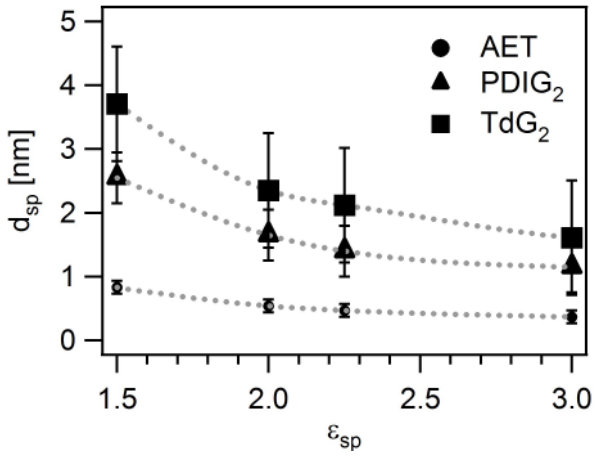

Figure 5.4. d_{sp} values obtained by setting different values for ε_{sp} determined by surface plasmon spectroscopy.

5.3.2 Variation of the gold nanoparticle sphere radius

The gold nanoparticle sphere radius was tuned by changing the trisodium citrate concentration during the preparation. Gold nanoparticles with diameters in the range from 20 nm to 150 nm were prepared yielding different sample architectures. The sample name convention used is: 'spacer-radius' where for spacer, the spacer name: **AET**, **$PDIG_2$** or **TdG_2** is used and the radius of the gold nanoparticles is given in nanometers. Figure 5.3b) shows scanning electron micrographs of different examples proving a good coverage of the gold surface predominantly by individual nanoparticles. These scanning electron micrograph images allow for a direct measurement of the gold nanoparticle radius showing a dispersion of about 5 nm for radii smaller than 75 nm and of about 10 nm for the bigger radii.

5.3.2.1 Polarisability of the sphere-on-plane resonators with air as a surrounding medium

From the measured reflectivity a polarisability α per unit area A: α/A was extracted for each sample following a routine as described earlier (see chapter 4). The extracted polarisability shows clear resonances which resemble the form of a Lorentz-type resonator (Bohren and Huffmann 1983). The resonances are seen with all three different spacers. Furthermore, depending on the nanoparticle radius and spacer the position of the resonance can be tuned to shift to wavelengths longer than the resonance wavelength of the sphere (~ 510 nm). Figure 5.5a) shows that for a 19 nm radius nanoparticle and the spacer **TdG_2** the resonance is seen at around 600 nm. Changing the spacer to **AET** (Figure 5.5b)) makes the resonance shift into the red to around 700 nm. Using very big nanoparticles like those shown in Figure 5.5c) with

80 nm radius shifts the resonance further into the red to around 800 nm. Since the experimentally accessible wavelength range is restricted to 550 nm < λ < 800 nm (see chapter 4), the resonance of the isolated sphere cannot be seen.The extracted polarisability for all samples investigated is shown in Appendix A.

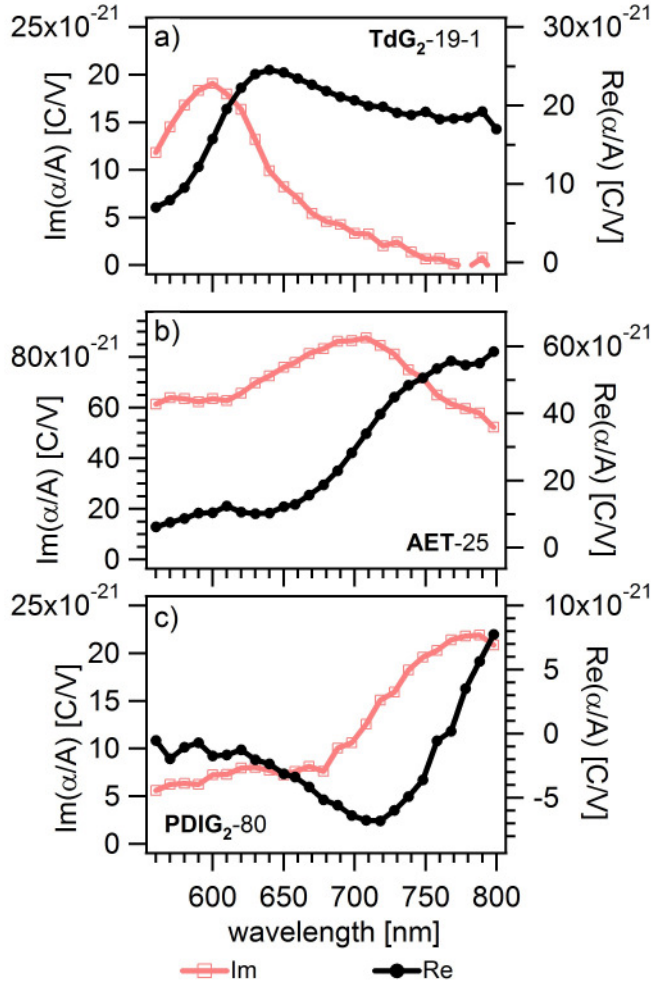

Figure 5.5. Polarisability per unit area α/A for a) TdG_2-19-1 b) AET-25 c) $PDIG_2$-80.

5.3.3 Variation of the surrounding medium

A great advantage of surface plasmon spectroscopy is the possibility to measure in liquids. Contrary to extinction experiments, where transmission through a highly absorbing gold film and through the liquid has to be measured, in surface plasmon spectroscopy no light has to propagate through the liquid. Therefore, the dielectric response of the surrounding medium can be varied experimentally by immersion in water and heptane.

Any changes in the system architecture such as solvent-induced swelling of the spacer

introduce variations in the response of the sphere on plane resonators which are not due to the new surrounding medium alone. To experimentally exclude this systematic error the optical response of the sample was measured in air once more after the measurements in air, water and heptane had been performed. The minimum position of the reflectivity dip was seen to return to the same place as measured before indicating that the sample did not irreversibly change its optical response.

Nevertheless, this does not exclude the possibility of reversible changes. To experimentally test this, besides water (ε=1.77), a non polar solvent: heptane (ε=1.86) was used. From an analysis of the reflectivity of the reference samples 'Au' and 'Au+spacer' in water and in heptane no significant difference was noticed when comparing the measurements in both solvents. It is not probable that these two chemically very different liquids affect the sphere-on-plane resonators on the molecular level in the same way. Thus, the observed shift can be interpreted in terms of the increase in refractive index of the surrounding medium.

From the measured reflectivity the polarisability per unit area α/A was extracted for each sample analogous to the measurements in air. The Clausius-Mossotti relationship was modified to account for a different surrounding medium:

$$\frac{\alpha}{A} = 3\varepsilon_0 \frac{\varepsilon_f / \varepsilon_{sm} - 1}{\varepsilon_f / \varepsilon_{sm} + 2} d_f \qquad (5.1)$$

with ε_0 the permittivity of free space, ε_f and d_f the dielectric function and thickness of the effective film formed by the sphere-on-plane resonators and ε_{sm} the dielectric function of the surrounding medium. ε_{sm} is extracted by adjusting the position of the total reflection edge of the reference sample when measured in water or heptane respectively. ε_f and d_f are extracted as explained in chapter 4. Figure 5.6 shows the real and imaginary part of α/A for three samples in air (circles), water (triangles) and heptane (squares). The resonance in air for **AET**-23 is quite weak in Im(α/A) but it can be clearly seen in the Re(α/A). In all cases a red-shift of approximately 40 nm was measured. The red-shift in heptane is slightly bigger due to its higher index of refraction. A small offset in the magnitude of the polarisability arises when comparing air with water and heptane. This may be due to slight changes in the optical

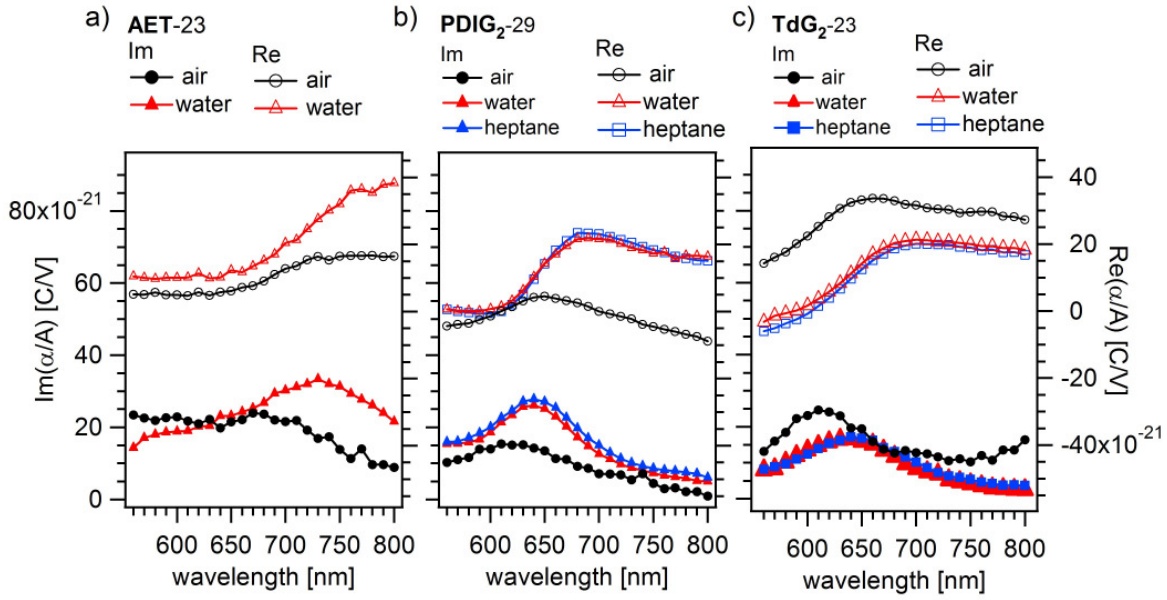

Figure 5.6. Polarisability per unit area α/A for some of the samples investigated. a) AET-23 b) $PDIG_2$-29 and c) TdG_2-23 with air (circles), water (triangles) and heptane (squares) as a surrounding medium.

response of the gold surface or the spacer layer when immersed in liquid. The offset in water or heptane is positive for **AET**-23 and **TdG_2** - 23 and negative for **$PDIG_2$**-29.

5.3.4 Summary of results

Figure 5.7 shows the resonance wavelength λ_{SOP}, defined as the wavelength for which Im(α/A) reaches its maximum, as a function of 1/R. λ_{SOP} was extracted by estimating the approximate position of the maximum from the calculated polarisability. For each individual spacer, i.e. a fixed gap distance, the bigger the radius the longer the wavelength of resonance. For the samples **AET**-23, **$PDIG_2$**-29 and **TdG_2**-23 a red-shift of the resonance occurs when immersed in liquid.

5.4 Theory

5.4.1 The AC model

The dependence of λ_{SOP} on R, d, the dielectric function of the surrounding medium ε_{sm} and ε_{Au} has been calculated analytically using the AC-model (Figure 5.1a). Different mathematical formalisms for this problem are known (Rendell and Scalapino 1981; Aravind and Metiu 1983; Ruppin 1983; Wind, Vlieger et al. 1987). Apart from the choice of the

coordinate system they are equivalent (Okamoto and Yamaguchi 2003).

An analytical expression for the polarisability per resonator area α/A can be calculated provided that the entire system is significantly smaller than the wavelength of light. Furthermore, it is assumed that the bulk dielectric function of gold describes the dielectric response of the nanosphere and that the gold plane is semi-infinite. Throughout this work the model of Wind et al. (Wind, Vlieger et al. 1987) was used to calculate α/A.

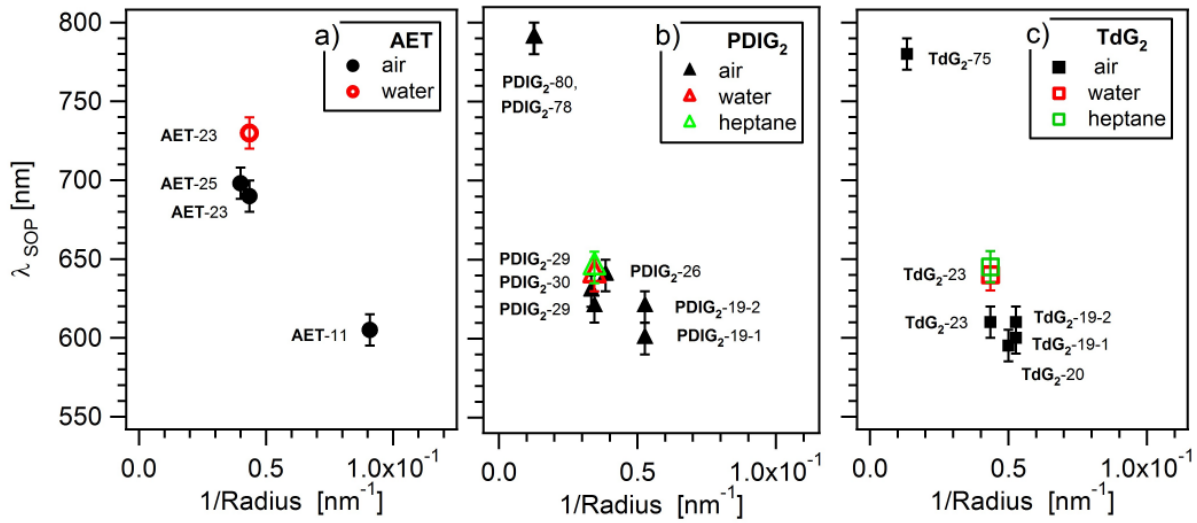

Figure 5.7. Summary of the wavelength of resonance λ_{SOP} as a function of 1/R for a) AET, b) $PDIG_2$ and c) TdG_2.

In the following some properties of this model are discussed which are required for the description of the experiments presented. First, it should be noted that in the static approximation, the sphere-on-plane system is scale invariant depending only on the gap/radius ratio, compare Nordlander et al. (Nordlander and Le 2006). Then, the complex polarisability α is a function of three parameters: $\alpha(\varepsilon_{sm}, d_{sp}/R, \lambda)$. Figure 5.8 gives an overview of the functional dependence of α on the parameters ε_{sm}, d_{sp}/R and λ. Figure 5.8a) shows α as a function of λ for $\varepsilon_{sm}=1.0$ and $d_{sp}/R=0.02$. The calculations were done using ε_{Au} obtained from the interpolation of the data from Johnson and Christy (Johnson and Christy 1972). Two resonances are seen at λ=535 nm and λ=635 nm, both resemble Lorentz-type resonators. In Figure 5.8b) the dependence of the imaginary part of α is shown as a function of λ keeping ε_{sm} = 1.0 fixed and varying d_{sp}/R. For d_{sp}/R=1 only one resonance is observed at

λ=510 nm. For this d_{sp}/R ratio the sphere is far away from the plane and the resonance corresponds to that of the sphere alone. As the d_{sp}/R ratio is decreased a second resonance appears, the gap resonance, which progressively shifts into the red. For $d_{sp}/R = 0.01$ a third resonance exists at λ=560 nm. It should be noted that for the gap resonances to appear, d_{sp}/R=0.1 or smaller is needed. Figure 5.8c) shows the influence of ε_{sm}, for a fixed d_{sp}/R ratio. All resonances shift further into the red as ε_{sm} is increased. The change in ε_{sm} induces a greater shift in the gap resonances as for the resonance of the sphere alone.

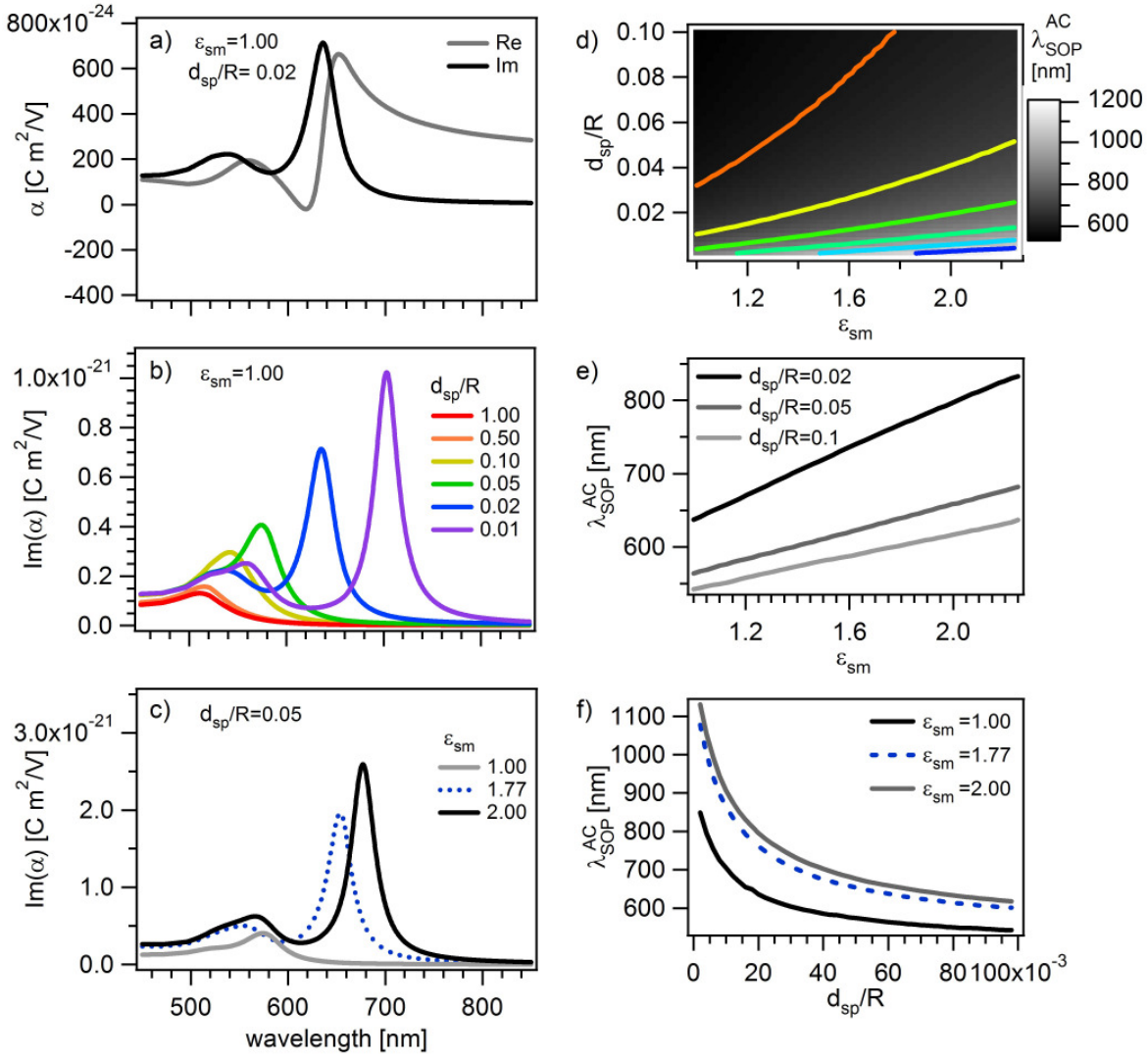

Figure 5.8. a) Complex polarisability α as function of the wavelength λ. b) Influence of d_{sp}/R on the imaginary part of α. c) Influence of ε_{sm} on the imaginary part of α. d) λ^{AC}_{SOP} as a function of d_{sp}/R and ε_{sm}. e) λ^{AC}_{SOP} as a function of d_{sp}/R. f) λ^{AC}_{SOP} as a function of ε_{sm}.

From the calculations, the wavelength of maximum Im(α) can be extracted. This sphere-on-plane resonance wavelength is a function of two parameters λ_{SOP}^{AC} (ε_{sm}, d_{sp}/R), shown in Figure 5.8d). In colour, the lines of constant λ_{SOP}^{AC} from λ_{SOP}^{AC} = 600 nm to λ_{SOP}^{AC} = 1100 nm in 100 nm steps are shown. Each value of λ_{SOP}^{AC} can be achieved by a whole set of (ε_{sm}, d_{sp}/R) combinations. The dependency of λ_{SOP}^{AC} on ε_{sm} is approximately linear (Figure 5.8e) whereas the relationship between λ_{SOP}^{AC} and d_{sp}/R is non linear (Figure 5.7f).

5.4.2 The ASpC model

To include the influence of the spacer on λ_{SOP}, we use the idealized ASpC (Ambient-Spacer-Colloid) model shown in Figure 1b). In the ASpC model $\lambda_{SOP}^{ASpC} = f(\varepsilon_{sp}, \varepsilon_{sm}, d_{sp}/R)$. Hence, for a full description of the ASpC system, the whole plane spanned by (ε_{sp}, ε_{sm}) is important. Although the AC model can only calculate $\varepsilon_{sp} = \varepsilon_{sm}$ it can be used to determine a range of possible values for d_{sp}/R if the following assumption is made: for a fixed d_{sp}/R, the resonance wavelength λ_{SOP}^{ASpC} increases monotonically when somewhere in the surrounding medium the dielectric function increases. We believe this is a reasonable assumption due to the fact that in the analytical calculations λ_{SOP}^{AC} always shifts to the red whenever ε_{sm} is increased. The only difference in our assumption is that ε_{sm} is not increased homogeneously in the surrounding. In particular, we can start increasing the dielectric function first in the gap area, i.e. only increase ε_{sp}, until the spacer layer is formed and then continue increasing the dielectric function, now only in the surrounding medium, until the entire system is surrounded by spacer. This path in the (ε_{sm}, ε_{sp}) plane is sketched in Figure 9a. Only when $\varepsilon_{sm} = \varepsilon_{sp}$ (dotted line in Figure 5.9a) we can use the AC model to calculate d_{sp}/R. Figure 5.9b sketches λ_{SOP}^{ASpC} along this path. A monotonous increase of the resonance wavelength directly leads to the inequality:
$\lambda_{SOP}^{AC}(\varepsilon_A,\ d_{sp}/R) < \lambda_{SOP}^{ASpC}(\varepsilon_A, \varepsilon_{sp},\ d_{sp}/R) < \lambda_{SOP}^{AC}(\varepsilon_{sp},\ d_{sp}/R)$

Instead of using the AC model, the influence of the spacer could be taken into account by numerical calculations as it has been done for silver nanoparticle dimers (Futamata, Maruyama et al. 2005) and for rectangular nanoparticles on a plane (Leveque and Martin 2006). However, firstly: it is not trivial to calculate this system numerically due to problems encountered when discretizing the small gap.

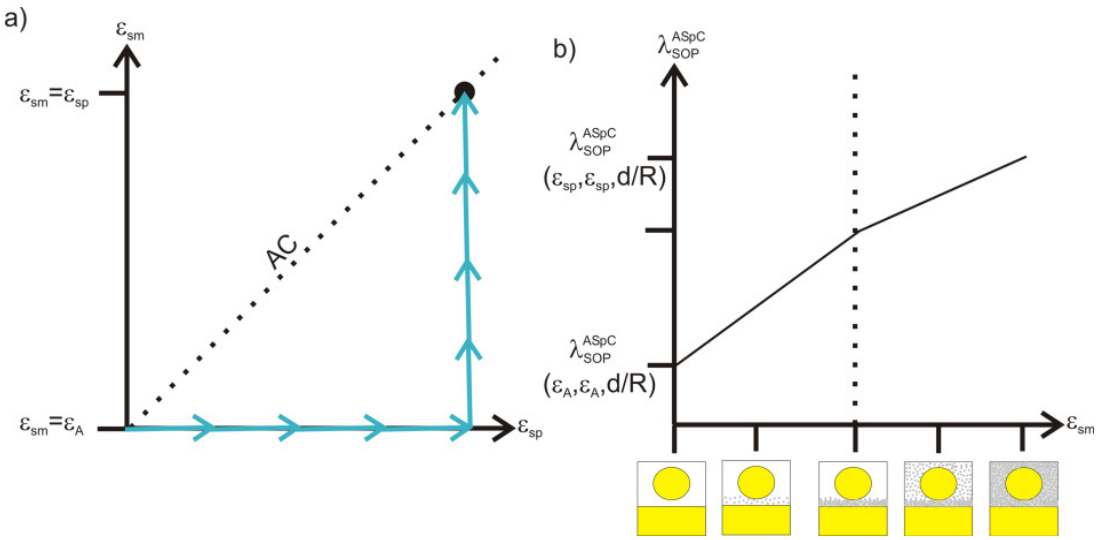

Figure 5.9. a) Path in the (ε_{sm}, ε_{sp}) plane for a fixed d_{sp}/R ratio to reach the value where $\varepsilon_{sm}=\varepsilon_{sp}$. b) Monotonic increase of λ_{SOP}^{ASpC} as a function of ε_{sm}.

Secondly, the central experimental problem: the ambiguity in the determination of the spacer thickness and its refractive index remains also when comparing with full numerical models.

5.5 Quantitative analysis: determining a gap thickness interval

In the following, the measured values of λ_{SOP} in the different surrounding media together with the calculated dependence on d_{sp}/R and ε_{sm} will be used to determine a gap thickness interval if a value for ε_{sp} is assumed. We will use exemplarily $\varepsilon_{sp} = 2.00$ which is reasonable for non-close-packed organic molecules as estimated in 3.1.3. Though, this analysis works for any ε_{sp} and gives comparable results for all reasonable choices $1.77 < \varepsilon_{sp} < 2.5$.

5.5.1 Interval analysis

Figure 5.10a) shows the dependency of λ_{SOP}^{AC} on d_{sp}/R calculated for different values of ε_{sm} (solid lines). Two values for d_{sp}/R can be calculated for a fixed λ_{SOP}: those given by assuming the system is completely embedded in spacer $\varepsilon_{sm} = 2.00$ and those assuming that the system is totally surrounded by air ($\varepsilon_{sm} = 1$) or water ($\varepsilon_{sm} = 1.77$). In both cases, intervals of possible

d_{sp}/R are obtained which are indicated as black and blue solid lines for air and water respectively. Given that the radius can be estimated, an interval for d is obtained. Figure 5.10b) shows these intervals using air and water as surrounding medium.

Due to the huge uncertainty of about 60%, the measurements in air do not provide very valuable information. The immersion experiments yield new values for d_{sp}, the limits being given now by the surrounding medium water and the spacer. The values fall into the range calculated before in air and the uncertainty is reduced.

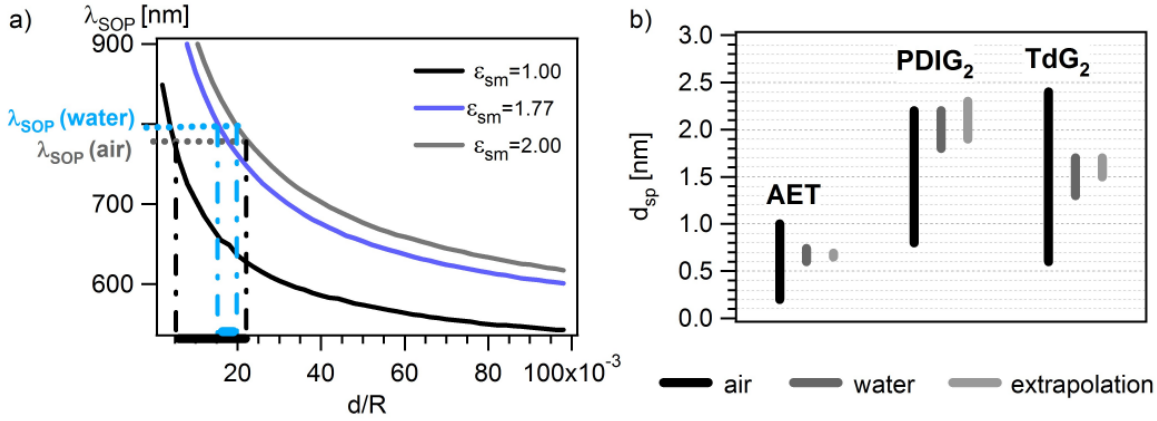

Figure 5.10. a) d_{sp}/R interval in water and in air determined by the measured λ_{SOP}. b) Intervals for d_{sp} calculated using the experiments in air, water and with the interpolation approach assuming ε_{sp}=2.00.

5.5.2 d_{sp}/R from interpolation approach

Next, it is introduced as a further assumption, that the values measured for λ_{SOP} in air, water and heptane can be linearly extrapolated to a certain value of ε_{sm}. For example, if we extrapolate to the value of the spacers' dielectric response ε_{sp}, we arrive at a situation that can be modelled analytically. In this way, we replace a full analytical ambient-spacer-colloid model by an empirical extrapolation. The linear extrapolation approach is justified by the fact that in the AC model the dependence of λ_{SOP}^{AC} is approximately linear. Calculations on more complex geometries yield similar linear dependencies (Leveque and Martin 2006). Figure 5.11a) shows the λ_{SOP} obtained from the immersion experiments in air, water and heptane for the three different spacers. The shaded area delimitates the possible λ_{SOP} when the values are linearly extrapolated. The λ_{SOP} (ε_{sm}) extracted from the interpolation determine a unique d_{sp}/R

value with an error which is due to experimental uncertainty in the measured λ_{SOP} as illustrated exemplarily for **TdG$_2$**-23 in Figure 5.11b). The interval of possible d_{sp}/R values for any ε_{sp} is directly read from this graph. If again ε_{sm} =2.00 is assumed, we obtain a better estimate for d_{sp}/R which agrees with the earlier analysis (see Figure 5.10b).

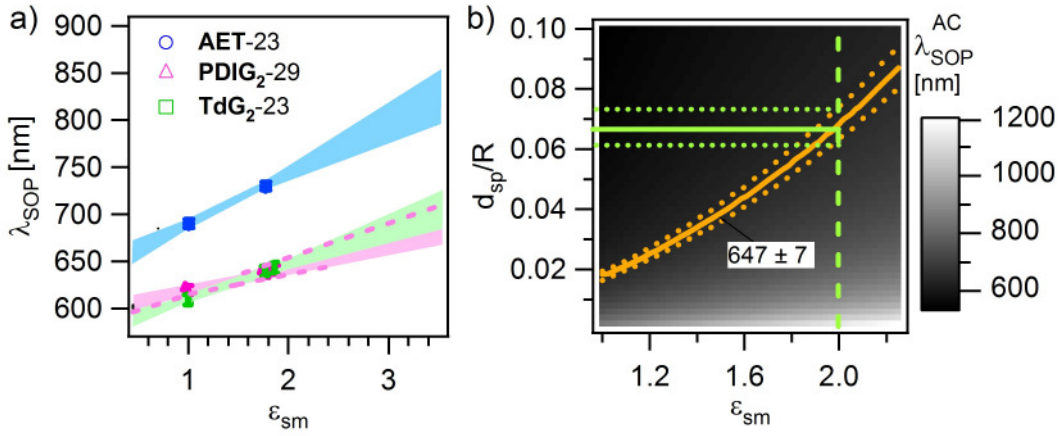

Figure 5.11. a) λ_{SOP} for ε_{sm} =1 (air), ε_{sm} =1.77 (water) and ε_{sm} =1.86 (heptane). The shaded regions show the possible range for λ_{SOP} taking into account the error bars in the extrapolation. b) The λ_{SOP} determined from a) for TdG$_2$-23 is shown as a solid contour line which determines a $d_{sp}/R(\varepsilon_{sm})$. The dotted contour lines show the regions of uncertainty when determining $d_{sp}/R(\varepsilon_{sm} = 2.00)$.

5.5.3 Scale invariant representation of the results

With these (d_{sp}, ε_{sp}) combinations, the measured λ_{SOP} can be related with the gap/radius ratio of the sample. Figure 5.12 shows the results obtained using the values obtained in 5.5.2.

Within the error, all resonances lie between the range predicted by the theory using either air or spacer as surrounding medium. They seem not to behave as if the system were completely embedded in air or in spacer but in a mixture of both environments with similar weight of ε_{sp} and ε_A. This result is reasonable, since much more air than spacer is surrounding the sphere (compare Figure 5.1b) but the field concentration in the gap gives more weight to the dielectric response there. For small d_{sp}/R a tendency to a dominating ε_{sp} is observed but this could be due to the breaking of the quasi-static condition for the large nanoparticle radii. Only the values for **PDIG$_2$**-26 and **PDIG$_2$**-19-2 lie outside the trend line. In general the experimental results agree very well with the simple analytical model.

Importantly, independent of the thickness of the three different spacers used the results

can be described with this type of master curve. This indicates that at least down to the gap distances investigated here, no significant influence of corrections due to the very small length scales involved play a big role.

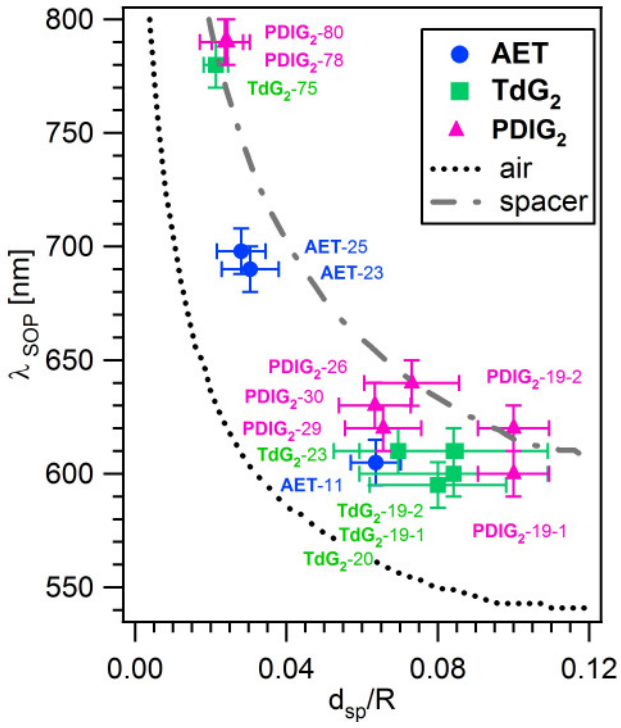

Figure 5.12. λ_{SOP} as a function of d_{sp}/R. The calculations using the AC-model for air and spacer as surrounding medium are shown for comparison.

5.6 Resolving the ambiguity in ε_{sp} /d_{sp}

In chapter 5.5 we have described a way to determine a set of possible pairs (d_{sp}, ε_{sp}) for arbitrary ε_{sp}. Thus, if d_{sp}/R is known ε_{sp} is determined in a unique way and vice versa. Since neither of those quantities is determined from the sphere-on-plane resonance alone, an independent experiment is required to resolve this ambiguity. By surface plasmon spectroscopy a very similar situation is found and only a set of possible (d_{sp}, ε_{sp}) combinations but no unique values are obtained (compare section 5.3.1.3). The combination of the information from the two techniques though, resolves this ambiguity as shown in Figure 5.13. The pairs (d_{sp}, ε_{sp}) that agree with both experiments are readily determined as crossing points.

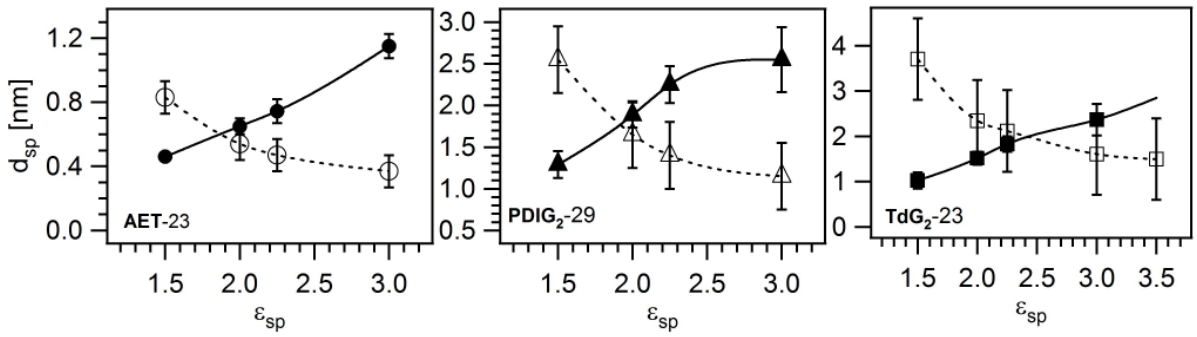

Figure 5.13. d_{sp} as a function of ε_{sp} for a) AET-23, b) $PDIG_2$-29 and c) TdG_2-23 using surface plasmon spectroscopy (empty symbols) and using the extrapolated values for λ_{sop} from the immersion experiments and the theory of Wind et al. (filled symbols). The solid lines connect the symbols as a guide to the eye.

Due to the small errors in the determination of d_{sp} for **AET**, a precise determination of $\varepsilon_{sp} = 1.9 \pm 0.1$ and $d_{sp} = (0.6 \pm 0.1)$ nm is possible. This determination without free parameters, but assuming a perfect ASpC system yields exactly the layer thickness as estimated from the molecular structure indicating no sign of an imperfect geometry as suggested in Figure 5.1c. Although this may be a coincidence, the agreement remains remarkable. For **$PDIG_2$** and **TdG_2** large errors in the surface plasmon spectroscopy experiments do not allow for a very precise conclusion but reasonable estimates for (ε_{sp}, d_{sp}) are obtained. For **$PDIG_2$** $\varepsilon_{sp} = 2.0 \pm 0.3$ and $d_{sp} = (1.8 \pm 0.3)$ nm is found. For **TdG_2** we find $\varepsilon_{sp} = 2.3 \pm 0.5$ and $d_{sp} = (2.0 \pm 0.5)$ nm.

5.7 Conclusions

Sphere-on-plane resonators were fabricated using three different kinds of spacers. In particular we succeeded in fabricating these systems using the polyphenylene dendrimers **$PDIG_2$** and **TdG_2** which posses different physical and chemical properties and allow for further functionalization making them a more versatile type of spacer than the commonly used alkanethiols. By combining the three different spacers and varying the nanoparticle radius the gap resonance wavelength could be tuned in the range between 550 nm and 850 nm. The dielectric response of the surrounding medium was varied by immersion in water and heptane. The influence of the dielectric function of spacer and surrounding on the resonance wavelength was found to be roughly equal in spite of the considerably smaller volume of the spacer. A spacer thickness interval was determined using a ASpC (Ambient-Spacer-Colloid) system based on the analytical calculations of a AC (Ambient-Colloid) system. In combination with surface plasmon spectroscopy the gap distance and spacer

dielectric function could be determined without adjustable parameters. To our surprise the gap distance is in agreement with an estimate from its molecular structure. No evidence of geometrical imperfections or modifications to Maxwell's theory on the sub-nanometer scale is seen in our experiments. Further experiments should show if this agreement with a simple theory applies as well to the local field enhancements and other measurable quantities or if it is pure coincidence.

5.8 Acknowledgements

[Removed]

6 Surface-enhanced fluorescence from the 'hot spots' of sphere-on-plane systems

In this chapter experiments towards a quantitative understanding of the field enhancements taking place in the gap of the sphere-on-plane systems will be shown. The objective was to compare the fluorescence of a metal-supported monolayer of the molecule **$PDIG_2$** upon decoration of the surface with nanoparticles. As a start for a systematic study, the metal used, the colloid mean size and the surface roughness were varied and the fluorescence of the system was measured in ensemble before and after colloid deposition. These measurements were thought as a first step to achieve optimal systems for single object studies.

6.1 Introduction

Surface enhanced luminescence is a process connected with the enhancement of the incident electromagnetic field and a change of the radiative and non-radiative decay rates of molecules placed for example near metallic nanostructures or planes (Weitz, Garoff et al. 1983; Xu, Wang et al. 2004). The most effective location for the enhancement are interstitial sites between metallic structures called 'hot spots' (Kneipp, Kneipp et al. 2002). The dimensions of these sites are in the order of nanometers.

Even though the mechanisms behind surface enhanced fluorescence have been studied for decades (Gersten and Nitzan 1981; Wokaun 1985; Barnes 1998; Xu, Wang et al. 2004) a quantitative understanding is still lacking. One of the reasons for this is the undefined geometry in which these experiments have been carried out. In the past most experiments carried out were done on nanoparticle aggregates (Kneipp, Kneipp et al. 1999) or on rough surfaces (Glass, Liao et al. 1980; Ritchie and Burstein 1981; Wokaun, Lutz et al. 1983).The effects were dependent on the cluster geometry which is undefined, uncontrollable and cannot be reproduced.

A defined system in which these 'hot spots' can be achieved is the sphere-on-plane system in which a metallic nanosphere is placed at nanometer distances from a metal plane creating a nanometer gap between them. Enhancements of the incident field intensity of up to 10^4

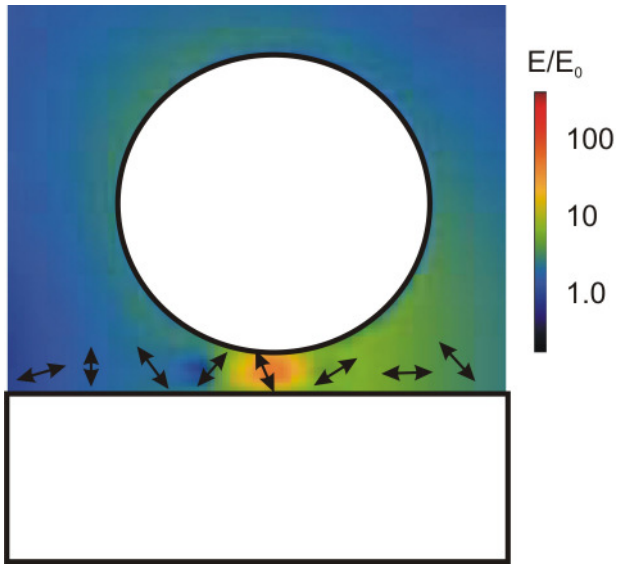

Figure 6.1: Sketch of an idealized sphere-on-plane system in which a fluorescent molecule depicted as a dipole is localized in the gap. The electromagnetic field amplitude enhancements (E/E_0) are represented in a rainbow scale. The highest enhancements (red) are located at the gap.

(Aravind and Metiu 1983) are possible in such systems. The electromagnetic fields in sphere-on-plane systems depend critically on the gap distance and the form of the gap, the nanoparticle size and the dielectric function of the materials (see chapter 5). The idealized geometry is shown schematically in Figure 6.1. A perfect sphere is placed on top of a perfectly flat plane. The emitters are sketched as point dipoles (shown as arrows) which are present in the gap between the sphere and the plane. When illuminated with light, the system becomes resonant at certain wavelengths and the incident field is enhanced. The field enhancement shown in a color scale in Figure 6.1 is strongest in the gap (red and yellow regions). It decreases in magnitude around the sphere (green) and is lowest in the blue regions. Due to the strong fields to which the emitter is exposed, there is an enhancement in the absorption. The emission is also enhanced but since upon excitation maximum one photon can be emitted, there is not generally an increase in brightness due to emission enhancement. This process competes with radiation-less energy transfer to the surface (quenching). The two mechanisms have different distance dependences (Wokaun, Lutz et al. 1983). Quenching is severe at much more shorter distances from the surface.

Experimentally, the gap is achieved by a molecular spacer that attaches to the metal nanoparticle and the metal plane. The idealized junction is deformed due to factors as the surface roughness and the actual geometry of the crystallites of which the nanostructure is

composed (see chapter 5). In this experiment, the polyphenylene dendrimer with perylenediimide core **$PDIG_2$** was used as spacer. This new class of spacer molecules allows for the simultaneous nanometer separation and inclusion of the chromophore in the gap. This permits a much better defined control of the positioning of the emitter in the gap and distance of the emitter to the metal surface compared to the usually employed alkanethiols (Anderson and Moskovits 2006).

The following experiment shows measurements of the fluorescence of **$PDIG_2$** under different experimental conditions. The surface roughness was controlled by different surface preparation techniques. Evaporated surfaces and template stripped surfaces were compared. Gold and silver systems were prepared to compare their different performances.

6.2 Experimental

A schematic representation of the three different sample architectures used in this study is shown in Figure 6.2a)-c). Silver and gold sphere-on-plane systems were fabricated using different types of surfaces. For the silver systems, two different surfaces were used: one prepared by evaporation and one prepared by the method of template stripping of silver (TSS) from silicon using the procedures developed for carbon and gold surfaces (Butt, Wang et al. 1991; Butt, Müller et al. 1993; Hegner, Wagner et al. 1993; Stamou, Gourdon et al. 1997). To separate the metal colloids from the surface, two different molecules were used as spacer: the polyphenylene dendrimer **TdG_2** and the polyphenylene dendrimer with a chromophore core **$PDIG_2$** (see Figure 6.2d) which were presented in chapter 5. For the gold systems, the surface was prepared by the method of template stripping of gold (TSG) from mica (Butt, Wang et al. 1991; Butt, Müller et al. 1993; Hegner, Wagner et al. 1993) (see chapter 2.4.3).

To fabricate the silver layers by evaporation (see Figure 6.2a) first, a thin (~2 nm) chromium layer was deposited onto a BK7 (Menzel-Gläser) objective slide by thermal evaporation (Edwards FL 400). Subsequently a silver layer (approximately 50 nm thickness) was evaporated. One of these samples was kept as "Ag_{Evap}" reference. To prepare the template stripped silver (TSS) layers (see Figure 6.2b) a silver layer of 200 nm nominal thickness was thermally evaporated (Edwards FL 400) on a silicon single crystal wafer. The silicon slide was obtained as a 26 x 45 mm^2 precut wafer (Crystec Kristalltechnologie). It was pre-cleaned for one hour in a solution of 50 ml H_2O, 10 ml NH_3 and 10 ml of H_2O_2 at 75°C, rinsed

extensively in ultra clean water (Milli-Q Gradient A10) and dried under nitrogen flow. It was then directly placed into the vacuum chamber for evaporation. The silver layer evaporated on the silicon wafer was then used to prepare a surface by the method of template stripping of silver from silicon TSS (template stripped silver). To fabricate this sample, the evaporated silver on the silicon wafer was immediately glued onto a clean BK7 glass substrate using the epoxy glue EPO-TEK 375 (Epoxy Technology) following the manufacturer's instructions. For curing, the sample was heated to 120°C for 60 min and let to cool down. Prior to the optical measurements, the silver surface was mechanically separated from the silicon wafer using a scalpel as a lever. One of these samples was kept as "TSS" reference sample for later reference measurements. To fabricate the template stripped gold (TSG) layers (see Figure 6.2c) mica slides (PELCO Mica from Plano GmbH) were heated to 650°C for 10 min to evaporate the crystal water present. Prior to gold evaporation, the mica slides were mechanically separated from each other with a scalpel. A gold layer of 200 nm nominal thickness was thermally evaporated (Edwards FL 400). The evaporated gold on mica was immediately glued onto a clean BK7 glass substrate using the epoxy glue EPO-TEK 377 (Epoxy Technology) following the manufacturer's instructions. The sample was then heated to 120°C for 60 min and let to cool down. Prior to the optical measurements the gold surface was chemically separated from the mica slide by immersing for 10 min in tetrahydrofurane. One of these samples was kept as "TSG" (template stripped gold) reference.

To create the spacer layer, the slides were submerged in a solution in tetrahydrofurane (HPCL Grade, Sigma Aldrich) containing the spacer molecule. The spacer concentration and submersion time was 2µM for 1.5 h for the evaporated silver surfaces and 5 µM for 1 h for the TSS. The slides were then rinsed in tetrahydrofurane and dried with air. For the TSG surfaces, the spacer was spin coated (Headway Research Inc, 3 ml suspension at 2000 rpm) using a 5 µM solution of the spacer molecule to avoid long time contact with tetrahydrofurane which makes the glue layer unstable. The use of spin coating to create the spacer layer had been previously tested by systematic studies of sphere-on-plane systems where it was found out that the immersion in the spacer solution is much more effective and gave a better surface coverage. Nevertheless, due to the glue instability this method had to be used in this case. One of these samples was kept as "Ag_{Evap} -spacer", "TSS-spacer" and "TSG-spacer" respectively for later reference measurements.

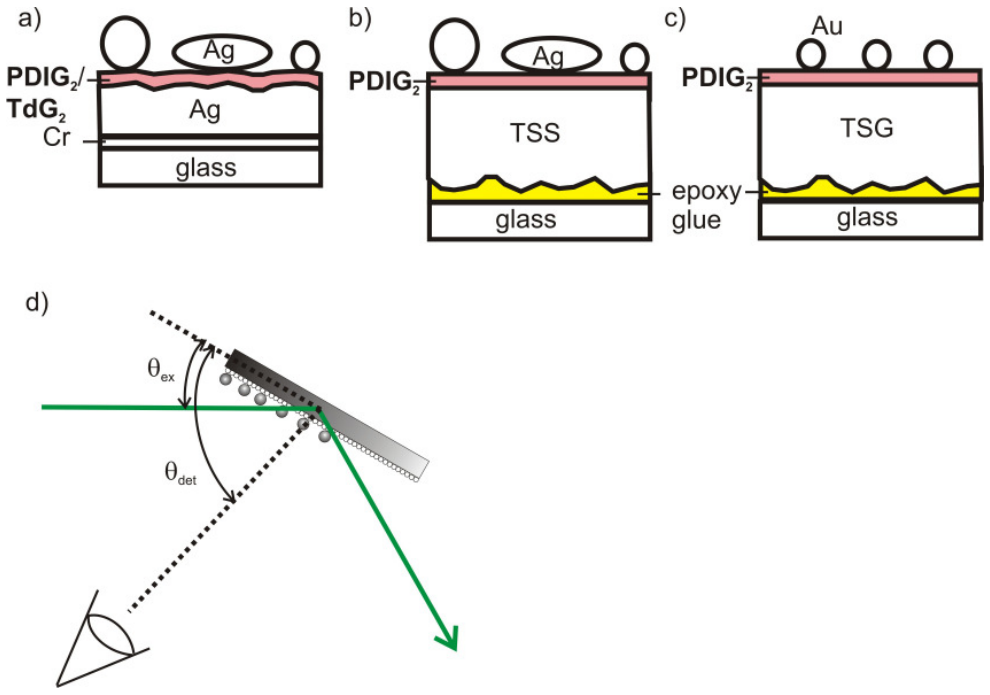

Figure 6.2: a) Silver sphere on plane system with an evaporated silver surface. b) Silver sphere on plane system with a template stripped silver surface. c) Gold sphere on plane system with a template stripped gold surface. d) Schematic representation of the experimental setup.

Silver nanoparticle sols of different size and shapes (rods, triangles, spheres) were synthesized using a modified citrate reduction method for gold nanoparticles (Turkevich, Stevenson et al. 1951; Frens 1973). In a 250 ml two-neck round-bottom flask, 20 mg of silver nitrate powder ($AgNO_3$ 99.9+%, Aldrich) dissolved in 100 ml ultra clean water (Milli-Q Gradient A10) was heated to reflux, and 120 mg trisodium citrate dihydrate (99+%, Aldrich) dissolved in 3 ml H_2O was injected quickly. After approximately 7 – 10 min the color changed from clear colorless into a cloudy yellow brown, indicating the formation of silver nanoparticles. The larger brown colored particles were separated from the smaller yellow colored ones by a 72 hour sedimentation process. To attach the nanoparticles to the surface the slides were dipped in the nanoparticle suspension. For the evaporated silver systems, the slides were submerged in the yellow colloid suspension for 3 h. These samples will be called Ag_{Evap}-**$PDIG_2$**-yellow and Ag_{Evap}-**TdG_2**-yellow. The same procedure was repeated for the brown suspension. These samples will be called Ag_{Evap}-**$PDIG_2$**-brown and Ag_{Evap} -**TdG_2**-brown. For the TSS system the slides were submerged in the yellow colloid suspension for 3 h. This sample will be called TSS-**$PDIG_2$** -yellow. Another slide was submerged in the brown colloid suspension for 2 h. This sample will be called TSS-**$PDIG_2$**-brown. For the TSG system, gold nanoparticle sols

(40 nm nominal diameter) were prepared as described in chapter 4 using a 0.015 M solution of trisodium citrate (Aldrich). The colloidal suspension prepared in this way had a mean particle radius of 20 nm as determined by scanning electron microscopy. Two different samples with different colloid concentrations were fabricated by submerging the samples in the gold nanoparticle suspension for one and two days. The sample submerged one day will be called "TSG- **$PDIG_2$**-c1" and the one submerged for two days will be called "TSG-**$PDIG_2$**-c2", the subscripts c1 and c2 standing for the two different concentrations: $c_1 = 7$ particles/μm^2 and $c_2 = 24$ particles/μm^2

The fluorescence spectrum of the samples was measured using an Andor iDus spectrometer (Shamrock 303i spectrometer, Du420A CCD camera from Andor Technologies). The 532 nm light from a diode laser (Polytec, PDL-DPGL-532-20) was passed through a 532 nm line filter (Omega Optical, XLK08/532NB3 0143 DTM). The sample was tilted to achieve an excitation angle $\theta_{ext} = 30°$ (see Figure 6.2d). At this angle of incidence the laser spot looked elliptical and had an area of approximately 1 cm x 5 mm. The detection angle was set to $\theta_{det} = 77°$ to avoid the detection of the specularly reflected light. The emitted light was filtered with a 532 nm notch filter (Semrock Razor Edge, NF01-532U-25) and a 538 nm long pass filter (Omega Optical, EL00123848) and collected by a fiber bundle coupled to the spectrometer opening slit. For the experiments with the silver nanoparticles on evaporated silver surfaces and the silver nanoparticles on template stripped silver surfaces the distance from the sample to the fiber entrance was 16 cm. The detection time was 120 s. For the experiments with gold nanoparticles on template stripped gold surfaces $\theta_{det} \approx 100°$ and the distance from the sample to the fiber entrance was 19 cm. The detection time was 40 s.

The combined emission excitation spectra as a function of the excitation and detection wavelengths of **TdG_2** (2 µM), **$PDIG_2$** (1 µM) and of the solvent tetrahydrofurane (HPCL Grade, Sigma Aldrich, used as purchased) were measured in a fluorescence spectrograph (J&M Tidas).

6.3 Fluorescence of the spacer molecules

In chapters 4 and 5 it was shown that sphere-on-plane systems can be fabricated using polyphenylene dendrimer spacers. This is of particular interest due to the possibility of

functionalizing the spacer to include fluorophores and directly position them in the gap.

Two types of functional polyphenylene dendrimers were employed in the present study. The molecule **TdG_2** will be used as reference. The second dendrimer used is the second generation dendrimer **$PDIG_2$** (see chapter 5.3.1.1).

Figure 6.3 shows their fluorescence intensity as a function of excitation and emission wavelength, I(λ_{ex}, λ_{em}) (J&M Tidas spectrometer) in tetrahydrofurane. The neat solvent shows no fluorescence, the weak signal for $\lambda_{ex} = \lambda_{em}$ is due to scattering (Figure 6.3a). For **TdG_2** (Figure 6.3b), a small signal for λ_{ex} between 430 nm and 500 nm is seen probably due to contamination. This wavelength region is not of interest for this study and **TdG_2** represents a non-fluorescent reference. Figure 6.3c) shows that **$PDIG_2$** fluoresces for λ_{ex} between 510 nm and 700 nm with a maximum in the fluorescence intensity at λ_{em} = 600 nm as can be seen in Figure 6.3d) where the intensity is shown for λ_{ex} = 457 nm as a function of λ_{em}.

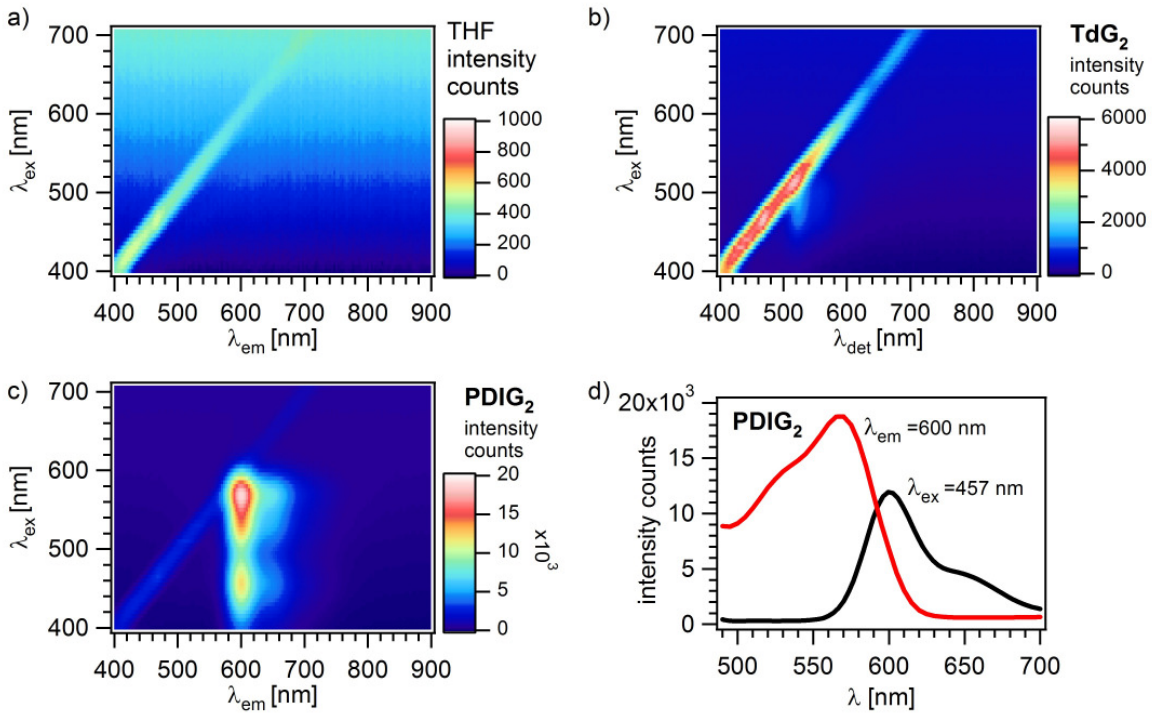

Figure 6.3: Fluorescence intensity as a function of λ_{ex} λ_{em}. a) Solvent Tetrahydrofurane (THF), b) TdG_2 2 µM in THF and c) $PDIG_2$ 1 µM in THF. d) Emission spectrum (black) at λ_{ex} = 457 nm and excitation spectrum (red) at λ_{em} = 600 nm for $PDIG_2$. (These measurements were done by Marcus Schmelzeisen).

6.4 Sample characterization

Figure 6.4a) shows the samples fabricated for the silver sphere-on-plane systems with evaporated surfaces. Eight different samples were investigated. One set of samples was fabricated with the molecule **TdG_2** as a reference. The other set with the molecule **$PDIG_2$** was fabricated simultaneously exchanging only the spacer used during the sample preparation. Two different silver colloid suspensions with different radii distribution were used. They will be called yellow or brown due to the color the suspension shows. Figure 6.4b) shows scanning electron micrographs of the samples with nanoparticles. The bright white spots are the silver nanoparticles. For the representation, only one micrograph with high resolution is shown. The statements here are however based on an analysis of various micrographs taken at different scales. The nanoparticles are not monodisperse. A huge variety of forms are formed during the fabrication with different axis lengths. The nanoparticles are in general well separated, with a low surface coverage. The poor surface coverage is due to the hydrophobic nature of the surface when covered with the spacer whereas the nanoparticles are suspended in water. To characterize the samples the averaged projected area per nanoparticle and the number of nanoparticles per μm^2 was extracted from the scanning electron micrographs (SEM). For the analysis, all micrographs with areas $< 10x10\ \mu m^2$ were used and their values were averaged. The results are listed in Table 6.1. The gray structures seen in the scanning electron micrographs are due to the surface roughness and show the polycrystalline nature of the surface. The sample name is given according to the notation: 'surface-spacer-yellow' or 'surface-spacer-brown' depending on the nanoparticle suspension used.

A smoother silver surface can be fabricated by using TSS. Figure 6.5 shows schematically the four samples fabricated with this type of surface. The problem when using TSS is the fluorescence of the glue EPO-TEK-377 which is used to attach the silver layer to the glass (see Figure 6.2b). To solve this problem, the silver films were made 200 nm thick. In this way either the excitation light from the laser is absorbed before reaching the glue layer or any fluorescence signal from the glue layer is absorbed before reaching the detector. Like in the case of the evaporated surface, two different nanoparticle suspensions were used: the yellow and the brown suspension. Only the spacer **$PDIG_2$** was used. Figure 6.5b) shows scanning electron micrographs from the samples fabricated. Due to the much smoother nature of the surface, now the silver nanoparticles can be easily distinguished as white structures. As in the case for evaporated silver, the surface coverage is poor, the nanoparticles are well

separated and a variety of forms are present as for example the very long rod-like structure seen for TSS- **$PDIG_2$**-yellow. The mean projected area per nanoparticle and the number of nanoparticles per μm^2 is listed in Table 6.1. The gray structures show how the surface is formed by large smooth crystallites.

Figure 6.6a) shows the four samples prepared using gold nanoparticles on TSG. For the gold systems only the spacer **$PDIG_2$** was tested. Two different surface coverages were used: $c_1 = 7$ particles/μm^2 and $c_2 = 24$ particles/μm^2. Again, a thick gold layer of 200 nm was used to absorb the fluorescence signal from the epotek glue (see Figure 6.2c). Figure 6.6b) shows

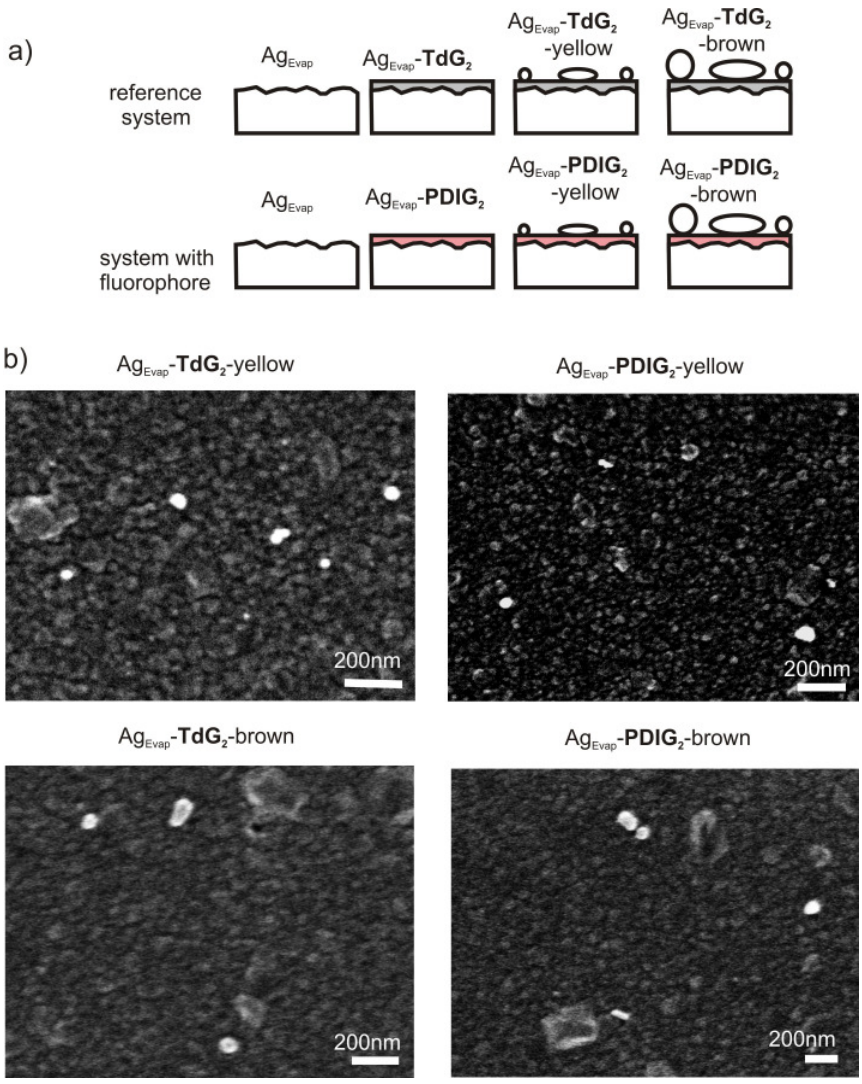

Figure 6.4: a) Schematic of the 8 different samples fabricated with an evaporated silver surface. b) Scanning electron micrographs of the samples with silver nanoparticles.

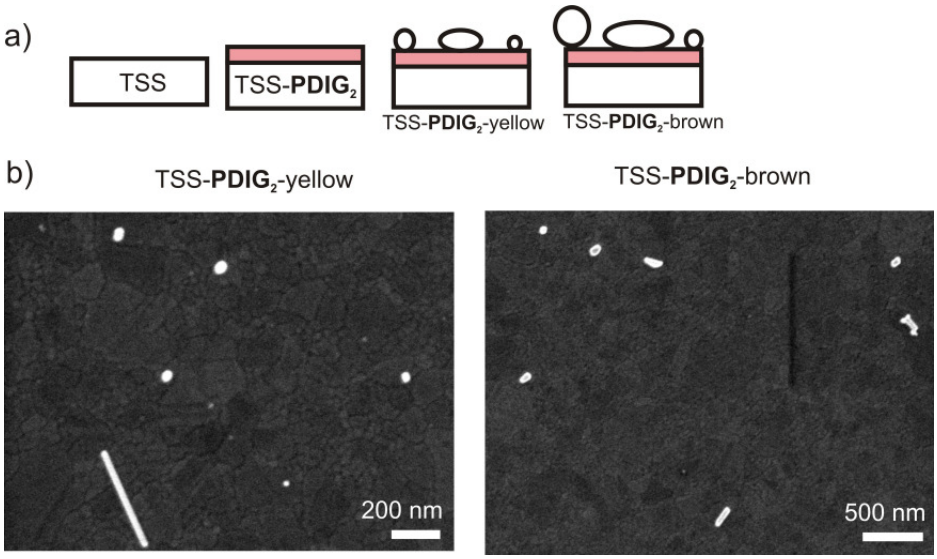

Figure 6.5: a) schematic of the 4 different samples fabricated with a template stripped silver surface. b) Scanning electron micrographs of the samples with silver nanoparticles.

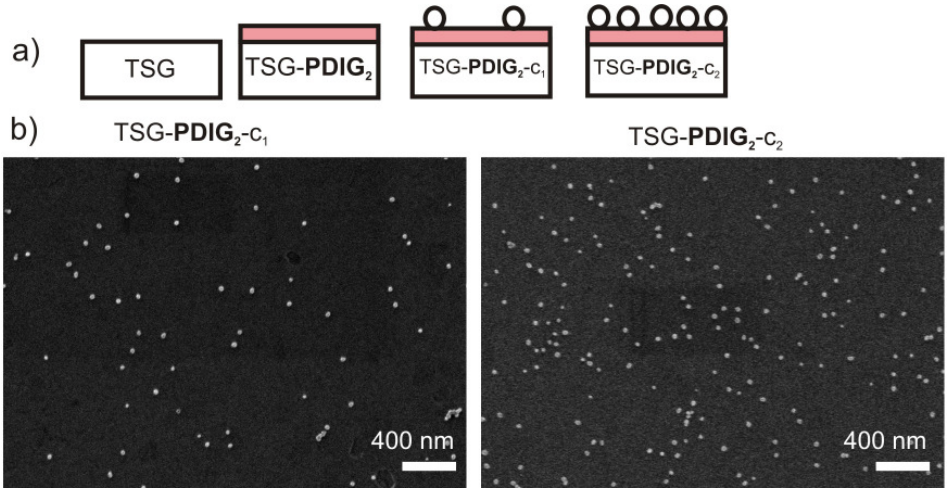

Figure 6.6: a) schematic of the 4 different samples fabricated with a template stripped gold surface. b) Scanning electron micrographs of the samples with gold nanoparticles.

the scanning electron micrographs of the samples with nanoparticles. The white spots are the gold nanoparticles which are well separated and, contrary to the silver nanoparticles, are monodisperse and create a good surface coverage. The better surface coverage is due to the smaller average dimensions of the particles present and the fact that the samples were immersed in the nanoparticle suspension for days. Even though an average radius makes sense in this case, the samples were characterized in the same way as the silver nanoparticles. The average projected area and number of nanoparticles per μm^2 is listed in Table 6.1. In the

case of gold, the surface structure cannot be well seen in the SEM.

Table 6.1 summarizes the values for the projected area per nanoparticle and number of particles per μm^2 for the samples fabricated.

Table 6.1: Number of particles per μm^2 and averaged projected area for the samples

sample	No. particles/μm^2	average projected area x10^{-6} [μm^2]
Ag_{Evap}-**$PDIG_2$**-yellow	0.94	1800
Ag_{Evap}-**$PDIG_2$**-brown	0.30	2950
Ag_{Evap}-**TdG_2**-yellow	0.91	1770
Ag_{Evap}-**TdG_2**-brown	0.40	2050
TSS-**$PDIG_2$**-yellow	1.42	1580
TSS-**$PDIG_2$**-brown	0.43	3860
TSG-**$PDIG_2$**-c1	7	1280
TSG-**$PDIG_2$**-c2	24	1280

6.5 Influence of the surface roughness

The objective is to learn about the field enhancements due to the presence of the particles near the surface. Any enhancement due to other factors has to be excluded. The surface roughness is expected to play a major role because it can create particle-like protrusions on the surface where field enhancements can take place. Furthermore, to ensure that the enhancements are really due to the presence of the perylenediimide core of **$PDIG_2$** and not due to any other chemical or physical properties of the polyphenylene dendrimer molecules, a reference measurement with the molecule **TdG_2** was made for the system with the better enhancement factor (silver nanoparticles on evaporated silver surfaces). The molecule **TdG_2** is similar in chemical composition as **$PDIG_2$** but it has no chromophore core.

The fluorescence spectra were background corrected and smoothed using the Savitzky-Golay method (Savitzky and Golay 1964) which basically performs a local polynomial regression. This smoothing routine preserve features of the distribution such as relative maxima, minima and width, which are usually 'flattened' by other adjacent averaging techniques.

The surface of the samples fabricated was not homogeneous on a nanometer scale. It was seen to have features like scratches and holes. When illuminated with the laser beam some areas were seen to have point scatterers which scattered stronger than other parts of the

surface. To see in how far these surface imperfections influenced the fluorescence spectrum, the fluorescence of the sample was measured at different spots choosing imperfect spots intentionally which could be compared with the signal from spots which apparently looked homogeneous. By correlating the presence of scratches, holes and other imperfections with the form of the fluorescence spectrum it could be assessed whether these played an important role or not.

For the system with silver nanoparticles on an evaporated silver surface each of the eight samples was measured at four different spots. Figure 6.7 shows the fluorescence spectrum measured at each spot for the system with **$PDIG_2$**. The fluorescence of **$PDIG_2$** in solution is shown as reference. The features present in the spot are shown in the sketch below the spectra. Figure 6.7a) shows the signal from the silver surface. No significant change in the signal is seen from spot to spot. When the **$PDIG_2$** molecules is added (Figure 6.7b) a small broad peak at around 600 nm can be seen. Again no significant change in the signal was observed dependent on the spot chosen. When the smaller (yellow) nanoparticles are added (Figure 6.7c), there is no significant increase of the fluorescence signal. With the bigger nanoparticles the increase of the signal is clear (Figure 6.7d). In this case, the form of the signal is similar from spot to spot but its magnitude changes slightly. No correlation with the surface inhomogeneity was found. For example in Figure 6.7d) a spot with a crack (spot 3) was measured. In this spot the signal's magnitude was lower as in the homogeneous spot (spot 1) contrary as it would be expected if the surface roughness plays a major role. The peak at 532 nm is due to the laser light used for the excitation. A small peak can be seen in every spectrum at around 610 nm and is due to the laser. This could be verified by measuring the signal when the glass substrate was illuminated showing that this peak is not originated by any features from the surface. The small negative values at each side of the laser line are created by the smoothing routine. These measurements show that despite the huge surface roughness, this factor is not playing the major role in the fluorescence enhancement. A strong, reproducible effect is seen when the bigger (brown) nanoparticles are added. The background signal without nanoparticles is low despite the surface roughness.

Figure 6.8 shows the results with **TdG_2** as a spacer, used as a reference. The signal does not change significantly from spot to spot and from sample to sample. The addition of the nanoparticles does not change the signal significantly. The absence of any signal due to

fluorescence shows that the enhancement signal seen in Figure 6.7d) is entirely due to the presence of **$PDIG_2$**.

Figure 6.9 shows the fluorescence from five different spots of each of the samples with silver nanoparticles on a template stripped silver surface. Figure 6.9a) shows the results for the reference template stripped silver surface. Four of the spots show very similar signals. However, spot 5 shows a huge increase of the signal showing a peak with maximum at around 600 nm. This signal is the fluorescence signal from the EPO-TEK glue. The presence of the signal from the glue is probably due to deep scratches in the gold film leaving the glue layer uncovered. Figure 6.9b) shows the results when the **$PDIG_2$** spacer is added. A slight change of the signal is seen depending on the spot measured. Spot 5 shows clearly the fluorescence signal of **$PDIG_2$**. When the nanoparticles are added, the fluorescence signal from **$PDIG_2$** can be seen. Considerable changes in the intensity can be seen from spot to spot (Figure 6.9c). With the bigger nanoparticles (Figure 6.9d) the signal becomes independent of the spot showing only slight changes in intensity. For the systems with a TSS, some spots show considerable increase of the fluorescence signal due to features of the surfaces and the EPO-TEK glue which are superimposed on the effect due to the sphere-on-plane field enhancements.

The effects due to the presence of EPO-TEK glue can be easily seen due to the fact that its fluorescence spectrum has a different form as the spectrum from **$PDIG_2$**. Although TSS has less surface roughness, the presence of the glue and the increase in sample manipulation in the fabrication steps for the template stripping makes the samples more inhomogeneous than the samples prepared by evaporation making them less appropriate for ensemble measurements.

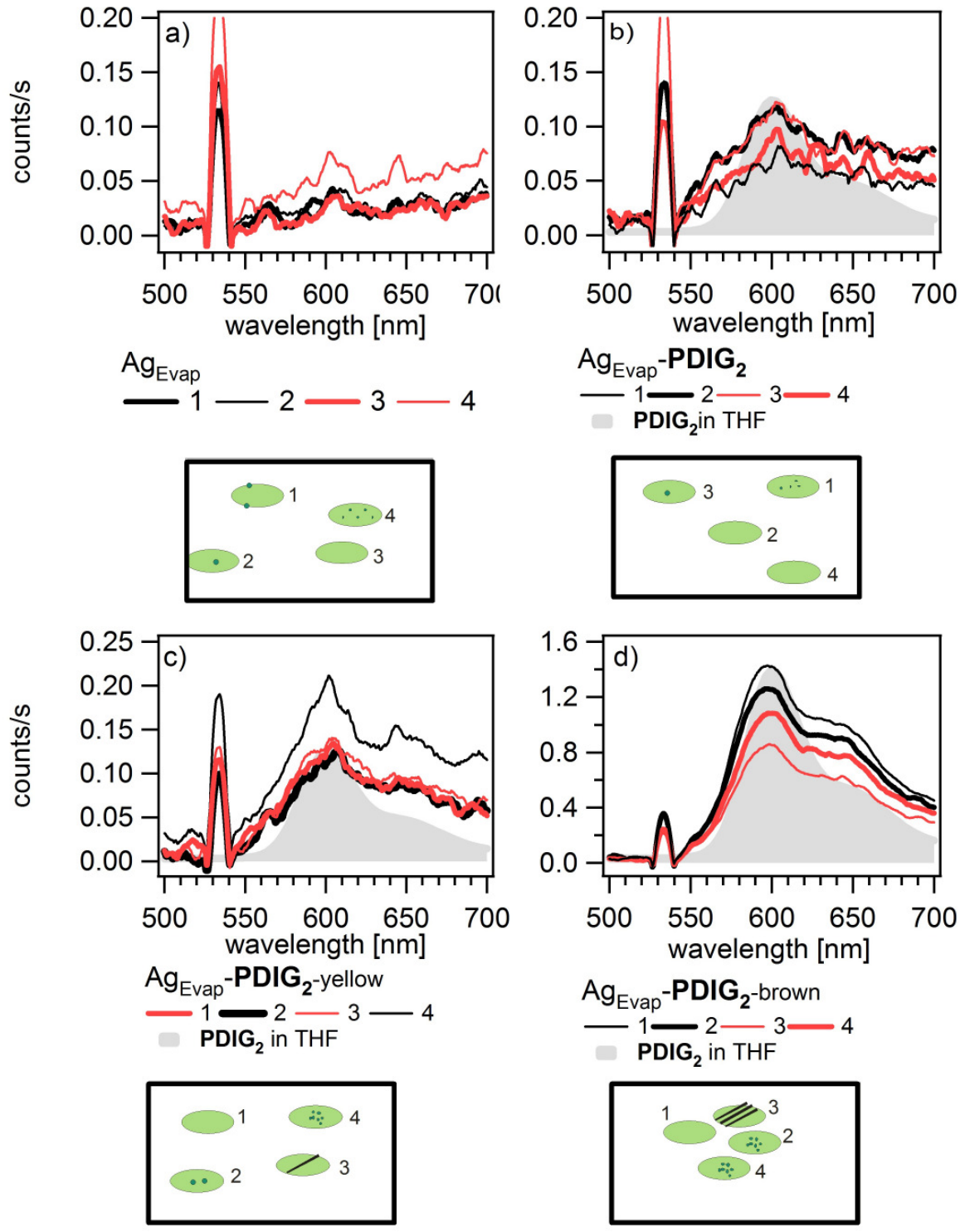

Figure 6.7: Fluorescence spectrum at different sample positions for a) Ag_{Evap}, b) Ag_{Evap}-$PDIG_2$, c) Ag_{Evap}-$PDIG_2$-yellow and d) Ag_{Evap}-$PDIG_2$-brown. The fluorescence of $PDIG_2$ in solution is shown as reference in light grey.The sketch shown at the bottom illustrates the features found in the illuminated area. The elliptical light green shaded area represents the laser spot. The small dark green spots symbolize the scatter sources. The lines in c) and d) represent scratches of the surface.

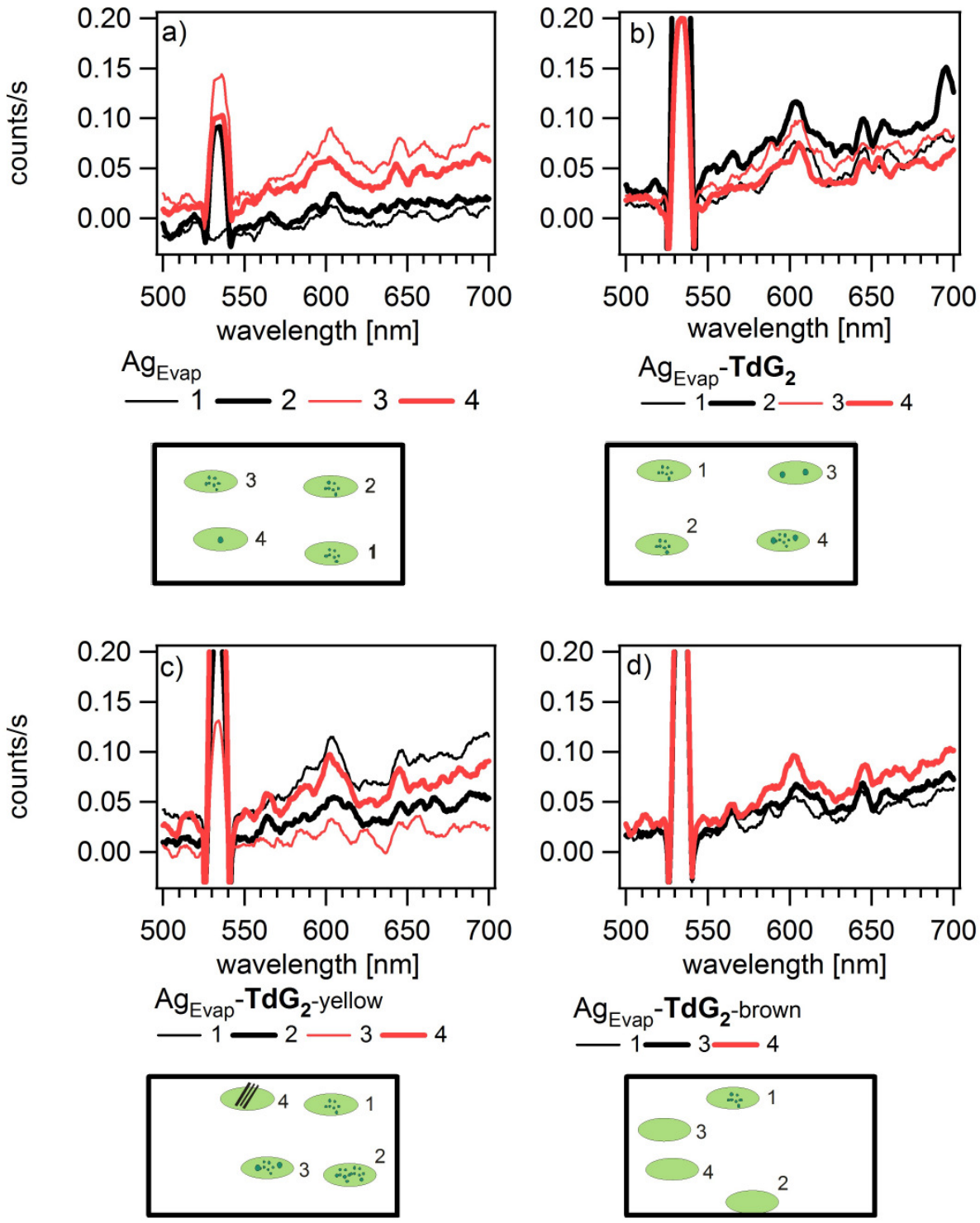

Figure 6.8: Fluorescence spectrum at different sample positions for a) Ag_{Evap}, b) Ag_{Evap}-TdG_2, c) Ag_{Evap}-TdG_2-yellow and d) Ag_{Evap}-TdG_2-brown. The sketch shown at the bottom illustrates the features found in the illuminated area. The elliptical light green shaded area represents the laser spot. The small dark green spots symbolize the scatter sources. The lines represent scratches on the surface.

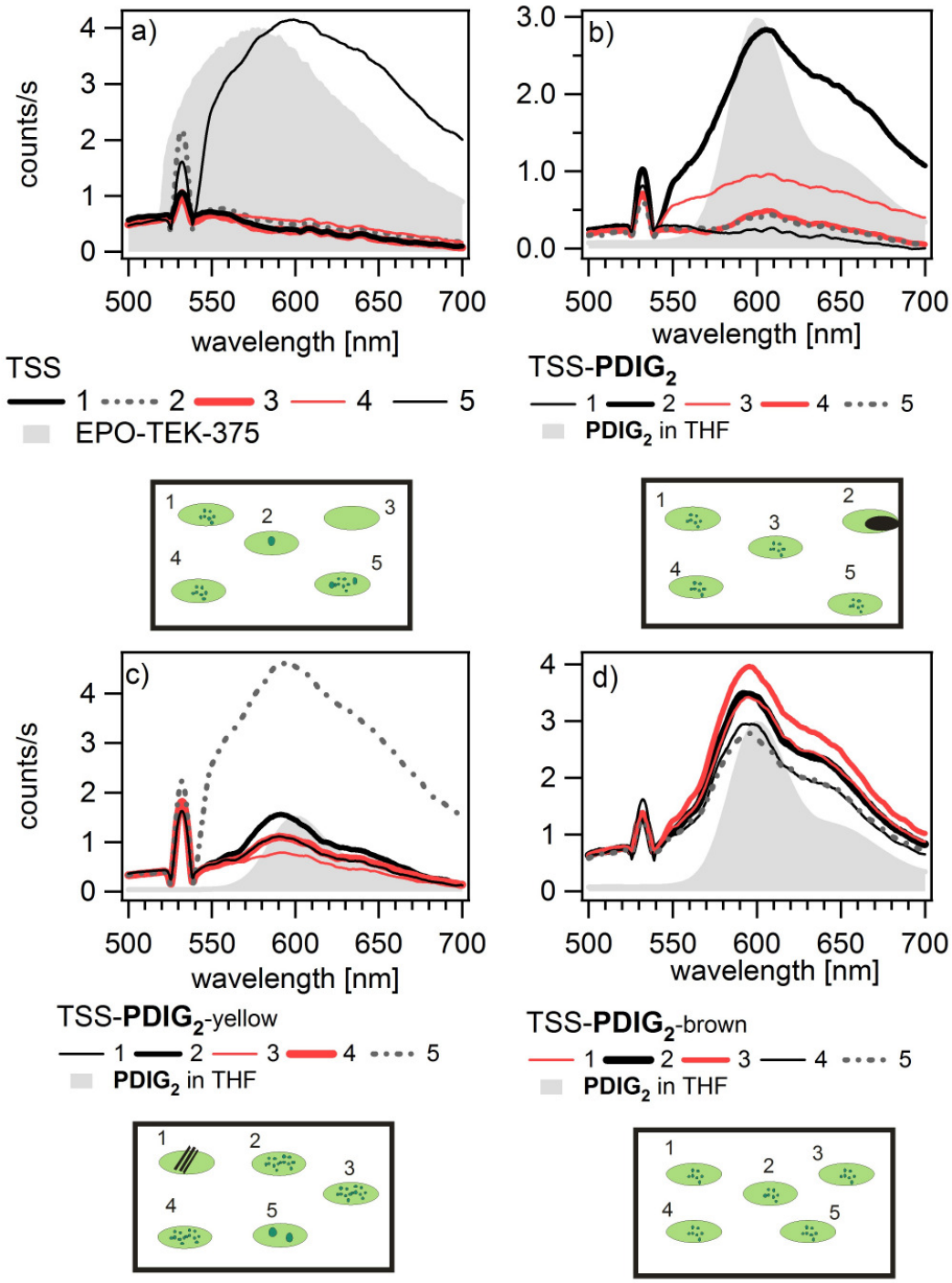

Figure 6.9: Fluorescence spectrum at different sample positions for a) TSS, b) TSS- $PDIG_2$, c) TSS-$PDIG_2$-yellow and d) TSS- $PDIG_2$-brown. In a), the fluorescence spectrum of the EPO-TEK-375 glue is shown for comparison in light grey. In b), c) and d) the fluorescence of $PDIG_2$ in solution is shown as reference in light grey. The sketch shown at the bottom illustrates the features found in the illuminated area. The elliptical light green shaded area represents the laser spot. The small dark green spots symbolize the scatter sources. The lines represent scratches on the surface. The black circle in b) represents a hole in the surface.

Figure 6.10) shows the fluorescence spectra from three different spots measured on the systems with gold nanoparticles on the TSG surface. Figure 6.10a) shows the results for

the bare surface. As seen before with the TSS surface, the spectra depend on the spot measured. Additionally, during the chemical separation of the mica from the gold surface, mica rests are left on the surface (spot 3 of Figure 6.10a, mica symbolized by a red circle). These small rests are distributed along the entire surface and cannot be generally avoided a priori when choosing spots. The signal form does not change but its magnitude is changed on spot 3. Figure 6.10b) shows the results when the **$PDIG_2$** is added. Two spots show similar fluorescence signals. One of the spots shows clearly the signal due to the **$PDIG_2$** fluorescence. When the nanoparticles are added (Figure 6.10c and 6.10d) the signal becomes independent of the spot measured, showing only slight changes in the intensity. No considerable increase of the signal was seen for the higher concentration sample. A systematic increase of the signal for increasing detection wavelength is seen for all samples. The reasons for this increase are unknown.

As for the TSS surface, it must be concluded that the sample manipulation to fabricate the TSG layer makes this surface inappropriate for ensemble measurements. In particular, the presence of mica rests on the surface creates a big problem.

6.6 Enhancement

For the following, representative spots are selected to compare the signal form and intensity between the samples with and without nanoparticles. Figure 6.11 shows a summary of the experiments.

Figure 6.11a) shows a comparison between spot 1 from all the samples for the spacer **TdG_2**. Fully reproducible measurements were obtained independent of the presence of the nanoparticles. No fluorescence enhancement is seen demonstrating that the increase of the signal when using **$PDIG_2$** is entirely due to the fluorescence of its chromophore core. Figure 6.11b) shows a comparison between spot 1 from all the samples for the spacer **$PDIG_2$**. A clear fluorescence enhancement is seen which only occurs in the presence of the silver nanoparticles and which is at least 11 times higher than the signal obtained with the surface without nanoparticles. The measurements are fully reproducible. The background signal is very low in spite of the surface roughness

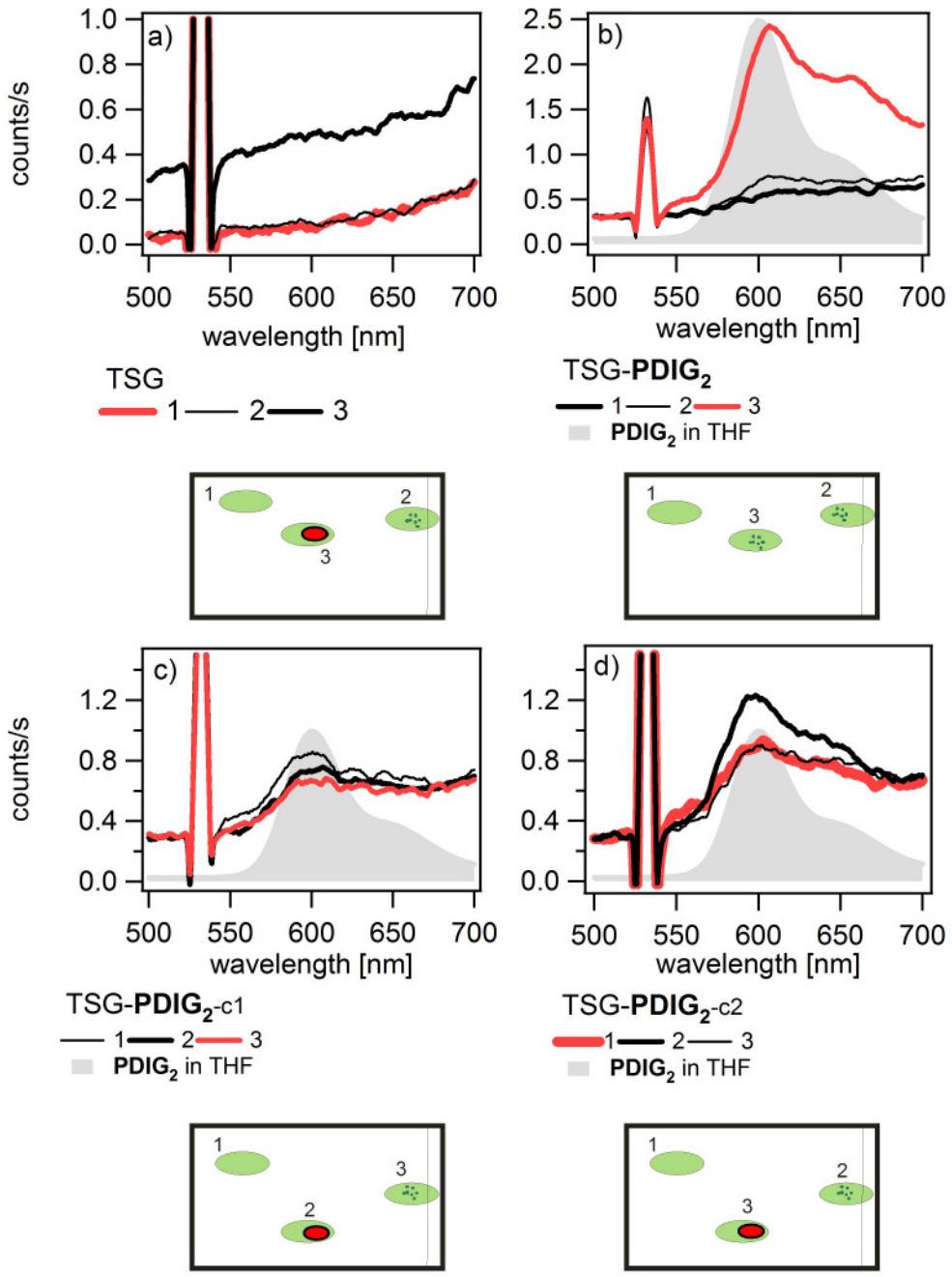

Figure 6.10: Fluorescence spectrum at different sample positions for a) TSG, b) TSG-$PDIG_2$, c) TSG-$PDIG_2$-33-c1 and d) TSG- $PDIG_2$-33-c2. The fluorescence of $PDIG_2$ in solution is shown as reference in light grey. The sketch shown at the bottom illustrates the features found in the illuminated area. The elliptical light green shaded area represents the laser spot. The small dark green spots symbolize the scatter sources. The lines near the edge symbolize the edge of the gold surface. Spots 3 in a), 2 in c) and 3 in d) had mica rests on the surface, symbolized by the red colored circle.

Figure 6.11c) shows a comparison of the measurements done with TSS which possesses a nominally smoother surface. Already without silver nanoparticles the fluorescence signal from **$PDIG_2$** can be seen. Large variations of the signal were obtained from spot to spot which makes the quantification more difficult but the fluorescence enhancement due to the

addition of the nanoparticles can be clearly seen. Figure 6.11d) shows the measurements done with gold nanoparticles on TSG surfaces. Again, as with TSS, already without nanoparticles the fluorescence signal from **$PDIG_2$** can be seen providing a poor reference. Not much increase of the fluorescence signal is observed upon addition of the nanoparticles despite the higher concentration of gold nanoparticles in the surface compared to the silver samples.

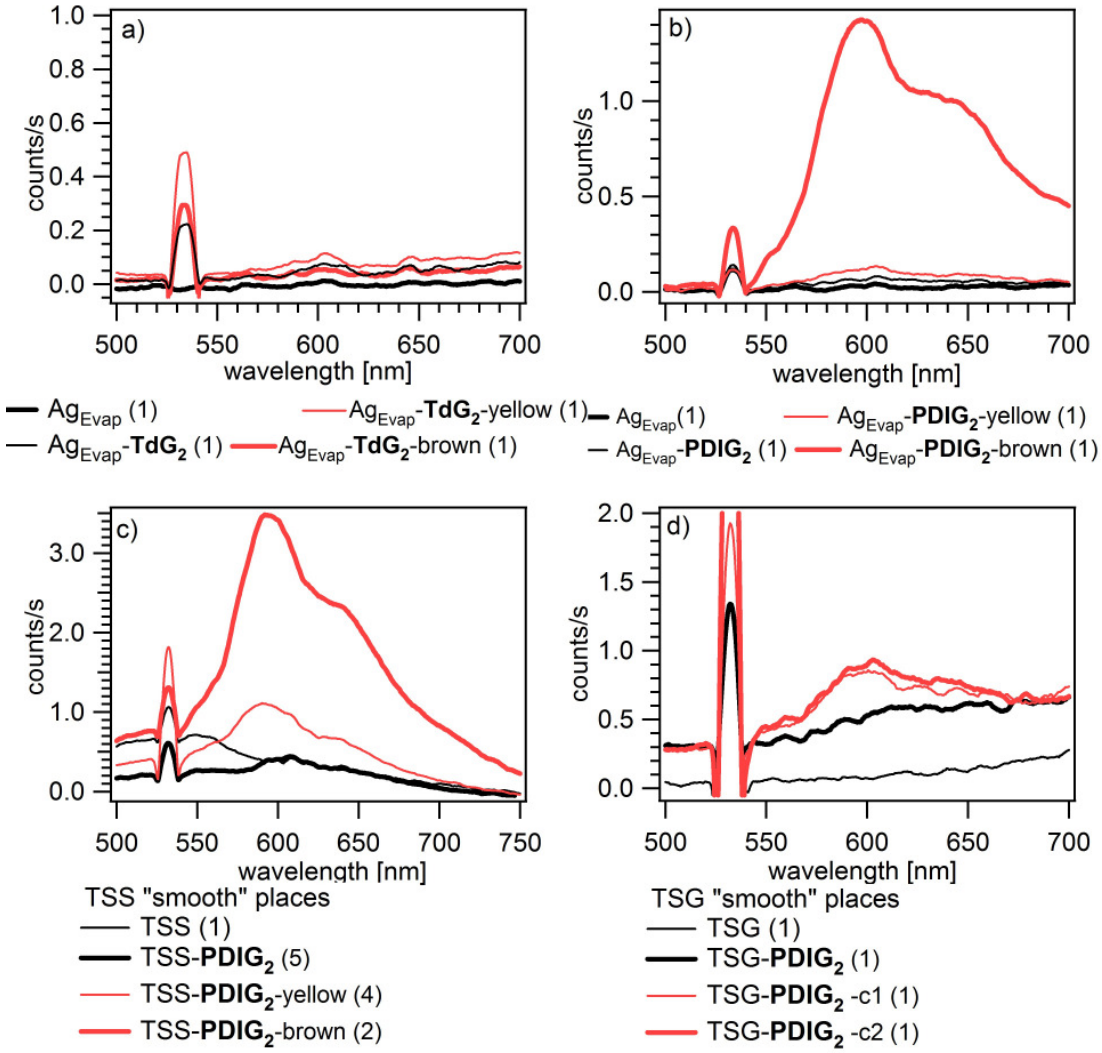

Figure 6.11: a) Signal from spot 1 for the system with evaporated silver surface with TdG_2 and b) with $PDIG_2$. c) Signal from the spots indicated in brackets for the system with template stripped silver surface and with d) template stripped gold surface.

The raw data does not give too much information on the enhancements effects since the particle concentration is not considered. One can only calculate enhancements relative to dyes very close to the metal, where it is almost perfectly quenched. A rough estimate for an "effective enhancement factor" EF, for the molecules experiencing an enhancement can be calculated according to:

$$EF = \frac{\text{Intensity with np}}{\text{Intensity without np}} \tag{6.1}$$

with np standing for nanoparticle. It is important to note that only a small fraction of the surface is covered by colloids and only a small fraction of the dyes experience an enhancement. Taking into account the surface coverage:

$$EF = \frac{\left(\frac{\text{Intensity measured with np}}{A_{covered}}\right)}{\left(\frac{\text{Intensity measured without np}}{A_{illuminated}}\right)} = \underbrace{\frac{\text{Intensity measured with np}}{\text{Intensity measured without np}}}_{IR} \cdot \underbrace{\frac{A_{illuminated}}{A_{covered}}}_{AR} \tag{6.2}$$

with $A_{covered}$ the effective surface area covered by the nanoparticles and $A_{illuminated}$ the total illuminated area. The ratio $A_{covered}$ / $A_{illuminated}$ can be calculated by multiplying the number of particles per μm^2 and the average area per nanoparticle listed in Table 6.1. The maximum measured intensity with nanoparticles was extracted from the fluorescence spectra of the samples with nanoparticles shown in Figure 6.11 at around 600 nm where the maximum fluorescence of **$PDIG_2$** takes place. The intensity without nanoparticles was extracted from the corresponding reference spectrum of the sample with spacer. The enhancement factors for the three different systems are shown in Table 6.2. The effective enhancement factor calculated in this way is a lower estimate when a background enhancement induced by the surface is present.

The greatest enhancement factors are achieved with the brown silver nanoparticle suspension which contains bigger nanoparticles in average. Surprisingly, the rough evaporated surface shows a better enhancement factor as the smooth TSS surface. The gold systems show a lower enhancement factor. This is not surprising, a better enhancement factor is expected for silver systems (Aravind and Metiu 1983).

Table 6.2: Enhancement factor calculated according to equation 1. The abbreviation np stands for nanoparticle. The abbreviations IR and AR stand for intensity and area ratio correspondingly (see equation 2).

sample	Intensity without np[counts/s]	Intensity with np [counts/s]	IR	AR [x10^2]	EF [x10^3]
Ag_{Evap}-**$PDIG_2$**-yellow	0.063	0.112	1.8	5.91	1.1
Ag_{Evap}-**$PDIG_2$**-brown		1.426	22.6	11.3	25.6
TSS-**$PDIG_2$**-yellow	0.390	1.099	2.8	4.45	1.3
TSS-**$PDIG_2$**-brown		3.474	8.9	6.03	5.4
TSG-**$PDIG_2$**-c1	0.545	0.842	1.5	1.18	0.2
TSG-**$PDIG_2$**-c2		0.928	1.7	0.32	0.05

Besides the change in intensity of the fluorescence due to the strong electromagnetic effects taking place in the gap, a change in the spectral profile of the fluorescence emission has been reported (Le Ru, Etchegoin et al. 2007; Trugler and Hohenester 2008) which is not due to any modifications of the energy levels of the emitter but entirely due to the coupling to the electromagnetic resonances. A small blue shift of about 10 nm is observed which appears only when the nanoparticles are added (compare in Figures 6.7, 6.9 and 6.10 the respective graphs b) and d)). The spectrum of **$PDIG_2$** in solution has two maxima, one at around 600 nm and a small second peak at around 650 nm. The intensity ratio between these peaks changes when measured at the surface but is not due to the presence of the nanoparticles because it is seen also in the reference spectra with spacer. Nevertheless, no drastic change in the spectrum of **$PDIG_2$** was observed probably due to the great variation in particle size which creates variations in the gap resonances throughout the sample.

6.7 Conclusions

Sphere-on-plane systems were fabricated using the polyphenylene dendrimer **$PDIG_2$** which contains in its core the chromophore perylenediimide. This unique feature of the spacer allows for the fabrication of systems in which a chromophore can be accurately positioned exactly in the gap where the near field enhancements of the sphere-on-plane systems is expected to take place. A systematic variation of the metal used, the sample's surface roughness and the size of the colloids added was done. Some increase in fluorescence upon

decoration with colloids is seen in all cases. In spite of its roughness, the evaporated silver surface efficiently quenches the fluorescence of a **$PDIG_2$** monolayer while the smoother template stripped surface apparently has some defects. The same can be said for the template stripped gold surface. Decoration with large silver crystallites leads to the most pronounced fluorescence enhancements while smaller silver crystallites are less efficient. Some small changes are seen in the emission spectrum of **$PDIG_2$** compared with the spectrum in solution. No surface enhanced Raman scattering signal was observed. A most promising sample architecture for the study of field enhancements was identified which not only shows high enhancement factors but has the incredible advantage to be simple to fabricate and characterize.

6.8 Acknowledgements

[Removed]

7 Conclusions

In this work, a contribution towards a quantitative understanding of the electromagnetic resonances of metallic sphere-on-plane systems with sub-wavelength dimensions was presented. Even though these systems have been studied in the past, the understanding remained always qualitative due either to an undefined geometry of the sample architecture or due to the ambiguity when determining the gap thickness and dielectric environment of the system simultaneously.

As a contribution towards a better defined geometry of the system, sphere-on-plane systems utilizing a more versatile class of molecules as the commonly used alkanethiols were successfully fabricated. A great challenge when fabricating sphere-on-plane systems are the very small gaps needed (-3 nm). Polyphenylene dendrimers proved to be a good choice for a molecular spacer due to their outstanding rigidity and size. Furthermore, they can be functionalized to include chromophores in their cores which can be accurately positioned in the gap of the sphere-on-plane systems.

Investigations were done on smooth and rough gold films before decoration with spheres to see how the surface roughness affected the description of the film as a single layer. Two gold films were prepared with a smooth and a rough side which were as similar as possible. Both were characterized by surface plasmon spectroscopy in Kretschmann-configuration. Even though in an unambiguous way surface plasmon spectroscopy is unable to resolve inhomogenities in the metal film, it could be shown that it is not necessary to know the depth dependence of the dielectric function in the metal film if the experimental goal is the optical investigation of thin adlayers as is the case in this work. Hence, the metal film can be modeled as a single layer without compromising the results obtained for the thickness of the adlayer.

The use of multi-wavelength surface plasmon spectroscopy in Kretschmann-configuration as a tool to study quantitatively the optical response of sphere-on-plane systems was established. Qualitatively, the resonances lead to characteristic changes in the surface plasmon dispersion. For a quantitative study, an analysis was proposed in which the sphere-on-plane resonators are treated as an effective layer for which the polarisability pro unit area α/A is extracted. This analysis avoids the ambiguity in the choice of a thickness for the effective layer and

constitutes a better defined physical quantity. In this respect, this new approach constitutes a contribution not only for the study of sphere-on-plane systems but for any kind of system provided it meets the criteria discussed in detail in chapter 4.

Using this technique, a systematic study of the sphere-on-plane systems was conducted changing three parameters. By changing the spacer molecule used, the sphere radius and the surrounding medium, a quantitative agreement of the resonance wavelength of the system was found with a simple analytical model. The influence of the dielectric function of spacer and surrounding on the resonance wavelength was found to contribute with approximate equal weight even though the spacer has a considerably smaller volume. An analytical description of the system is only possible if the difference in optical response between spacer and ambient is neglected. An extrapolation scheme based on this analytical description was developed that allows for an estimation of the effect of the spacer. Most important, in combination with surface plasmon spectroscopy the gap distance and spacer dielectric function could be determined without adjustable parameters allowing for an unambiguous determination of the gap thickness and dielectric function. This is surprising since both geometrical imperfections and corrections to the description of the material in terms of a constant dielectric function could be expected. Maybe different effects compensate each other in the overall response.

As a proof of principle, to show that not only it is possible to use a polyphenylene dendrimer with a chromophore core as a rigid molecule to create sphere-on-plane systems supporting gap resonances, but that the chromophore present in its core can be used as a probe for the fields present in the gap. Preliminary experiments were performed to see in how far the fluorescence of these molecules changed due to the sphere-on-plane interaction and surface roughness. The experiments were done using different surface roughness and different types of metals. It could be shown that these systems constitute a promising system for further studies of the field enhancements present on sphere-on-plane systems. A systematic study of these systems in which the nanoparticle size and excitation wavelength is changed should be carried on.

Appendix A

A.1 Synthesis of $PDIG_2$

The polyphenylene dendrimer **$PDIG_2$** was synthesized by Dr. Roland Bauer who provided the following information. The first step in which the first generation dendrimer (**3**) (see Figure A.1) is synthetized was taken from (Qu, Zhang et al. 2004).

The perilenediimide core (PDI) (**1**) was prepared according to (Herrmann, Weil et al. 2001; Qu, Pschirer et al. 2004). Starting from this fluorescent core the first generation dendrimer (**3**) bearing ethynyl groups was prepared by Diels-Alder addition of the cyclopentadienone (**2**) substituted with ethynyl groups deactivated by silyl substituents followed by deprotection (Ito, Wehmeier et al. 2000). For the building up of the second generation an eightfold Diels-Alder cycloaddition of the methoxy-functionalised tetraphenylcyclopentadienone (**4**) was done to obtain the dendrimer having 16 methoxy-groups at its periphery. The same solvents as for the formation of the first generation are employed. Subsequently these methoxy groups underwent a multiple ether cleavage reaction in the presence of an excess of PBr_3 leading to the sixteenfold hydroxyl-functionalised polyphenylene dendrimer (**6**). The latter was then used in a dicyclohexylcarbodiimide-coupling sequence together with the thioctic acid (5-[1,2]dithiolan-3-ylpentanoic acid) (**7**) leading to the final target molecule (**8**). All final compounds and intermediates resembled the characteristic properties of polyphenylene dendrimers and where unambiguously identified by the routine analytical methods.

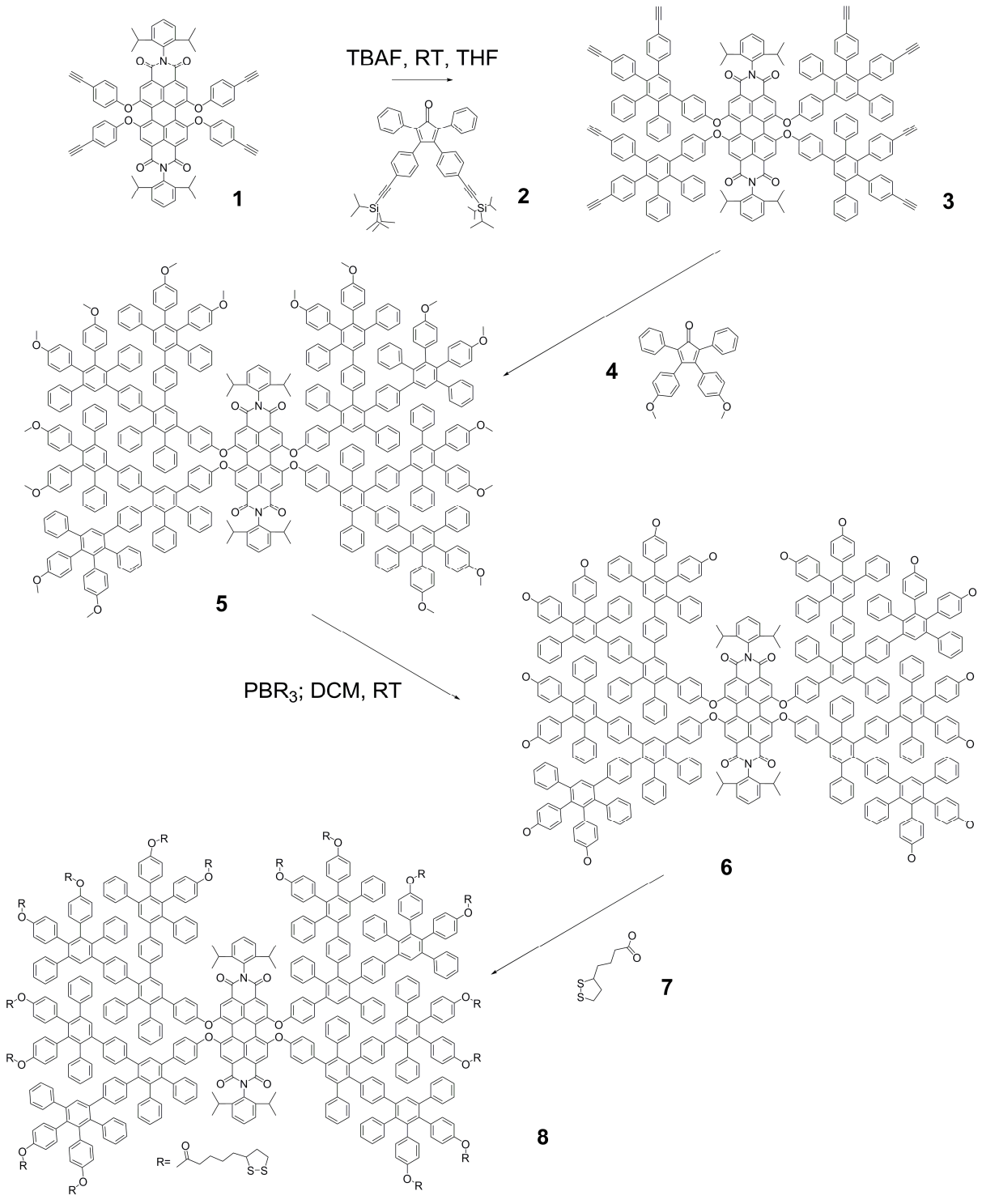

Figure A.1. Synthesis of the polyphenylene dendrimer 8 ($PDIG_2$) with a PDI core and 16 dithiolane units R at the periphery.

A.2 Summary of samples

In this section a summary of all samples used for this study is presented.

A.2.1 Preparation

Table A.1 shows a list of all the samples used in this study. The spacer concentration and submersion time is given together with the method to deposit the nanoparticles. Additionally the nanoparticle radius and area pro resonator estimated from the scanning electron micrographs are listed.

Table A.1: Summary of sample preparation, nanoparticle radius and area pro resonator for every sample used in this study.

Sample name	Spacer	Nanoparticles	Radius [nm]	Area pro Resonator A [μm^2]
AET-11	16 h submersion in 1 mM solution of AET in ethanol	3.5 h submersion	11 ± 1	0.0023
AET-23	16 h submersion in 1 mM solution of AET in ethanol	15 min submersion	23 ± 5	0.10
AET-25	16 h submersion in 1 mM solution of AET in ethanol	8.5 h submersion	25 ± 5	0.10
TdG_2-16	45 min submersion in 1 µM solution of **TdG_2** in THF	1 week submersion	16 ± 5	0.29
TdG_2-19-1	10 min submersion in 2 µM solution of **TdG_2** in THF	0.5 V potential applied for 15 min	19 ± 5	0.10
TdG_2-19-2	10 min submersion in 2 µM solution of **TdG_2** in THF	0.7 V potential applied for 15 min	19 ± 5	0.06
TdG_2-20	10 min submersion in 2 µM solution of **TdG_2** in THF	0.1 V-1 V potentials applied for 15 min	20 ± 4	0.14
TdG_2-23	60 min submersion in 2 µM solution of **TdG_2** in THF	0.5 V potential applied for 15 min	23 ± 5	0.06

Sample name	Spacer	Nanoparticles	Radius [nm]	Area pro Resonator A [μm^2]
TdG_2-75	45 min submersion in 1 µM solution of **TdG_2** in THF	1 week submersion	75 ± 10	1.00
$PDIG_2$-19-1	15 min submersion in 5 µM solution of **$PDIG_2$** in THF	3 ml suspension spin coating at 2000 rpm	19 ± 2	0.06
$PDIG_2$-19-2	15 min submersion in 5 µM solution of **$PDIG_2$** in THF	5 days submersion	19 ± 2	0.01
$PDIG_2$-26	15 min submersion in 1 µM solution of **$PDIG_2$** in THF	1 week submersion	26 ± 5	0.50
$PDIG_2$-29	3 min submersion in 5 µM solution of **$PDIG_2$** in THF	0.5 V potential applied for 15 min	29 ± 5	0.06
$PDIG_2$-30	10 min submersion in 1 µM solution of **$PDIG_2$** in THF	1 week submersion	30 ± 5	0.14
$PDIG_2$-78	15 min submersion in 1 µM solution of **$PDIG_2$** in THF	1 week submersion	78 ± 15	2.00
$PDIG_2$-80	10 min submersion in 1 µM solution of **$PDIG_2$** in THF	1 week submersion	80 ± 25	2.00

A.2.2 Extracted polarisability

Figure A.2 and Figure A.3 show the extracted polarizability for all samples used in this study.

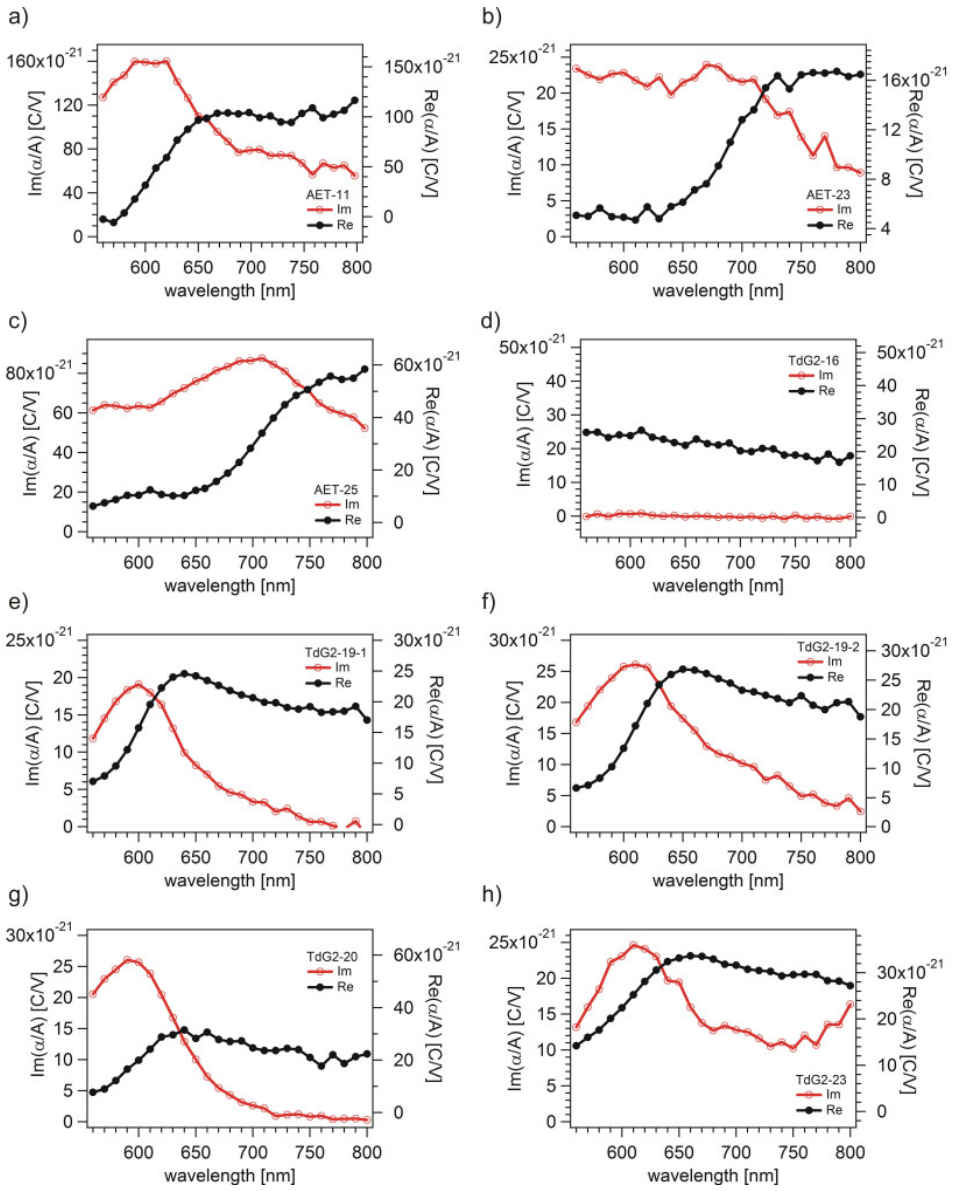

Figure A.2: Polarisability per unit area α/A for all of the samples investigated. a) AET-11 b)AET-23 c) AET-25 d) TdG_2-16 e) TdG_2-19-1 f) TdG_2-19-2 g) TdG_2-20 h) TdG_2-23

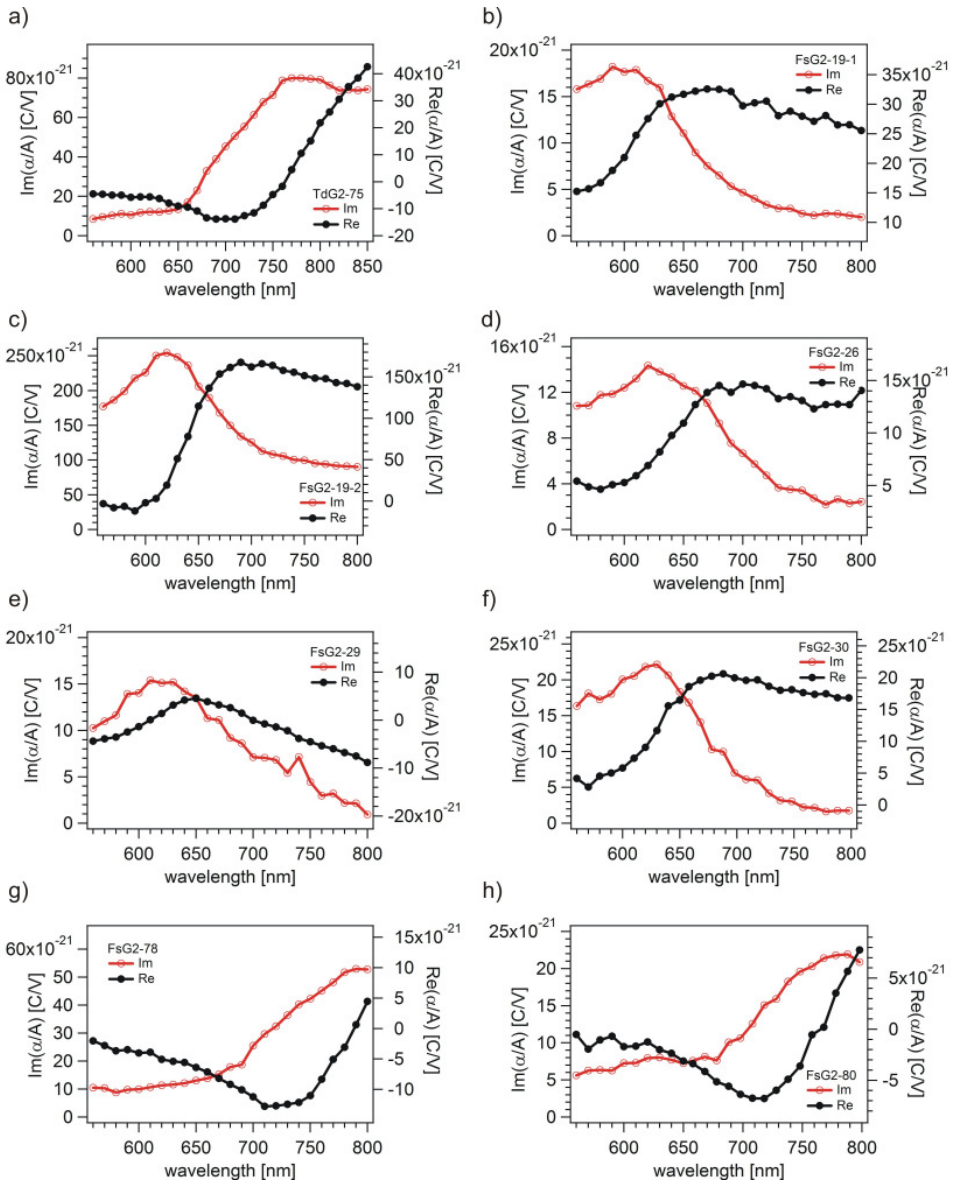

Figure A.3: Polarisability per unit area α/A for all of the samples investigated. a) TdG_2-75 b) $PDIG_2$-19-1 c) $PDIG_2$-19-2 d) $PDIG_2$-26 e) $PDIG_2$-29 f) $PDIG_2$-30 g) $PDIG_2$-78 h) $PDIG_2$-80.

A.3 Spacer layer investigations

A.3.1 AFM

The adsorption of the polyphenylene dendrimers on the gold surface was characterized using atomic force microscopy (AFM). The images were taken in air at room temperature with a commercial AFM (Nanocope IIIa, Veeco) in tapping mode. The dendrimer **TdG_2** was used for these studies. For AET no measurements were done. A gold slice fabricated with the method of template stripping of gold from mica (Butt, Wang et al. 1991; Butt, Müller et

al. 1993; Hegner, Wagner et al. 1993) was dipped in a 1 µM solution of **TdG_2** in tetrahydrofurane for 10 s, 15 min and 2 hours. The topography images for each slide are shown in Figure A.4. The objective was to obtain information about the surface distribution (aggregates, holes, multilayers) of the dendrimer molecules on the surface depending on the dipping time.

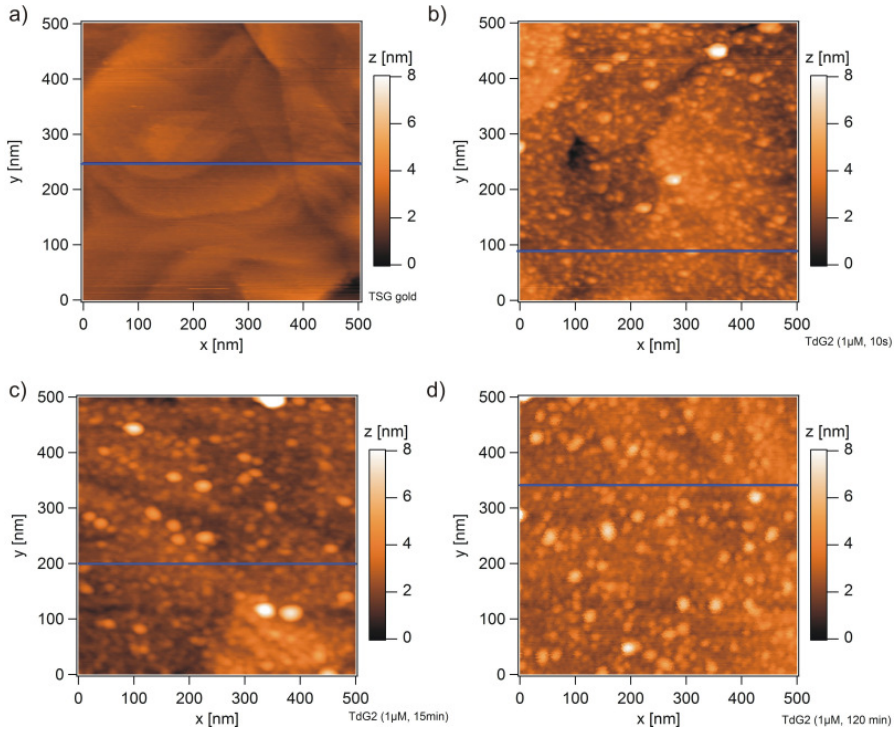

Figure A.4: Atomic force microscope images of a) Reference gold layer and of TdG_2 dipped for b) 10 s, c) 15 min and d) 2 hours in a 1 µM solution in tetrahydrofurane. The blue line indicates the position for the height profile shown in Figure I4.

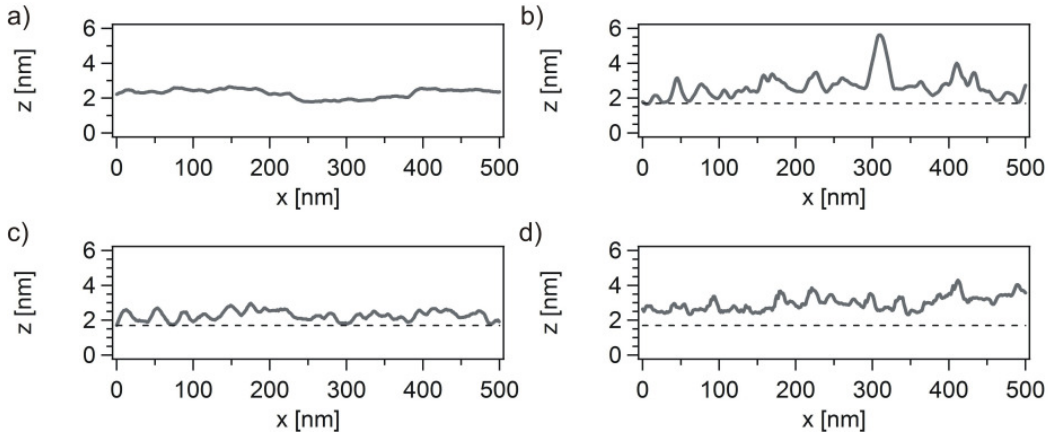

Figure A.5: Height profiles of the AFM images shown in Figure I3 at the y position indicated by the blue line. The dashed line in b), c) and d) shows the height due to the gold roughness.

Figure A.4a) and Figure A.5a) show the AFM image and height profile of the gold surface before dendrimer deposition. Steps approximately 200 nm wide and 1 nm high are seen. These steps are typical for the mica surface. After 10 s in the **TdG_2** solution many bright spots appear on the surface. Some spots are big, approximately 30 nm wide but most of them are approximately 10 nm wide. The height profile (Figure A.5b)) shows for example at $x \approx$ 320 nm one of the wide ones which is 3 nm high approximately. Most of the spots have a height of 1 nm to 1.5 nm. We believe this spots to be the dendrimer molecules which seem to adsorb on the surface in a disordered way. The big spots are probably aggregates. After 15 min slightly more of these aggregates can be seen. Otherwise no much change is observed. The same can be said after 2 hours. The surface roughness after 10 s, 15 min and 2 hours is similar and amounts to approximately 1 nm.

From these results, it seems that after 15 min the surface is covered with a dendrimer layer. Although not a monolayer most of the surface seems to be covered. These results are confirmed by surface plasmon resonance changes as a function of an applied potential to the surface. If the single peaks seen correspond to one dendrimer molecule then the height of the molecule is approximately 1.5 nm to 2 nm. It should be noted that these characterization was done on template stripped gold from mica (roughness 0.3 nm) whereas the gold layer used throughout these work was fabricated by thermal evaporation (roughness 1 nm rms). Nevertheless, the low roughness of template stripped gold allows for the detection of small changes on the surface due to the small dendrimer molecules.

A.3.2 Surface plasmon spectroscopy

In section 5.3.1.3 surface plasmon spectroscopy of the three different spacers was presented. In this section, the variations in the thickness as a function of the wavelength of the incident light are shown. This is important most of all for **$PDIG_2$** for which the chromophore core could influence the optical measurements dependent on the wavelength used. Figure A.6 shows the spacer layer thickness d_{SPR} obtained from the fit setting $\varepsilon_{sp} = 2.25$ fix for AET. The average thickness is dentoed by $< d_{SPR} >$. Variations of d_{SPR} depending on the wavelength are always obtained. Whereas for AET-11 and AET-25 a similar thickness is obtained with small variations from wavelength to wavelength for AET-23 an increase of the thickness for longer wavelengths is observed. This is not related to the concentration of AET used or the

submersion time or with the goodness of the fit given by s^2:

$$s^2 = \frac{\sum_{i=1}^{n} e^2}{n} \qquad \text{(A.1)}$$

Here, $e = R(\theta_i) - R(\theta_i)_{fit}$ where $R(\theta_i)$ is the measured reflectivity value for a given angle θ_i, $R(\theta_i)_{fit} = cR_{calc}(\theta_i)$ is the fitted value at this same angle and n is the total number of points measured.

A value of $s^2 \approx 1\text{x}10^{-4}$ means the fit is good. $<s^2>$ denotes the average value of s^2 for each fit at a fixed wavelength. The thickness of AET was determined using the results from AET-11 and AET-25.

Figure A.7 shows the spacer layer thickness d_{SPR} obtained from the fit setting $\varepsilon_{sp} = 2.25$ fix for **PDIG$_2$**. Only the results from **PDIG$_2$**-78 and **PDIG$_2$**-80 were taken into account. For **PDIG$_2$**-19 the goodness of the fit is low and for **PDIG$_2$**-29 huge variations from wavelength to wavelength were observed. The thickness of **PDIG$_2$** was determined using the results from **PDIG$_2$**-78 and **PDIG$_2$**-80.

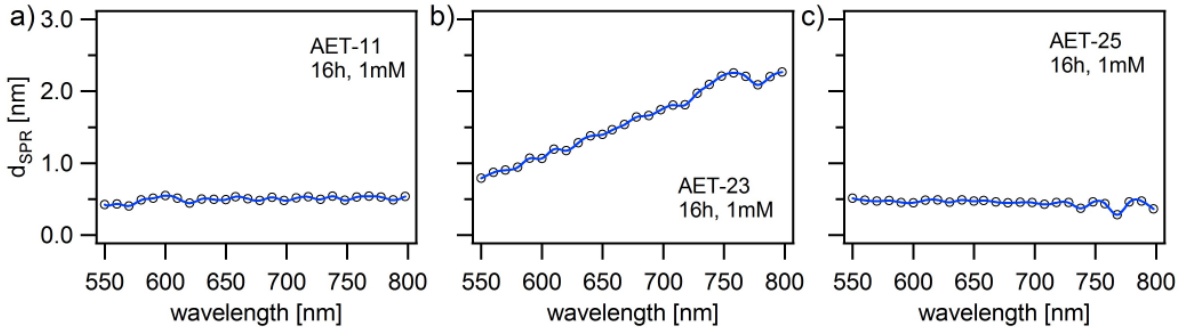

Figure A.6: d_{SPR} as a function of wavelength for AET a) $<d_{SPR}> = 0.49 \pm 0.04$, $<s^2> = 4\text{x}10^{-5}$ b) $<d_{SPR}> = 1.27 \pm 0.50$, $<s^2> = 8\text{x}10^{-5}$ c) $<d_{SPR}> = 0.44 \pm 0.05$, $<s^2> = 8\text{x}10^{-5}$.

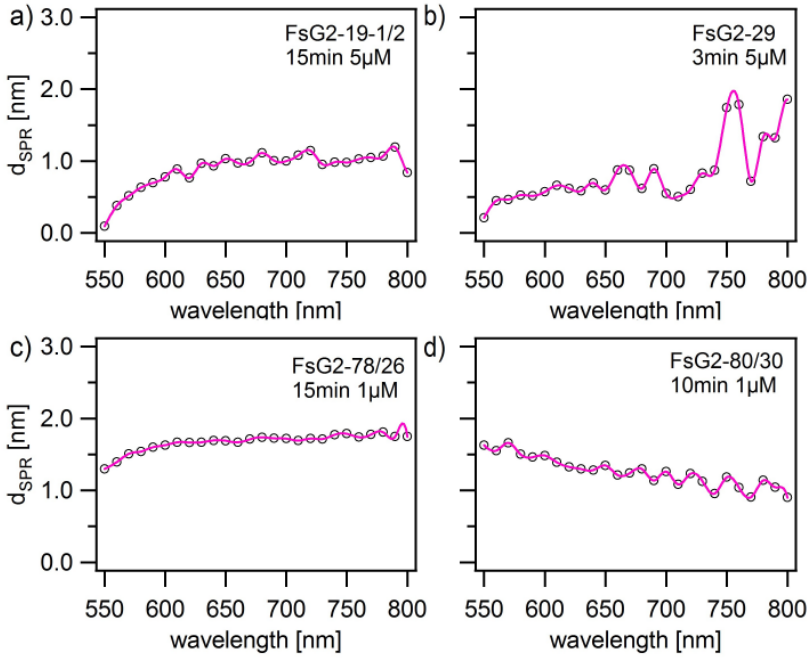

Figure A.7: d_{SPR} **as a function of wavelength for PDIG$_2$ a)** $\langle d_{SPR}\rangle = 0.9 \pm 0.2$, $\langle s^2\rangle = 1.6\text{x}10^{-3}$ **b)** $\langle d_{SPR}\rangle = 0.9 \pm 0.5$, $\langle s^2\rangle = 4\text{x}10^{-5}$ **c)** $\langle d_{SPR}\rangle = 1.6 \pm 0.1$, $\langle s^2\rangle = 1.6\text{x}10^{-4}$ **d)** $\langle d_{SPR}\rangle = 1.2 \pm 0.2$, $\langle s^2\rangle = 2.8\text{x}10^{-4}$.

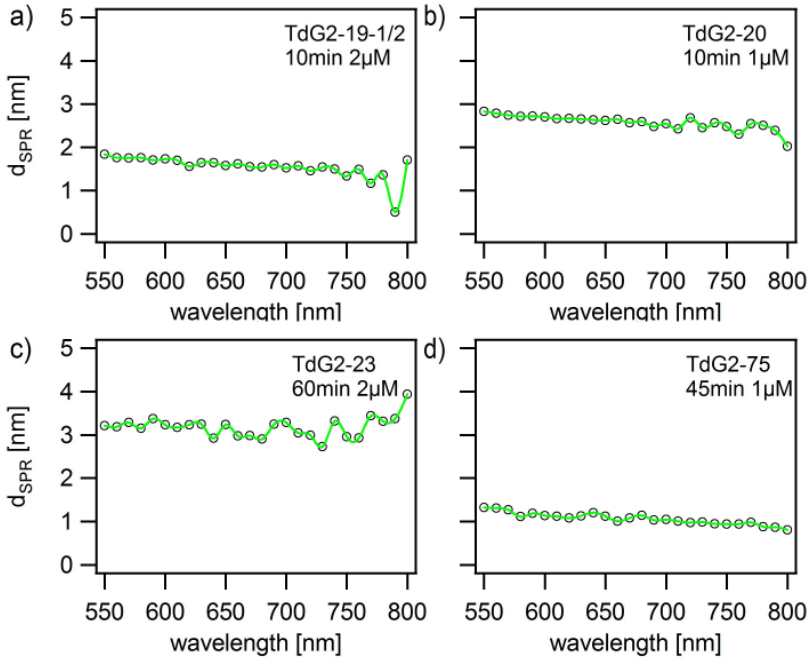

Figure A.8: d_{SPR} **as a function of wavelength for TdG$_2$ a)** $\langle d_{SPR}\rangle = 1.6 \pm 0.2$, $\langle s^2\rangle = 2.8\text{x}10^{-4}$ **b)** $\langle d_{SPR}\rangle = 2.6 \pm 0.2$, $\langle s^2\rangle = 3.2\text{x}10^{-4}$ **c)** $\langle d_{SPR}\rangle = 3.2 \pm 0.2$, $\langle s^2\rangle = 8.0\text{x}10^{-5}$ **d)** $\langle d_{SPR}\rangle = 1.1 \pm 0.1$, $\langle s^2\rangle = 8.0\text{x}10^{-5}$.

Figure A.8 shows the spacer layer thickness d_{SPR} obtained from the fit setting $\varepsilon_{sp} = 2.25$ fix for **TdG$_2$**. For **TdG$_2$** the goodness of the fit was good for the four samples investigated. Nevertheless big variations from the results obtained from sample to sample were

observed. Whereas for **TdG$_2$**-75 and **TdG$_2$**-19 thickness in the order of 1 nm were obtained, **TdG$_2$**-23 and **TdG$_2$**-20 show thicknesses in the order of 3 nm. The thickness of **TdG$_2$** was determined using all results.

List of abbreviations

AC	*Ambient-Colloid model*
AET	*Spacer molecule 2-Aminoethanethiol (see Figure 5.3)*
AFM	*Atomic force microscope*
AIP	*American Institute of Physics*
AR	*Area ratio*
ASpC	*Ambient-Spacer-Colloid model*
BK7	*Type of borosilicate crown glass (K from the German krone=crown)*
CCD	*Charge-coupled device*
EF	*Enhancement factor*
Evap	*Evaporated*
FWHM	*Full width at half maximum*
HPCL	*High performance liquid chromatography*
IR	*Intensity ratio*
J&C	*Johnson and Christy*
LasFN9	*Dense lanthanum flint glass*
NIR	*Near infrared*
np	*Nanoparticle*
PDI	*Perylenediimede dye*
$PDIG_2$	*Spacer molecule. Type of polyphenylene dendrimer. Abbreviation stands for Perylenediimede generation 2*
PPD	*Polyphenylene dendrimer*
rms	*Root mean squared*
SAM	*Self assembled monolayer*
SEF	*Surface enhanced fluorescence*
SEM	*Scanning electron microscope*
SERS	*Surface enhanced Raman scattering*
SNOM	*Scanning near field optical microscope*
SOP	*Sphere-on-plane*
SOP7	*Sample name. Stands for sphere-on-plane sample with 7 particles pro μm^2 (see Figure 4.1)*
SOP22	*Sample name. Stands for sphere-on-plane sample with 7 particles pro μm^2 (see Figure 4.1)*
STM	*Scanning tunneling microscopy*

TdG$_2$	*Spacer molecule. Type of polyphenylene dendrimer. Abbreviation stands for Tetrahedric dendrimer generation 2*
TE	*Transverse electric*
THF	*Tetrahydrofurane*
TM	*Transverse magnetic*
TSG	*Template stripped gold. Type of very smooth gold.*
TSS	*Template stripped silver. Type of very smooth silver*
UV	*Ultraviolet*
Vis	*Visible*

References

Abe, H., K. Manzel, et al. (1981). "Surface-Enhanced Raman-Spectroscopy Of Co Adsorbed On Colloidal Silver Particles." Journal Of Chemical Physics **74**(2): 792-797.

Albrecht, M. G. and J. A. Creighton (1977). "Anomalously Intense Raman-Spectra of Pyridine at a Silver Electrode." Journal of the American Chemical Society **99**(15): 5215-5217.

Anderson, D. J. and M. Moskovits (2006). "A SERS-active system based on silver nanoparticles tethered to a deposited silver film." Journal of Physical Chemistry B **110**(28): 13722-13727.

Anger, P., P. Bharadwaj, et al. (2006). "Enhancement and quenching of single-molecule fluorescence." Physical Review Letters **96**(11): 113002.

Aravind, P. K. and H. Metiu (1983). "The Effects Of The Interaction Between Resonances In The Electromagnetic Response Of A Sphere-Plane Structure - Applications To Surface Enhanced Spectroscopy." Surface Science **124**(2-3): 506-528.

Ashcroft, N. W. and N. D. Mermin (1976). Solid States Physics. USA, Harcourt College Publishing.

Aspnes, D. E. (1982). "Optical-Properties of Thin-Films." Thin Solid Films **89**(3): 249-262.

Aussenegg, F. R., A. Leitner, et al. (1987). "Novel Aspects of Fluorescence Lifetime for Molecules Positioned Close to Metal-Surfaces." Surface Science **189**: 935-945.

Barkowski, S. L. and K. Hedberg (1987). "Conformational-Analysis .11. 2-Aminoethanethiol - an Electron-Diffraction Investigation of the Molecular-Structure, Conformational Composition, and Anti-Gauche Energy and Entropy Differences - Evidence for an Intramolecular Sh...N Hydrogen-Bond." Journal of the American Chemical Society **109**(23): 6989-6994.

Barnes, W. L. (1998). "Fluorescence near interfaces: the role of photonic mode density." J. Modern Optics **45**(4): 661-699.

Bauer, R., D. Liu, et al. (2007). "Polyphenylene dendrimers with pentafluorophenyl units:

Synthesis and self-assembly." Macromolecules **40**(14): 4753-4761.

Bauer, R. E., A. C. Grimsdale, et al. (2005). Functionalised polyphenylene dendrimers and their applications. Functional Molecular Nanostructures**:** 253-286.

Bek, A., R. Jansen, et al. (2008). "Fluorescence enhancement in hot spots of AFM-designed gold nanoparticle sandwiches." Nano Letters **8**(2): 485-490.

Bellessa, J., C. Bonnand, et al. (2004). "Strong coupling between surface plasmons and excitons in an organic semiconductor." Physical Review Letters **93**(3): 036404.

Benner, R. E., P. W. Barber, et al. (1980). "Observation Of Structure Resonances In The Fluorescence-Spectra From Microspheres." Physical Review Letters **44**(7): 475-478.

Bohren, C. F. and R. D. Huffmann (1983). Absorption and Scattering of Light by Small Particles. New York, Wiley and Sons.

Brocorens, P., R. Lazzaroni, et al. (2007). "Molecular modeling simulations of the morphology of polyphenylene dendrimers." Journal of Physical Chemistry B **111**(31): 9218-9227.

Buffat, P. A., M. Flueli, et al. (1991). "Crystallographic Structure of Small Gold Particles Studied by High-Resolution Electron-Microscopy." Faraday Discussions(92): 173-187.

Butt, H. J., T. Müller, et al. (1993). "Immobilizing Biomolecules for Scanning Force Microscopy by Embedding in Carbon." Journal of Structural Biology **110**(2): 127-132.

Butt, H. J., D. N. Wang, et al. (1991). "Effect of Surface-Roughness of Carbon Support Films on High-Resolution Electron-Diffraction of 2-Dimensional Protein Crystals." Ultramicroscopy **36**(4): 307-318.

Chen, Y., K. Munechika, et al. (2007). "Dependence of fluorescence intensity on the spectral overlap between fluorophores and plasmon resonant single silver nanoparticles." Nano Letters **7**(3): 690-696.

Clark, C. G., R. J. Wenzel, et al. (2007). "Controlled MegaDalton assembly with locally stiff but globally flexible polyphenylene dendrimers." Journal of the American Chemical Society

129(11): 3292-3301.

Clark, C. G., R. J. Wenzel, et al. (2007). "Solvophobically-driven 3-D self-assembly of "exploded"-type polyphenylene dendrimers." New Journal of Chemistry **31**(7): 1300-1306.

Debruijn, H. E., B. S. F. Altenburg, et al. (1991). "Determination of Thickness and Dielectric-Constant of Thin Transparent Dielectric Layers Using Surface-Plasmon Resonance." Optics Communications **82**(5-6): 425-432.

Debye, P. (1909). "Der Lichtdruck auf Kugeln von beliebigem Material." Annalen der Physik **335**(11): 57-136.

Dieringer, J. A., A. D. McFarland, et al. (2006). "Surface enhanced Raman spectroscopy: new materials, concepts, characterization tools, and applications." Faraday Discussions **132**: 9-26.

Dintinger, J., S. Klein, et al. (2005). "Strong coupling between surface plasmon-polaritons and organic molecules in subwavelength hole arrays." Physical Review B **71**(3): 035424.

Drexhage, K. H. (1970). "Influence of a dielectric interface on fluorescence decay time." Journal of Luminescence **1-2**: 693-701.

Fano, U. (1938). "Zur Theorie der Intensitätsanomalien der Beugung." Annalen der Physik **424**(5): 393-443.

Faraday, M. (1857). "The Bakerian Lecture: Experimental Relations of Gold (and other Metals) to Light." Philosophical Transactions of the Royal Society **147**: 145-181.

Fedutik, Y., V. V. Temnov, et al. (2007). "Exciton-plasmon-photon conversion in plasmonic nanostructures." Physical Review Letters **99**.

Fischer, U. C. and D. W. Pohl (1989). "Observation Of Single-Particle Plasmons By Near-Field Optical Microscopy." Physical Review Letters **62**(4): 458-461.

Fleischmann, M., P. J. Hendra, et al. (1974). "Raman spectra of pyridine adsorbed at a silver electrode." Chemical Physics Letters **26**(2): 163-166.

Frens, G. (1973). "Controlled Nucleation for Regulation of Particle-Size in Monodisperse

Gold Suspensions." Nature-Physical Science **241**(105): 20-22.

Fuchs, R. and F. Claro (1987). "Multipolar response of small metallic spheres: Nonlocal theory." Physical Review B **35**(8): 3722.

Futamata, M., F. Maruyama, et al. (2004). "Adsorbed sites of individual molecules on Ag nanoparticles in single molecule sensitivity-surface-enhanced Raman scattering." Journal Of Physical Chemistry B **108**(35): 13119-13127.

Futamata, M., Y. Maruyama, et al. (2005). "Critical importance of the junction in touching Ag particles for single molecule sensitivity in SERS." Journal of Molecular Structure **735-36**: 75-84.

Gersten, J. and A. Nitzan (1981). "Spectroscopic Properties Of Molecules Interacting With Small Dielectric Particles." Journal Of Chemical Physics **75**(3): 1139-1152.

Glass, A. M., P. F. Liao, et al. (1980). "Interaction Of Metal Particles With Absorbed Dye Molecules - Absorption And Luminescence." Optics Letters **5**(9): 368-370.

Gray, D. E. (1972). American Institute of Physics Handbook, Mac-Graw Hill.

Hansma, P. K. and H. P. Broida (1978). "Light-Emission From Gold Particles Excited By Electron-Tunneling." Applied Physics Letters **32**(9): 545-547.

Hegner, M., P. Wagner, et al. (1993). "Ultralarge Atomically Flat Template-Stripped Au Surfaces for Scanning Probe Microscopy." Surface Science **291**(1-2): 39-46.

Henglein, F., D. M. Kolb, et al. (1993). "Electroreflectance Spectroscopy of Au(100) Covered by Adsorbed Pyridine Molecules." Surface Science **291**(3): 325-336.

Herrmann, A., T. Weil, et al. (2001). "Polyphenylene dendrimers with perylene diimide as a luminescent core." Chemistry-a European Journal **7**(22): 4844-4853.

Holland, W. R. and D. G. Hall (1984). "Frequency-Shifts Of An Electric-Dipole Resonance Near A Conducting Surface." Physical Review Letters **52**(12): 1041-1044.

Homola, J., S. S. Yee, et al. (1999). "Surface plasmon resonance sensors: review." Sensors

and Actuators B-Chemical **54**(1-2): 3-15.

Hutter, E., S. Cha, et al. (2001). "Role of substrate metal in gold nanoparticle enhanced surface plasmon resonance imaging." Journal Of Physical Chemistry B **105**(1): 8-12.

Hutter, E., J. H. Fendler, et al. (2001). "Surface plasmon resonance studies of gold and silver nanoparticles linked to gold and silver substrates by 2-aminoethanethiol and 1,6-hexanedithiol." Journal Of Physical Chemistry B **105**(45): 11159-11168.

Ito, S., M. Wehmeier, et al. (2000). "Synthesis and Self-Assembly of Functionalized Hexa-<I>peri</I>-hexabenzocoronenes." Chemistry - A European Journal **6**(23): 4327-4342.

Jeanmaire, D. L. and R. P. van Duyne (1977). "Surface Raman Spectroelectrochemistry .1. Heterocyclic, Aromatic, And Aliphatic-Amines Adsorbed On Anodized Silver Electrode." Journal Of Electroanalytical Chemistry **84**(1): 1-20.

Johansson, P., R. Monreal, et al. (1990). "Theory For Light-Emission From A Scanning Tunneling Microscope." Physical Review B **42**(14): 9210-9213.

Johnson, P. B. and R. W. Christy (1972). "Optical-Constants of Noble-Metals." Physical Review B **6**(12): 4370-4379.

Johnson, P. B. and R. W. Christy (1974). "Optical-Constants of Transition-Metals - Ti, V, Cr, Mn, Fe, Co, Ni, and Pd." Physical Review B **9**(12): 5056-5070.

Kittel, C. (1996). Introduction to solid state physics. USA, John Wiley & Sons, Inc.

Kneipp, K., H. Kneipp, et al. (1999). "Ultrasensitive Chemical Analysis by Raman Spectroscopy." Chem. Rev. **99**(10): 2957-2976.

Kneipp, K., H. Kneipp, et al. (2002). "Surface-enhanced Raman scattering and biophysics." Journal of Physics: Condensed Matter **14**(18): R597-R624.

Kneipp, K., Y. Wang, et al. (1997). "Single molecule detection using surface-enhanced Raman scattering (SERS)." Physical Review Letters **78**(9): 1667-1670.

Knoll, W. (1998). "Interfaces and thin films as seen by bound electromagnetic waves."

Annual Review Of Physical Chemistry **49**: 569-638.

Kolb, D. M. (1988). UV-Visible Reflectance Spectroscopy in Spectroelectrochemistry: Theory and Practice. New York, Plenum.

Krasteva, N., Y. Fogel, et al. (2007). "Vapor sorption and electrical response of Au-nanoparticle-dendrimer composites." Advanced Functional Materials **17**(6): 881-888.

Kreibig, U. and M. Vollmer (1995). Optical Properties of Metal Clusters. Heidelberg, Springer.

Kretschmann, E. (1971). "Determination Of Optical Constants Of Metals By Excitation Of Surface Plasmons." Zeitschrift Für Physik **241**(4): 313-324.

Kuhn, S., U. Hakanson, et al. (2006). "Enhancement of single-molecule fluorescence using a gold nanoparticle as an optical nanoantenna." Physical Review Letters **97**(1).

Kume, T., S. Hayashi, et al. (1996). "A new method of surface plasmon excitation using metallic fine particles." Materials Science And Engineering A-Structural Materials Properties Microstructure And Processing **217**: 171-175.

Kume, T., S. Hayashi, et al. (1997). "Light emission from surface plasmon polaritons mediated by metallic fine particles." Physical Review B **55**(7): 4774-4782.

Kume, T., N. Nakagawa, et al. (1995). "Interaction Between Localized And Propagating Surface-Plasmons - Ag Fine Particles On Al Surface." Solid State Communications **93**(2): 171-175.

Lambe, J. and S. L. McCarthy (1976). "Light-Emission from Inelastic Electron-Tunneling." Physical Review Letters **37**(14): 923-925.

Le, F., N. Z. Lwin, et al. (2005). "Plasmons in the metallic nanoparticle - Film system as a tunable impurity problem." Nano Letters **5**(10): 2009-2013.

Le Ru, E. C., P. G. Etchegoin, et al. (2007). "Mechanisms of spectral profile modification in surface-enhanced fluorescence." Journal of Physical Chemistry C **111**(44): 16076-16079.

Leveque, G. and O. J. F. Martin (2006). "Optical interactions in a plasmonic particle coupled

to a metallic film." Optics Express **14**(21): 9971-9981.

Leveque, G. and O. J. F. Martin (2006). "Tunable composite nanoparticle for plasmonics." Optics Letters **31**(18): 2750-2752.

Lyon, L. A., D. J. Pena, et al. (1999). "Surface plasmon resonance of Au colloid-modified Au films: Particle size dependence." Journal Of Physical Chemistry B **103**(28): 5826-5831.

Michota, A., A. Kudelski, et al. (2002). "Molecular structure of cysteamine monolayers on silver and gold substrates - Comparative studies by surface-enhanced Raman scattering." Surface Science **502**: 214-218.

Mie, G. (1908). "Articles on the optical characteristics of turbid tubes, especially colloidal metal solutions." Annalen Der Physik **25**(3): 377-445.

Morgenroth, F., C. Kübel, et al. (1997). "Nanosized polyphenylene dendrimers based upon pentaphenylbenzene units." Journal of Materials Chemistry **7**(7): 1207-1211.

Morgenroth, F., E. Reuther, et al. (1997). "Polyphenylene dendrimers: From three-dimensional to two-dimensional structures." Angewandte Chemie-International Edition in English **36**(6): 631-634.

Muskens, O. L., V. Giannini, et al. (2007). "Strong enhancement of the radiative decay rate of emitters by single plasmonic nanoantennas." Nano Letters **7**(9): 2871-2875.

Naud, C., P. Calas, et al. (2001). "Critical influence of the fluorinated chain length in the self-assembly of terminally perfluorinated alkanethiol monolayers on gold surfaces. An electrochemical study." Langmuir **17**(16): 4851-4857.

Nie, S. M. and S. R. Emory (1997). "Probing single molecules and single nanoparticles by surface-enhanced Raman scattering." Science **275**(5303): 1102-1106.

Nordlander, P. and F. Le (2006). "Plasmonic structure and electromagnetic field enhancements in the metallic nanoparticle-film system." Applied Physics B **84**: 35-41.

Novotny, L. and B. Hecht (2006). Principles of Nano-Optics. Cambridge, Cambridge University Press.

Nuzzo, R. G. and D. L. Allara (1983). "Adsorption of Bifunctional Organic Disulfides on Gold Surfaces." Journal of the American Chemical Society **105**(13): 4481-4483.

Okamoto, T. and I. Yamaguchi (2003). "Optical absorption study of the surface plasmon resonance in gold nanoparticles immobilized onto a gold substrate by self-assembly technique." Journal Of Physical Chemistry B **107**(38): 10321-10324.

Otter, M. (1961). "Optische Konstanten Massiver Metalle." Zeitschrift Fur Physik **161**(2): 163-&.

Otto, A. (1968). "Excitation Of Nonradiative Surface Plasma Waves In Silver By Method Of Frustrated Total Reflection." Zeitschrift für Physik **216**(4): 398-410.

Palik, E. D. (1984). "Handbook of Optical-Constants." Journal of the Optical Society of America a-Optics Image Science and Vision **1**(12): 1297-1297.

Philpott, M. R. (1975). "Effect of Surface Plasmons on Transitions in Molecules." Journal of Chemical Physics **62**(5): 1812-1817.

Plunkett, M. A., Z. H. Wang, et al. (2003). "Adsorption of pNIPAM layers on hydrophobic gold surfaces, measured in situ by QCM and SPR." Langmuir **19**(17): 6837-6844.

Pockrand, I., A. Brillante, et al. (1982). "Exciton Surface-Plasmon Coupling - An Experimental Investigation." Journal Of Chemical Physics **77**(12): 6289-6295.

Prodan, E., C. Radloff, et al. (2003). "A hybridization model for the plasmon response of complex nanostructures." Science **302**(5644): 419-422.

Qu, J., J. Zhang, et al. (2004). "Dendronized Perylene Diimide Emitters: Synthesis, Luminescence, and Electron and Energy Transfer Studies." Macromolecules **37**(22): 8297-8306.

Qu, J. Q., N. G. Pschirer, et al. (2004). "Dendronized Perylenetetracarboxdiimides with Peripheral Triphenylamines for Intramolecular Energy and Electron Transfer." Chemistry - A European Journal **10**(2): 528-537.

Raether, H. (1988). Surface Plasmons on Smooth and Rough Surfaces and on Gratings.

Berlin, Springer.

Rendell, R. W. and D. J. Scalapino (1981). "Surface-Plasmons Confined By Microstructures On Tunnel-Junctions." Physical Review B **24**(6): 3276-3294.

Ritchie, G. and E. Burstein (1981). "Luminescence of Dye Molecules Adsorbed at a Ag Surface." Physical Review B **24**(8): 4843-4846.

Ritchie, R. H. (1957). "Plasma Losses by Fast Electrons in Thin Films." Physical Review **106**(5): 874.

Ritchie, R. H. and A. L. Marusak (1966). "Surface Plasmon Dispersion Relation for an Electron Gas." Surface Science **4**(3): 234-+.

Ruppin, R. (1983). "Surface-Modes And Optical-Absorption Of A Small Sphere Above A Substrate." Surface Science **127**(1): 108-118.

Savitzky, A. and M. J. E. Golay (1964). "Smoothing and Differentiation of Data by Simplified Least Squares Procedures." Anal. Chem. **36**(8): 1627-1639.

Schmid, G. (2003). Nanoparticles. Weinheim, Wiley-VCH.

Schnatterly, S. E. and C. Tarrio (1992). "Local fields in solids: microscopic aspects for dielectrics." Reviews of Modern Physics **64**(2): 619.

Schulz, L. G. (1954). "The Optical Constants of Silver, Gold, Copper, and Aluminum .1. the Absorption Coefficient-K." Journal of the Optical Society of America **44**(5): 357-362.

Schulz, L. G. and F. R. Tangherlini (1954). "Optical Constants of Silver, Gold, Copper, and Aluminum .2. the Index of Refraction-N." Journal of the Optical Society of America **44**(5): 362-368.

Simovski, C. R., M. Popov, et al. (2000). "Dielectric properties of a thin film consisting of a few layers of molecules or particles." Physical Review B **62**(20): 13718-13730.

Stamou, D., D. Gourdon, et al. (1997). "Uniformly flat gold surfaces: Imaging the domain structure of organic monolayers using scanning force microscopy." Langmuir **13**(9): 2425-

2428.

Tam, F., G. P. Goodrich, et al. (2007). "Plasmonic enhancement of molecular fluorescence." Nano Letters **7**(2): 496-501.

Thèye, M.-L. (1970). "Investigation of the Optical Properties of Au by Means of Thin Semitransparent Films." Physical Review B **2**(8): 3060.

Trugler, A. and U. Hohenester (2008). "Strong coupling between a metallic nanoparticle and a single molecule." Physical Review B **77**(11).

Tsuboi, K., S. Abe, et al. (2006). "Second-harmonic spectroscopy of surface immobilized gold nanospheres above a gold surface supported by self-assembled monolayers." Journal of Chemical Physics **125**(17): 174703.

Tsuboi, K., S. Fukuba, et al. (2007). "Multichannel biosensing platform of surface-immobilized gold nanospheres for linear and nonlinear optical imaging." Applied Optics **46**(20): 4486-4490.

Turbadar, T. (1959). "Complete absorption of light by thin metal films." Proc. Phys. Soc. (London) **73**: 40-44.

Turkevich, J., P. C. Stevenson, et al. (1951). "A Study Of The Nucleation And Growth Processes In The Synthesis Of Colloidal Gold." Discussions Of The Faraday Society(11): 55-75.

Ulman, A. (1996). "Formation and structure of self-assembled monolayers." Chemical Reviews **96**(4): 1533-1554.

Vasilev, K. (2004). Fluorophores near metal interfaces. Halle-Wittenberg, Martin-Luther-Universität Halle-Wittenberg. **Doctoral Thesis**.

Vielma, J. and P. T. Leung (2007). "Nonlocal optical effects on the fluorescence and decay rates for admolecules at a metallic nanoparticle." Journal of Chemical Physics **126**(19).

Vossmeyer, T., B. Guse, et al. (2002). "Gold nanoparticle/polyphenylene dendrimer composite films: Preparation and vapor-sensing properties." Advanced Materials **14**(3): 238-

242.

Weatherby, S. (2005). Faraday Discussions 132: Surface enhanced Raman spectroscopy. London, RSC.

Weiss, K. (1948). "Uber Optische Konstanten Und Elektrischen Widerstand Dicker Metallschichten." Zeitschrift Fur Naturforschung Section a-a Journal of Physical Sciences **3**(3): 143-147.

Weitz, D. A., S. Garoff, et al. (1983). "The Enhancement Of Raman-Scattering, Resonance Raman-Scattering, And Fluorescence From Molecules Adsorbed On A Rough Silver Surface." Journal Of Chemical Physics **78**(9): 5324-5338.

Wiederrecht, G. P., J. E. Hall, et al. (2007). "Control of molecular energy redistribution pathways via surface plasmon gating." Physical Review Letters **98**(8): 083001.

Wiesler, U. M., A. J. Berresheim, et al. (2001). "Divergent synthesis of polyphenylene dendrimers: The role of core and branching reagents upon size and shape." Macromolecules **34**(2): 187-199.

Wind, M., K. Saalwächter, et al. (2002). "Solid-state NMR investigations of molecular dynamics in polyphenylene dendrimers: Evidence of dense-shell packing." Macromolecules **35**(27): 10071-10086.

Wind, M. M., J. Vlieger, et al. (1987). "The Polarizability Of A Truncated Sphere On A Substrate-I." Physica A **141**(1): 33-57.

Wokaun, A. (1985). "Surface Enhancement of Optical-Fields - Mechanism and Applications." Molecular Physics **56**(1): 1-33.

Wokaun, A., H. P. Lutz, et al. (1983). "Energy-Transfer In Surface Enhanced Luminescence." Journal Of Chemical Physics **79**(1): 509-514.

Wood, R. W. (1902). "On a remarkable case of uneven distribution of light in a diffraction grating spectrum." Philosophical Magazine(4): 396-402.

Xu, H. X. and M. Käll (2002). "Surface-plasmon-enhanced optical forces in silver

nanoaggregates." Physical Review Letters **89**(24): 246802.

Xu, H. X., X. H. Wang, et al. (2004). "Unified treatment of fluorescence and Raman scattering processes near metal surfaces." Physical Review Letters **93**(24): 243002.

Yeh, P. (1998). Optical waves in layered media. New York, John Wiley and Sons.

Yin, M., C. R. W. Kuhlmann, et al. (2008). "Novel Fluorescent Core-Shell Nanocontainers for Cell Membrane Transport." Biomacromolecules **9**(5): 1381-1389.

Yin, M., J. Shen, et al. (2008). "Fluorescent Core/Shell Nanoparticles for Specific Cell-Nucleus Staining." Small **x**(x): 1-5.

Zhang, H., K. Mullen, et al. (2007). "Pulsed-Force-Mode AFM Studies of Polyphenylene Dendrimers on Self-Assembled Monolayers." J. Phys. Chem. C **111**(23): 8142-8144.

Zhang, S., L. Berguiga, et al. (2007). "Surface plasmon resonance characterization of thermally evaporated thin gold films." Surface Science **601**(23): 5445-5458.

Summary

The optical resonances of metallic nanoparticles placed at nanometer distances from a metal plane were investigated. At certain wavelengths, these "sphere-on-plane" systems become resonant with the incident electromagnetic field and huge enhancements of the field are predicted localized in the small gaps created between the nanoparticle and the plane.

An experimental architecture to fabricate sphere-on-plane systems was successfully achieved in which in addition to the commonly used alkanethiols, polyphenylene dendrimers were used as molecular spacers to separate the metallic nanoparticles from the metal planes. They allow for a defined nanoparticle-plane separation and some often are functionalized with a chromophore core which is therefore positioned exactly in the gap.

The metal planes used in the system architecture consisted of evaporated thin films of gold or silver. Evaporated gold or silver films have a smooth interface with their substrate and a rougher top surface. To investigate the influence of surface roughness on the optical response of such a film, two gold films were prepared with a smooth and a rough side which were as similar as possible. Surface plasmons were excited in Kretschmann configuration both on the rough and on the smooth side. Their reflectivity could be well modeled by a single gold film for each individual measurement. The film has to be modeled as two layers with significantly different optical constants. The smooth side, although polycrystalline, had an optical response that was very similar to a monocrystalline surface while for the rough side the standard response of evaporated gold is retrieved. For investigations on thin non-absorbing dielectric films though, this heterogeneity introduces only a negligible error.

To determine the resonant wavelength of the sphere-on-plane systems a strategy was developed which is based on multi-wavelength surface plasmon spectroscopy experiments in Kretschmann-configuration. The resonant behaviour of the system lead to characteristic changes in the surface plasmon dispersion. A quantitative analysis was performed by calculating the polarisability per unit area α/A treating the sphere-on-plane systems as an effective layer. This approach completely avoids the ambiguity in the determination of thickness and optical response of thin films in surface plasmon spectroscopy. Equal area densities of polarisable units yielded identical response irrespective of the thickness of the layer they are distributed in. The parameter range where the evaluation of surface plasmon data in terms of α/A is applicable was determined for a typical experimental situation. It was shown that this analysis yields reasonable quantitative agreement with a simple theoretical model of the sphere-on-plane resonators and reproduces the results from standard extinction experiments having a higher information content and significantly increased signal-to-noise ratio.

With the objective to acquire a better quantitative understanding of the dependence of the resonance wavelength on the geometry of the sphere-on-plane systems, different systems were fabricated in which the gold nanoparticle size, type of spacer and ambient medium were varied and the resonance wavelength of the system was determined. The gold nanoparticle radius was varied in the range from 10 nm to 80 nm. It could be shown that the polyphenylene dendrimers can be used as molecular spacers to fabricate systems which support gap resonances. The resonance wavelength of the systems could be tuned in the optical region between 550 nm and 800 nm. Based on a simple analytical model, a quantitative analysis was developed to relate the systems' geometry with the resonant wavelength and surprisingly

good agreement of this simple model with the experiment without any adjustable parameters was found.

The key feature ascribed to sphere-on-plane systems is a very large electromagnetic field localized in volumes in the nanometer range. Experiments towards a quantitative understanding of the field enhancements taking place in the gap of the sphere-on-plane systems were done by monitoring the increase in fluorescence of a metal-supported monolayer of a dye-loaded dendrimer upon decoration of the surface with nanoparticles. The metal used (gold and silver), the colloid mean size and the surface roughness were varied. Large silver crystallites on evaporated silver surfaces lead to the most pronounced fluorescence enhancements in the order of 10^4. They constitute a very promising sample architecture for the study of field enhancements.

Zusammenfassung

Diese Arbeit befasst sich mit den optischen Resonanzen metallischer Nanopartikel im Abstand weniger Nanometer vor einer metallischen Flächen. Diese sogenannte „Kugel-auf-Fläche“-Systeme zeigen abhängig von der Wellenlänge ausgeprägte Resonanzen und eine große Verstärkung des einfallenden Feldes, welche im Spalt zwischen Nanopartikel und der Fläche lokalisiert ist.

Eine Architektur für die Herstellung von Kugel-auf-Fläche-Systemen mit Polyphenylen-Dendrimeren als molekulare Abstandshalter wurde zusätzlich zu den häufig verwendeten Alkanthiolen etabliert. Polyphenylen-Dendrimere erlauben die Einstellung eines definierten Kugel-Fläche-Abstands und können mit Chromophoren im Inneren funktionalisiert werden, was eine genaue Positionierung des Chromophors im Spalt erlaubt.

Die dünnen Gold- oder Silberfilme, die für die Herstellung der Kugel-auf-Fläche-Systeme benötigt werden, wurden durch thermisches Aufdampfen hergestellt. Aufgedampfte dünne Gold- oder Silberfilme besitzen eine glatte Grenzfläche zum Substrat und eine raue obere Seite. Um den Einfluss der Rauhigkeit auf die optische Antwort des Filmes zu untersuchen, wurden zwei Goldfilme mit einer rauen und einer glatten Oberseite parallel hergestellt. Die optische Antwort des Systems wurde durch Anregung von Oberflächenplasmonen an den glatten und rauen Oberflächen in Kretschmann-Konfiguration untersucht. Die Reflektivität des Systems konnte mit einem Einschicht-Modell für jede separate Messung gut beschrieben werden. Um gleichzeitig beide Reflektivitäten beschreiben zu können, muss ein Zweischicht-Modell mit deutlich unterschiedlichen optischen Konstanten eingeführt werden. Die glatte polykristalline Seite zeigte eine optische Antwort ähnlich monokristalliner Oberflächen, während die raue Seite optisch dem aufgedampften Gold ähnelt. Diese Heterogenität führt nur zu einem geringfügigen Fehler bei der Untersuchung nicht-absorbierender dünner Deckschichten.

Um die Resonanzwellenlänge der Kugel-auf-Fläche-Systeme zu bestimmen, wurde eine Strategie basierend auf Multiwellenlängen-Oberflächenplasmonenspektroskopie in Kretschmann-Konfiguration entwickelt. Das resonante Verhalten des Systems führt zu einer charakteristischen Änderung der Dispersionsrelationen der Oberflächenplasmonen. Die quantitative Analyse basiert auf der Modellierung der Kugel-auf-Fläche Resonatoren als eine effektive Schicht für die eine Polarisierbarkeit pro Flächeneinheit, α/A , bestimmt wurde. Dieser Ansatz vermeidet die nicht-Eindeutigkeit bei der gleichzeitigen Bestimmung der Dicke und der optischen Antwort eines dünnen Films in der Oberflächenplasmonenspektroskopie. Gleiche Flächendichten der polarisierbaren Einheiten führten zu einer identischen optischen Antwort unabhängig von der Dicke der Schichten, in der sie verteilt sind. Die Grenzen für die möglichen Parameterwerte, für die diese Auswertung möglich ist, wurden anhand einer typischen experimentellen Situation mit Kugel-auf-Fläche-Systemen bestimmt. Es wurde gezeigt, dass die Auswertung gute Übereinstimmung mit einem einfachen theoretischen Modell liefert. Die Ergebnisse von Standard-Extinktions-Experimenten konnten mit einem erhöhten Informationsgehalt und verbessertem Signal-Rausch-Verhältnis reproduziert werden.

Um den Einfluss der Geometrie auf die Resonanzwellenlänge der Kugel-vor-Fläche Systeme besser zu verstehen, wurden unterschiedliche Parameter systematisch variiert. Die Kugelradien wurden von 10 nm bis 80 nm variiert. Weiterhin wurden die molekularen

Abstandshalter und die dielektrische Umgebung verändert. Es konnte gezeigt werden, das Polyphenylen-Dendrimere als molekulare Abstandshalter für Kugel-auf-Fläche Systeme geeignet sind. Die Resonanzwellenlängen konnten im Bereich von 550 nm bis 800 nm eingestellt werden. Basierend auf einem einfachen analytischen Modell wurde ein Verfahren entwickelt die Wellenlänge der Resonanz in Abhängigkeit der Geometrie zu bestimmen. Eine erstaunlich gute Übereinstimmung dieses einfachen Modells ohne zusätzliche freie Parameter mit dem Experiment wurde gefunden.

Eine zentrale Eigenschaft der Kugel-auf-Fläche-Systeme ist die große Feldverstärkung lokalisiert auf wenigen Kubik-Nanometer im Spalt zwischen Kugel und Fläche. Zum besseren quantitativen Verständnis dieser Feldverstärkung wurde der Anstieg des Fluoreszenzsignals einer Monoschicht eines farbstoffgeladenen Dendrimers auf einem metallischen Substrat nach Auftragung metallischer Kolloide auf dem Substrat bestimmt. Die verwendeten Metalle (Gold/Silber), die Kolloidgröße und die Oberflächenrauhigkeit wurden variiert. Große Silberkristallite auf aufgedampften Silberoberflächen lieferten die größte Verstärkung des Fluoreszenzsignals (in der Größenordnung 10^4) und stellen eine vielversprechende Architektur für weitere Untersuchungen der Feldverstärkung dar.

Acknowledgements

[Removed]